Imperial College London

Cell and Extracellular Matrix Interactions: A Biomimetic Approach to Use Cryptic Extracellular Information to Regulate the Epithelial-to-Mesenchymal Transition

Alex J-S Wang

Submitted in part fulfilment for the degree of Master of Philosophy

Faculty of Engineering
Department of Materials

November 2014

Declaration of Originality

I, Alex J-S Wang, hereby declare that the following written work: *Cell and Extracellular Matrix Interactions: A Biomimetic Approach to Use Cryptic Extracellular Information to Regulate the Epithelial-to-Mesenchymal Transition* is my own. This work was done wholly while as a candidate for a research degree at Imperial College London. All research done by others is appropriately referenced, and all work done with the collaborations of others is acknowledged and clearly attributed.

Copyright Declaration

The copyright of this thesis rests with the author and is made available under a Creative Commons Attribution Non-Commercial No Derivatives licence. Researchers are free to copy, distribute or transmit the thesis on the condition that they attribute it, that they do not use it for commercial purposes and that they do not alter, transform or build upon it. For any reuse or redistribution, researchers must make clear to others the licence terms of this work

Abstract

The extracellular matrix (ECM) provides dynamic biochemical and structural cues that control cell proliferation, signalling, and homeostasis. A critical feature of the ECM is its cryptic sites, hidden biologically active sites exposed through structural alteration or proteolytic cleavage events. In this project, a cryptic signalling fragment derived from the laminin-111 protein is explored as a potential control switch for the epithelial-to-mesenchymal transition (EMT), a critical process in development, wound healing, and cancer progression. One EMT-related pathology in wound healing is fibrosis, the accumulation of excess scar tissue that inhibits normal tissue function. A potential strategy in treating this disease is to control or slow the EMT process during wound healing to prevent epithelial cells from transforming into myofibroblasts that contribute to fibrotic tissue. The effect of the cryptic fragment is characterised in *Mus musculus* mammary gland epithelial cells (NMuMGs) undergoing transforming growth factor β (TGFβ) induced EMT using imaging, biochemical, and molecular-biological techniques. The fragment is then used to engineer a biomimetic basement membrane (BM), using polydopamine coated poly(ε-caprolactone) as the structural scaffold. This system allows stable binding of proteins, as well as providing a suitable surface for epithelial cell proliferation. In this work it is shown that the cryptic fragment directly down-regulates crucial EMT genes in this artificial BM system in NMuMGs, providing a potential reduction of fibrosis pathology. Future and ongoing work will continue to optimise the system and lead to other applications of EMT control both for *in vivo* and *in vitro* studies. This project explores the still widely unused potential of cryptic ECM information in tissue engineering.

Acknowledgements

I would like to thank Professor Molly Stevens for giving me the opportunity to work in her research group, as well as Dr. Christine-Maria Horejs for her invaluable project guidance, advice, and support. I thank Dr. Jean-Philippe St. Pierre and Dr. Thomas von Erlach for their advice and experimental work for the project, and all members of the Stevens Group for their kind support and suggestions. I would also like to acknowledge my examiners, Professors Erhard Hohenester and Alvaro Mata for their input and time. Additional thanks to Chia-Chen Hsu and YJ Xie for helpful discussions. This project was made possible by the US-UK Fulbright – Imperial College London Award.

Table of Contents

1. Introduction

1.1 The Extracellular Matrix and Cryptic Sites

1.2 Laminin – A Crucial Protein of the ECM with Cryptic Sites

1.3 Overview of the Epithelial-to-Mesenchymal Transition

1.4 How a Laminin Cryptic Site Affects the EMT

1.5 Fibrosis and EMT – Contribution of MMPs

1.6 Tissue Engineering Materials

1.7 Polydopamine – A Method for Effective Protein Conjugation

1.8 Engineering a Wound Healing Material that Controls Fibrosis

1.9 Statement of Work

2. Results

2.1 Characterisation of Response of Epithelial Cells to Cryptic Laminin Fragment

2.1.1 Imaging Characterisation

2.1.2 Protein Expression Analysis

2.2 Designing a Biomimetic Cryptic Basement Membrane System

2.2.1 Protein Binding Characterisation

2.2.2 Characterisation of Effect of Biomimetic Material on Epithelial Cells

3. Discussion

3.1 Characterisation of NMuMGs Undergoing EMT Shows Genetic and Morphological Changes

3.2 The Biomimetic Material Affects EMT-Related Genes in NMuMGs

4. Conclusion

4.1 Applications to Fibrotic Disease

4.2 Future Work

5. Materials and Methods

5.1 Cell Culture

5.1.1 Cell Handling

5.1.2 EMT Induction and Fragment Addition

5.1.3 Recombinant β1LnLe1-4 Fragment Production

5.2 qPCR

5.2.1 Cell Sample Preparation

5.2.2 RNA Extraction and Purification

5.2.3 Reverse Transcription

5.2.4 qPCR of cDNA Samples

5.2.5 Primers

5.2.6 Analysis
5.3 Western Blot
5.4 Immunostaining
5.5 Polydopamine Coated Poly(ε-caprolactone)
5.5.1 Electrospinning
5.5.2 Polydopamine Coating
5.5.3 IR Protein Binding Assay
5.5.4 BCA Protein Assay
5.5.5 Protein Coating for Cell-Seeding
5.5.6 Preparation of PCL Cell Chambers
5.6 Cell Handling on PCL Mats
5.6.1 Cell Seeding on PCL
5.6.2 EMT Induction on PCL
5.7 Imaging
5.7.1 Light Imaging
5.7.2 TIRF and Confocal Imaging Sample Preparation
6. References
7. Appendix
7.1 List of Abbreviations
7.2 RT-PCR primer threshold validations

1. Introduction

1.1 The Extracellular Matrix and Cryptic Sites

The extracellular matrix (ECM) is the assortment of proteins that surround the outside of cells and define their environment. Critical signalling in all stages of a cell's life involves the interaction of cellular membrane proteins such as integrins with elements from the ECM.[1] The properties of the ECM are defined by its proteins, soluble growth factors, topology, stiffness, assembly, and dynamics. As such, the composition of the ECM proteins in both type and abundance varies greatly in different regions of the body, allowing highly specific properties. An example of this phenomenon is the specialised ECM in bone, which consists mostly of type I collagen that imparts stiffness and structural integrity.[2] The ECM is also responsive to cells, which can affect the properties of the ECM in response to changing conditions. One aspect of the ECM that lends to its dynamic role is the presence of cryptic sites, hidden signalling "switches" located in certain ECM proteins that are activated by a specific event that can originate from the cell or the environment.[3] A triggering event such as the release of proteases or a conformational shift allows for the specific processing of proteins and exposing of cryptic sites. This action alters cell signalling and allows the cell to give a dynamic response related to the circumstances that triggered activation. There are several examples of cryptic sites that have been discovered in ECM proteins fibronectin, laminin-111, and collagens IV, XV, XVIII.[3,4] In many cases, a cellular enzyme cleaves a sequence or structure-specific protein component of the ECM, which leads to the release of protein fragments or an alteration of protein conformation, revealing hidden sites that give rise to novel cell-ECM interactions.[5]

1.2 Laminin – A crucial protein of the ECM with Cryptic Sites

Laminin is a key protein in the ECM, particularly in the basement membranes (BM), cell-associated ECMs that cover the basal side of epithelial and endothelial cells. Basement membranes are composed mostly of laminins, type IV collagens, nidogens, fibronectin, and numerous proteoglycans, along with macromolecules including growth factors.[6,7] The laminin proteins are composed of three subunits, one of each of the α, β, and γ chains, with the nomenclature of each chain referring to its different chain isomers (e.g. laminin - 511).[8] Its polymerisation is mediated by Laminin N-terminal (LN) domains at the termini of the three short arms of the heterotrimer that allows stable association with other laminin arms into a mesh-like network in the presence of calcium.[9] The Laminin Globular (LG) domains of α chains and some Laminin-type Epidermal Growth Factor-like (LE) modules bind to perlecan, heparin, agrin, and nidogen, which bridges laminin to type IV collagen.[10] The laminin-

collagen network thus forms the core integral BM structure.[11,12] Laminins exhibit dynamic behaviour, and have the ability to self-assemble and bind macromolecules. They bind to cellular receptors mainly through integrins and dystroglycans, playing a large role in establishing epithelial polarity and development.[13] Distinct laminin domains have been shown to be biologically active and harbour cryptic sites, including specific LN domains, nidogen-binding sites, and cell-binding sites.[14] Different laminin isoforms are present depending on the tissue but all play several important roles in tissue morphogenesis, such as organising cellular tissues and protecting adherent cells.[15] One particular isoform, laminin-111, plays a critical role as the most abundant laminin during embryonic development, supporting a variety of functions including neurite outgrowth, cellular migration, and receptor clustering.[7]

In Molly Stevens's group at Imperial College, a previously unidentified cryptic fragment of laminin-111 has been shown to modulate the epithelial to mesenchymal transition (EMT) in mouse and human embryonic stem cells (mESCs and hESCs). This work demonstrates the still widely unknown potential of cryptic ECM sites that play a crucial role in cell differentiation. In allowing embryonic stem cells (ESCs) to differentiate both in monolayer culture and as embryoid bodies that mimic post-implantation embryonic tissue, ESCs undergo transformations that are significantly affected in the presence of the laminin cryptic fragment. Using mESCs and hESCs, this fragment appears to have properties that can alter the EMT, the cell differentiation process that provides the basis for development.[16,17]

1.3 Overview of the Epithelial-to-Mesenchymal Transition

The EMT is responsible for the formation of most adult tissues and organs. Cells of an epithelial type are phenotypically characterised by close contacts with each other, a firmly established axis of polarity. Precise arrangement of adherens junctions, desmosomes, gap junctions, and tight junctions mediate firm attachment to adjacent cells and maintenance of polarity.[18] These cells are prevalent throughout the body and exist in most organ systems. Conversely, cells of a mesenchymal phenotype are loosely organised with no polarity or tight junctions, which enables them to migrate. The conversion from epithelial cells involves the loss of cell-cell adhesion, polarity, and acquiring the ability to migrate. This transformation can be visualised as a dramatic remodelling of actin filaments and cell morphology, with a degradation of attachment proteins in the ECM.[19] The EMT is characterised genotypically by increased expression and activity of Slug and Snail transcription factors, increased matrix metalloproteinase (MMP) activity, vimentin expression and especially a decrease in E-cadherin expression and up-regulated N-cadherin expression, a process known as cadherin switching that plays a role in destabilizing the actin cytoskeletal arrangement.[17,20,21] The

process of EMT is crucial in early development, where cells attached to the early basement membrane need to detach and migrate to specific regions and differentiate into specific tissues. Evidence of EMT in the adult tissue occur in wound healing, where epithelial cells migrate from areas surrounding a wound to fill a cavity, and in cancer metastasis, where certain malignant tumour cells migrate from the primary tumour to establish a secondary tumour in a different area of the body.[22]

The proteolytic processing of proteins of the extracellular basement membrane during EMT is facilitated by MMPs. MMPs are cellular enzymes (zinc endopeptidases) that cleave a variety of proteins, usually by sequence-specific recognition. The set of MMPs produced by humans can cleave virtually any protein in the ECM, with both secreted and membrane-bound MMPs produced by the cell.[23,24] The role of MMPs in a variety of EMT processes is evident, including development, wound healing, and cancer.[4,24] In all of these processes, cells require MMPs to cleave the ECM to facilitate detachment and migration. MMPs have been the target of multiple drug inhibitors for cancer and fibrosis pathologies, largely with disappointing results.[25] The cause of these failures is likely being the large role MMPs play in all crucial processes, with complete inhibition of MMP activity a fatal event for many cells.

1.4 How a laminin-111 cryptic site affects the EMT

A cryptic site of laminin-111 is revealed specifically by MMP2, whose expression is highly up-regulated during EMT.[16] MMP2 (also known as gelatinase A), has been shown to degrade certain types of collagen (IV, V, VII, X), laminins, fibronectin, elastin, and contributes to the activation of other MMPs secreted by the cell.[24] MMP2 cleavage releases a fragment from the N-terminal part of the β1-chain containing LN and LE domains (Ln-Le1-4), which was identified using peptide fingerprinting with liquid-chromatography tandem mass spectrometry (LC-MS) (Figure 1A).[16] Cleavage of this domain by MMP2, which is up-regulated during EMT and embryonic differentiation, releases the fragment from the basement membrane and allows it to act as a signalling peptide (Figure 1B, C). Laminin-111 interacts with the α3β1 isoform of integrin receptors, which is responsible for cytoskeleton assembly, facilitating cell migration, cell-cell junctions, and also regulates MMPs through the EMMPRIN protein (Figure 1E).[26-28] Using laminin as both a soluble factor in solution and an immobilised factor on the surface of a tissue culture plastic (TCP), mouse and human ESCs were observed to have EMT genes significantly altered – there is evidence of E-cadherin up-regulation, slug and snail down-regulation, and MMP2 down-regulation (Figure 1D). Thus, the cryptic laminin fragment appears to initiate a negative-feedback mechanism using MMP2 to slow down the EMT process once the basement membrane has been affected to a certain point. As EMT is occurring in development, MMP2 cleaves the basement membrane to

release the fragment, and once enough fragment has been released it will signal to the cell via integrins to start to inhibit expression of EMT genes. Pathway studies involving an EMMPRIN-blocking antibody fully block the laminin fragment EMT influence, further supporting its binding and signalling pathway through MMP2 and integrin α3β1 (Figure 1F). Establishing this link between MMP-ECM interactions opens up new possibilities to engineer bioactive materials that use this novel control switch.

1.5 Fibrosis and the EMT – The Implication of MMPs

Fibrosis is one of the main pathologies involving both the ECM and the EMT. It is a detrimental condition in wound healing marked by the deposition of scar tissue after severe injury, often compromising organ function.[29] In functional homeostasis of many tissue systems, ECM turnover is regulated by MMPs and tissue inhibitors of metalloproteinases or TIMPS.[23] In fibrosis, epithelial cells, macrophages, T-cells and fibroblasts become activated and can either be recruited or differentiate into a fibroblast-like phenotype that is highly related to the expression and activity of multiple MMPs and TIMPs.[30] Degradation of the ECM by MMPs can lead to the release of ECM-bound cytokines such as TGF-β that can induce fibrogenesis.[23] In fibrotic tissues, fibroblasts display characteristics of myofibroblasts, which secrete excessive fibrous proteins, mainly composed of collagen type I. Studies have shown that these myofibroblasts are involved in a multitude of diseases, including cardiac and liver fibrosis, and that they can be derived from epithelial or endothelial cells; in the case of cardiac fibrosis, vascular endothelial cells undergo a specialised endothelial-to-mesenchymal transition (EndoMT) that is phenotypically similar to normal EMT.[31-33] EMT/EndoMT promotes the progression of the pathology by generating new cells of mesenchymal phenotype that can become myofibroblasts, as well as causing tissues to lose healthy epithelial cells. Lens epithelium, endothelium, hepatocytes, and cardiomyocytes can all undergo EMT and transform into fibrotic tissue.[18] Thus, a possible pathway to target fibrosis is to establish the regulatory systems of myofibroblasts and their pro-fibrotic behaviour.[34]

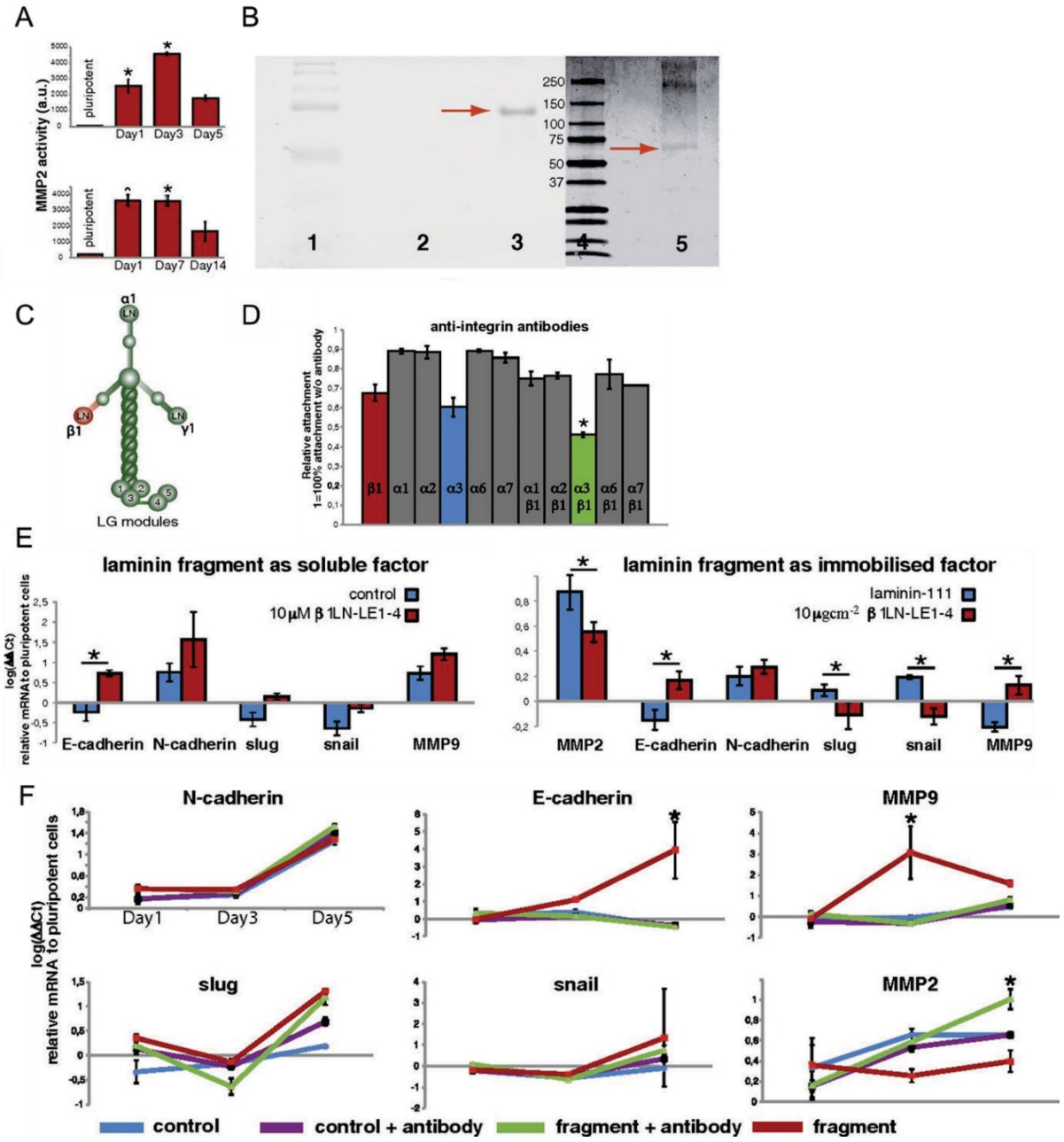


Figure 1 | The Laminin Cryptic Site

A, MMP2 activity assay for mouse (top) and human (bottom) embryonic stem cells (ESCs) on various days of differentiation in comparison to pluripotent cells. B, Native and denatured SDS-PAGE Coomassie blue-stained laminin-111. Lane 1: Molecular mass standard (MMS); Lane 2: Whole laminin-111 (too large to enter gel); Lane 3: Laminin-111 digested with MMP2; Lane 4: MMS; Lane 5: Denatured laminin-111 processed with MMP2. Top two bands correspond to the α, β, and γ chains with no processing, while a ~60 kDa fragment is present that is identified as the cryptic fragment Ln-Le1-4. C, Schematic of laminin-111 – the red segment shows the identified cryptic fragment. D, Cell attachment to Ln-Le1-4 was identified by blocking specific receptors using anti-integrin subunit antibodies and the binding is then quantified by crystal violet staining. Data is relative to non-blocked cells. E, qPCR relative EMT gene expression levels showing the influence of the laminin fragment. The fragment was administered both as a soluble factor in solution and as an immobilised peptide on the surface of a tissue culture plastic (both in monolayer culture). F, Use of an anti-EMMPRIN antibody blocks the effect of the fragment regarding gene expression by q-PCR in mouse ESCs. All significance in figures calculated as $P < 0.05$. All images adapted from Horejs et al. (Reference 16).

MMP2 and MMP14 up-regulation in particular is associated with progression of mild fibrosis to liver cirrhosis.[35] In previous studies, treatment with proteins interleukin-10 or interferon-α and γ reduced TIMP-1 and MMP2 levels while reducing fibrosis in rat models.[36,37] Due to the strong relationship between MMPs and the ECM, MMP inhibitors have been widely explored as a way of curbing excessive ECM proteolysis in a variety of pathologies.[30,38] Most of these therapies involve small molecules and were unable to translate into clinical application due to the side effects of systematically inhibiting MMP activity and due to issues with administered doses, as MMP activity is necessary for many pro-survival cellular processes.[25,39] There have been efforts to inhibit other parts of the EMT in cancer therapies, but due to the involvement of EMT in many pathways, the problem of non-specificity still arises.[40] As a result, recent studies have focused on local delivery of MMP inhibitors, such as through injectable hydrogels that release TIMPs.[41] One of the weaknesses, however, is the non-specificity of TIMPs, as they inhibit multiple MMPs. During the progression of wound healing related fibrosis, some EMT is required for normal repair and ECM turnover, and thus drastically decreasing MMP activity is not as desirable as moderately down-regulating it so that fibrotic scarring is reduced.

1.6 Tissue Engineering Materials

The field of tissue engineering for wound healing has seen marked progress in recent years. With the ever-expanding understanding of the crucial interplay between cells and their environment, much recent effort has been dedicated to creating an ECM environment *in vitro* that allows optimal regeneration of new tissue by delivering the correct structural guidance and bioactive cues.[42] One way to emulate signals from the ECM is to use specific small peptides that can be linked to scaffolds to provide cells with both mechanical support through the scaffold and growth signalling through the peptide.[43] Efforts have been made before to recreate synthetic matrices that are more tunable and consistently high quality.[44] However, such approaches involve complex protein conjugation methods such as chemical crosslinking, surface etching, or plasma treatment that may degrade larger peptides.[45] Besides the problems with protein conjugation, the base scaffold itself must also be consistently reproducible, high quality, and biodegradable. A promising avenue in creating artificial polymer materials with tunable properties is through electrospinning, which allows for the creation of fibrous scaffolds that can mimic the physical architecture of the ECM. These electro-spun fibres can be varied in diameter, alignment, and density to model both the topology of the ECM and its mechanical properties and are thus suitable to produce a biomimetic system that can be adapted to a variety of ECMs in different tissues. In

particular, Poly(ε-caprolactone) (PCL) fibre mats appear to fit the purpose of such a biomimetic scaffold base, as it can also be mixed with other polymers to vary its mechanical properties as well as being readily biodegradable.[46,47] Poly(ε-caprolactone) (PCL) electro-spun fibres have been shown to be conducive to cell growth on the surface and readily mimic an articular cartilage ECM (Figure 2A, B).[48] Thus, while there have been major advances in producing high quality scaffolds, there is still the challenge of how to effectively conjugate proteins to the surface in a way that does not denature or inhibit their bioactive properties.

1.7 Polydopamine – A Method for Effective Protein Conjugation

There has been much research in the development of functionalised biomimetic biomaterials that allow more sophisticated control of cell signalling and fate *in vitro* using signalling peptides, preferably without destructive chemical conjugations or inconsistent adsorption techniques.[43,44] One novel approach to creating these biomimetic materials is to use polydopamine (pDA), a material inspired by mussel adhesive pads.[49] L-dopamine is readily polymerised in alkaline conditions through reaction of its catechol groups to quinone in oxygen (Figure 2C). The resultant polymer can then be coated onto substrates in a thin layer.[49] These coatings show affinity for bioactive molecules that contain amine, thiol, or imidazole groups, thus presenting a wide variety of possible materials that can be bound to the surface.[50] Studies have shown that peptide and antibody immobilisation are possible on pDA surfaces.[43,51] Additionally, cells show increased adhesion on pDA alone with no detectable cytotoxicity, and are responsive to immobilised growth factors on the surface.[52,53] Polydopamine treated PCL scaffolds have already been shown to be a feasible system for cellular growth.[54] Thus, combining an electro-spun PCL biomimetic ECM coated with pDA would be an extremely modular and reliable biomimetic system that allows for the possibility of a complete and accurate artificial basement membrane for regenerative applications (figure 2D). A potential drawback of using pDA is the non-specificity of protein binding. As such, precaution must be used to expose the pDA surface only to desired proteins and that it be fully saturated. It appears that the long term binding stability of pDA to various peptides is not well characterised, and it may be that conditions such as forceful washing or constant fluid flow over the surface can displace previously-coated peptides over time.

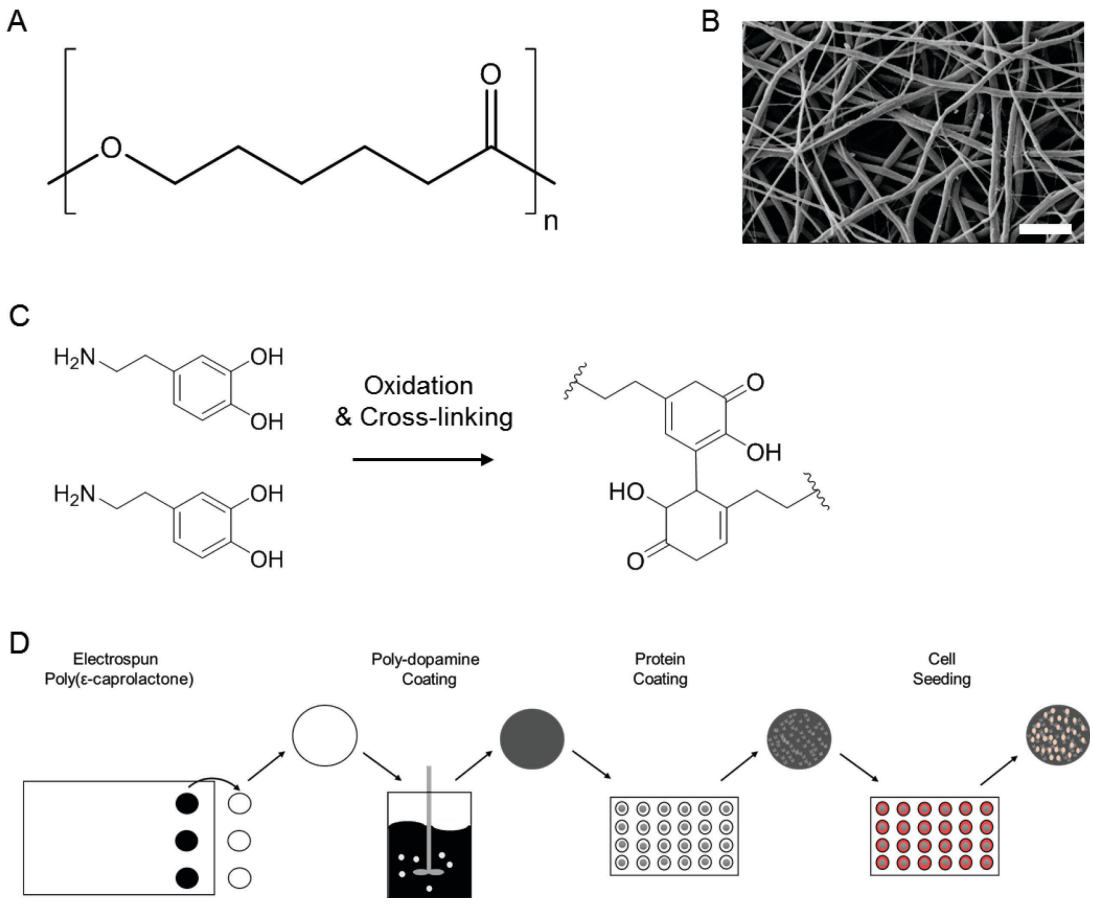


Figure 2 | Poly(ε-caprolactone) and Polydopamine Functionalisation
A, Chemical structure of Poly(ε-caprolactone) (PCL), a biodegradable polymer. B, PCL fibers can be spun together to model an artificial extracellular matrix environment in random-alignment shown in this scanning electron microscope (SEM) image. Scale bar = 10μm C, Dopamine is used by mussels as an adhesion technique. It can be polymerised via oxidation and coated on a surface to allow facile functionalisation of peptides without chemical conjugation methods. D, An artificial basement membrane system can be created using PCL coated polydopamine (pDA). Electrospun poly(ε-caprolactone) is punched from a sheet into small circular mats that are then exposed to a solution of polydopamine. Laminin and collagen are coated on the surface and epithelial cells are then seeded. (B) courtesy of Dr. Jean-Philippe St.-Pierre.

1.8 Engineering a Wound Healing Material that Controls Fibrosis

The goal of this thesis project is to create a biomimetic material that can actively impact the EMT process of epithelial cells and thus provide a novel approach to target tissue fibrosis. A targeted method using β1LnLe1-4 fragment on PCL coated with polydopamine provides a promising system. This system differs from traditional scaffold functionalisation that seeks to maximise cell growth, and instead seeks to control fibrotic accumulation by down-regulating critical EMT genes while still providing strong cell attachment and viability. Recombinant

laminin fragment can be produced and seeded onto the PCL pDA mats.[55] Epithelial cells are then seeded onto this artificial basement membrane and made to undergo EMT. TGFβ will be used to induce EMT in mouse epithelial cells through binding to Tsk7L type I receptors.[56] Sustained up-regulation of TGFβ is implicated during inflammation that precedes fibrosis and cancer progression, and is therefore a relevant activator of EMT.[57] TGFβ works through several pathways, including through Smad complexes, PI3K, ERK, and mTOR, and thus can reliably induce EMT in a wide variety of conditions.[34,58]

This project has three milestones:

1. Establishing the role of β1LnLe1-4 in EMT, first in mESCs and then in mouse epithelial cells.
2. Optimizing and characterising a material system that allows use of the fragment to control the EMT.
3. Characterising the role of β1LnLe1-4 on the EMT on the PCL pDA material using a variety of imaging, biochemical, and molecular biological techniques.

1.9 Statement of Work:

In the first part of my work as co-author on the paper: *Biologically-active laminin-111 fragment that modulates the epithelial-to-mesenchymal transition in embryonic stem cells*, I was involved in characterising the effect of the laminin fragment on murine ESCs in monolayer culture and as embryoid bodies.[16] Additionally, I prepared quantitative PCR (qPCR) experiments to determine change in protein expression due to blocking of extracellular matrix metalloproteinase inducer (EMMPRIN). As the data was collected for the purposes of the previously published work, it will not be mentioned other than in the introduction, and the data and discussion presented in the main section will comprise solely of the mouse epithelial cell system and its characterisation regarding EMT, fragment influence, and on the PCL scaffold. I was involved in planning, running, and analysing all experiments involving the mouse epithelial cells with the exception of confocal and TIRF images on PCL mats, in which I prepared the samples, and the imaging was done by Thomas von Erlach and Christine-Maria Horejs. The PCL mat was electrospun with the help of Jean-Philippe St.-Pierre. All images not credited to someone else were self-made.

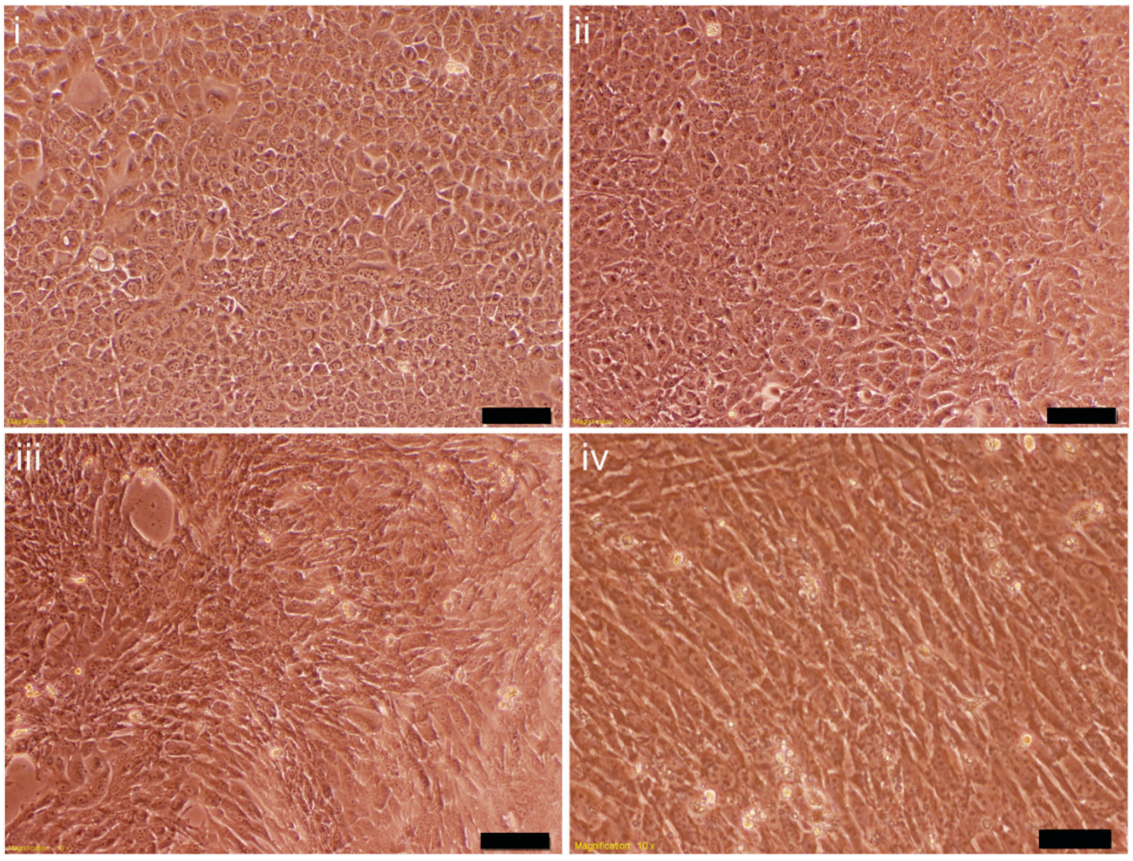
2. Results

2.1 Characterisation of Response of Epithelial Cells to Cryptic Laminin Fragment

2.1.1 Imaging Characterisation

The model system uses a specific type of mouse epithelial cells, the NMuMG line derived from mammary glands. In order to ascertain the effect of the laminin fragment on epithelial cell morphology during EMT, light and immunofluorescence microscopy was used. To induce EMT, both TGFβ3 and TGFβ1 were initially used to determine if initializing EMT through slightly different pathways would change the effect of the laminin fragment or vary EMT phenotype significantly. Figure 3 shows light microscopy images for both TGFβ3 and TGFβ1 induced EMT in NMuMG cells. Laminin fragment was added as a soluble factor before the induction of EMT. There is a dramatic change in morphology upon the addition of TGFβ3 and TGFβ1 after 24 hrs, but the fragment does not appear to significantly change the overall morphology.

A



B

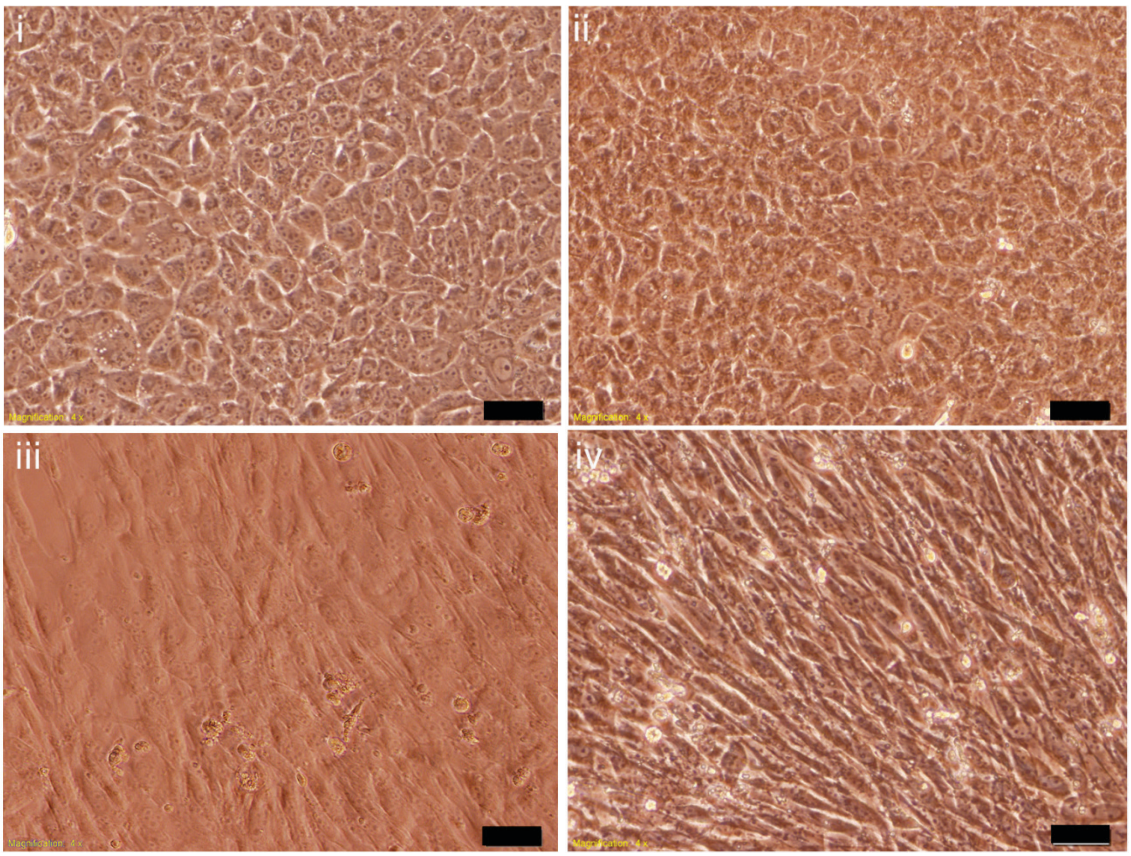
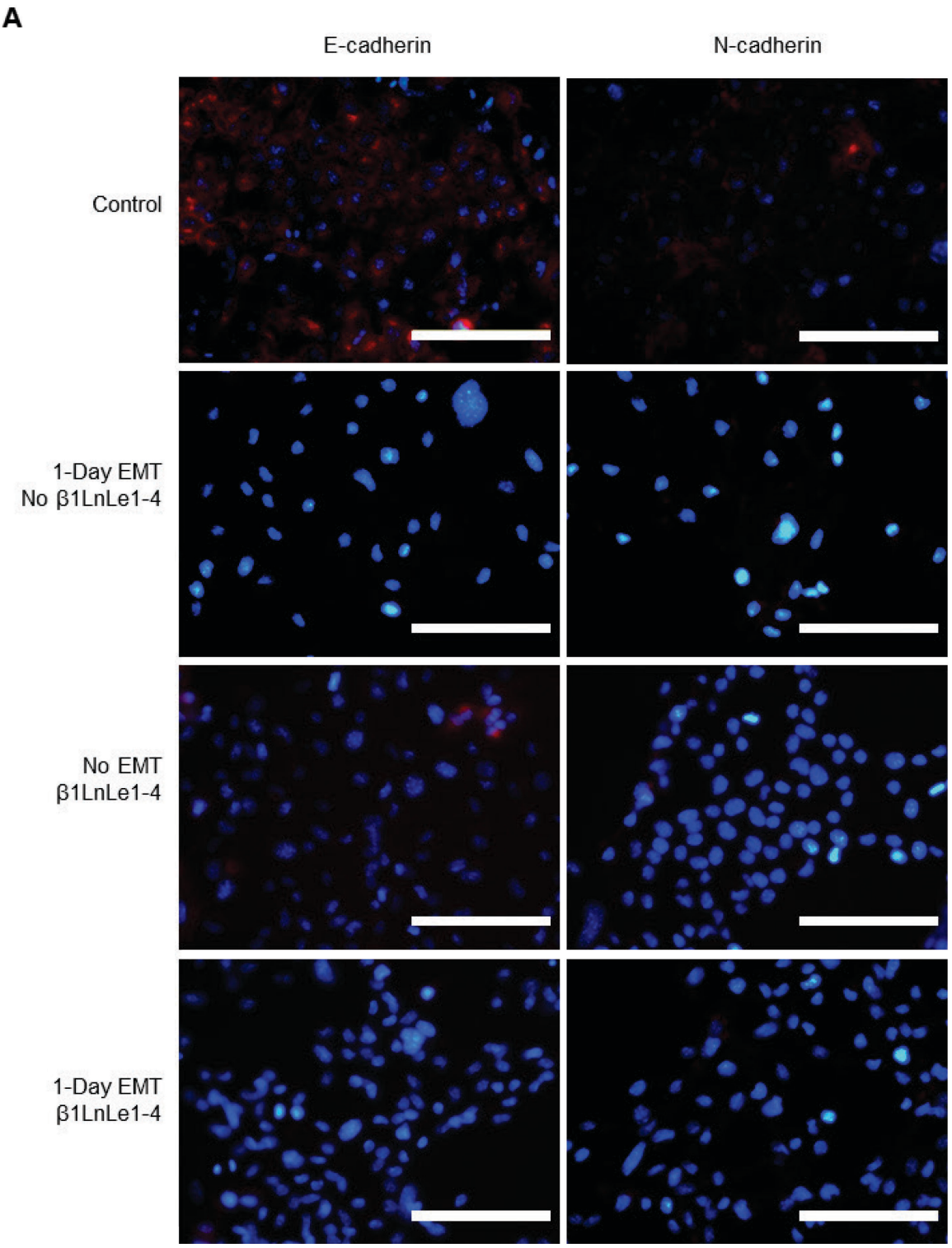


Figure 3 | Light Microscopy of NMuMG cells
A, Experiment with EMT induced via TGFβ3 for 24 hrs. (i) control; (ii) β1LnLe1-4; (iii) TGFβ3; (iv) β1LnLe1-4 and TGFβ3. Scale bar = 100μm. B, Experiment with EMT induced via TGFβ1 for 24 hrs. (i) control; (ii) β1LnLe1-4; (iii) TGFβ1; (iv) β1LnLe1-4 and TGFβ1. Scale bar = 200μm.

For immunostaining, time dependent fragment influence was also studied, as well as any potential differences between TGFβ3 and TGFβ1 (Figures 4-7). For TGFβ3, cells had EMT induced for 24 hrs or 48 hrs and were then fixed and stained for EMT-related proteins: E-Cadherin, N-Cadherin, Fibronectin, and Actin. For TGFβ1, cells had EMT induced for 48 hrs and were fixed and stained for EMT-related proteins: E-Cadherin, N-Cadherin, Fibronectin, and Collagen I. Immunostaining imaging for TGFβ1 induction at 24 hrs was not done after comparison of 48 hr results with TGFβ3 showed no qualitative difference, as it is likely that there would be no discernible differences at shorter stimulation times. Image results show that laminin fragment addition appears to have a qualitative effect on Collagen I, with treated samples showing reduced staining intensity. Fibronectin also appears to be qualitatively slightly different.


A
E-cadherin
N-cadherin
Control
1-Day EMT
No β1LnLe1-4
No EMT
β1LnLe1-4
1-Day EMT
β1LnLe1-4

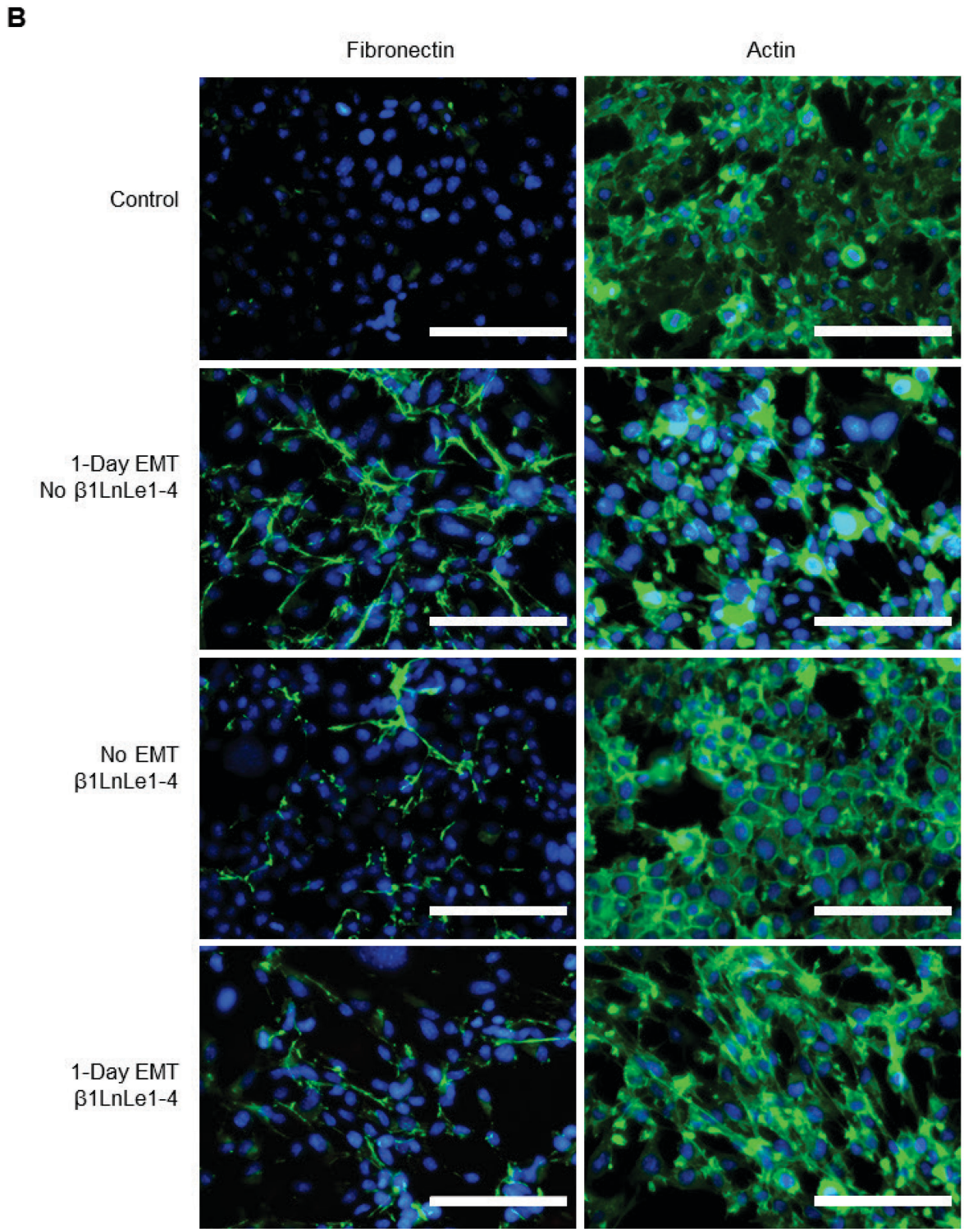
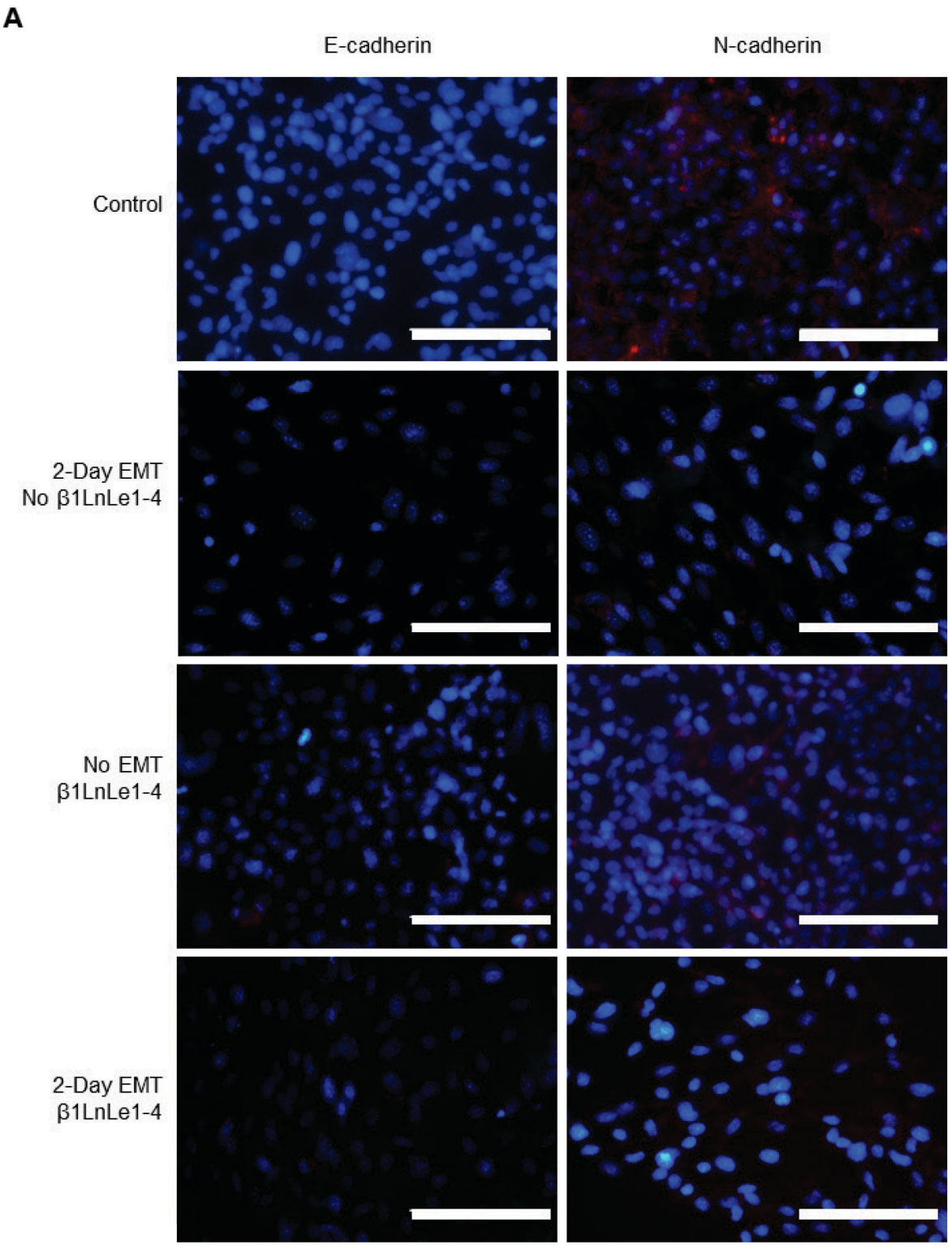


Figure 4 | Immunostaining of NMuMG Cells with TGFβ3 EMT Induction for 24 hrs

Representative images from fixed cells after 24 hrs of adding TGFβ3 and staining with antibodies for A, Anti-E-Cadherin, N-Cadherin and B, Anti-Fibronectin, and Actin. Some contrast and sharpening adjustments were made. Scale bar = 100μm.


A
E-cadherin
N-cadherin
Control
2-Day EMT
No β1LnLe1-4
No EMT
β1LnLe1-4
2-Day EMT
β1LnLe1-4

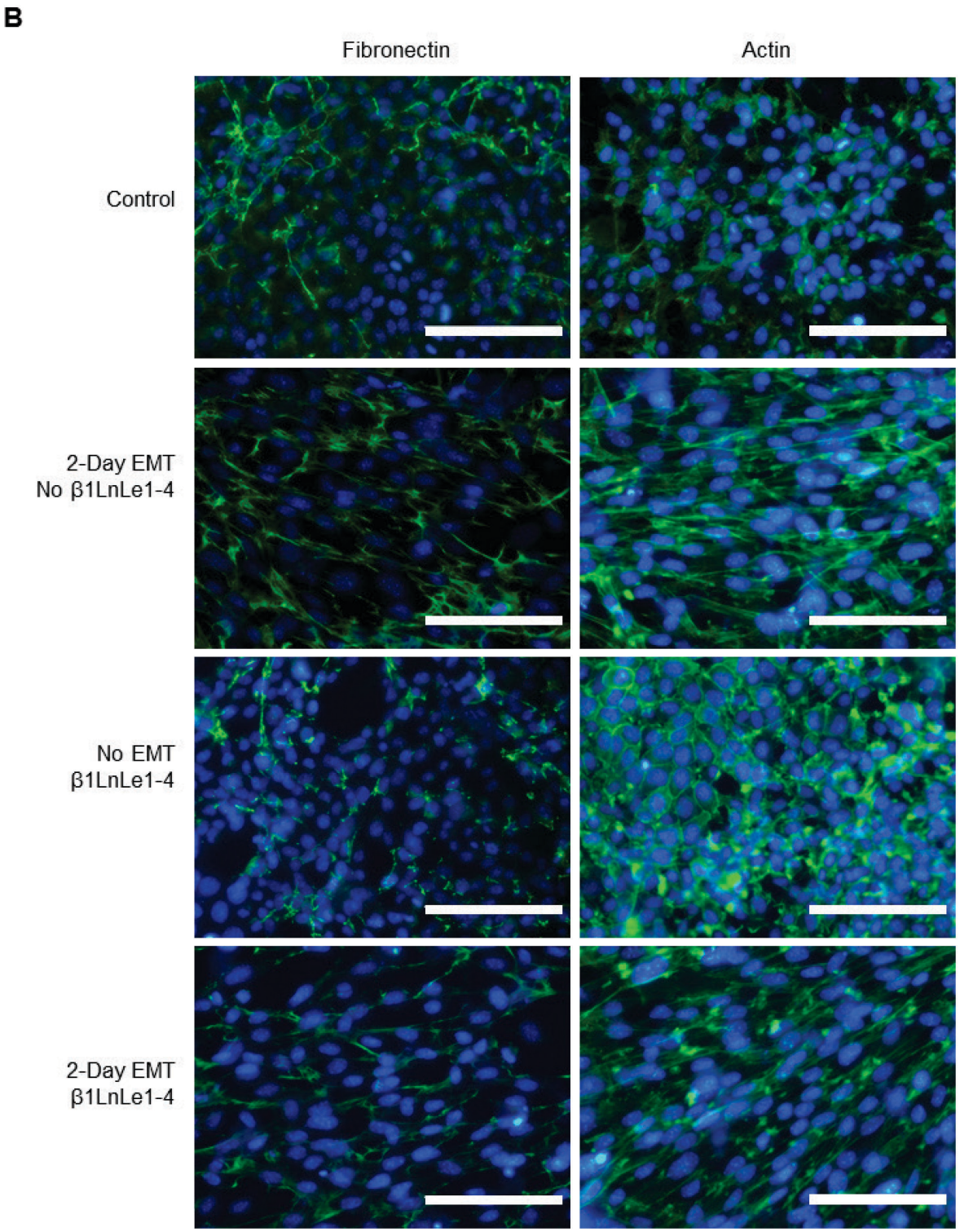
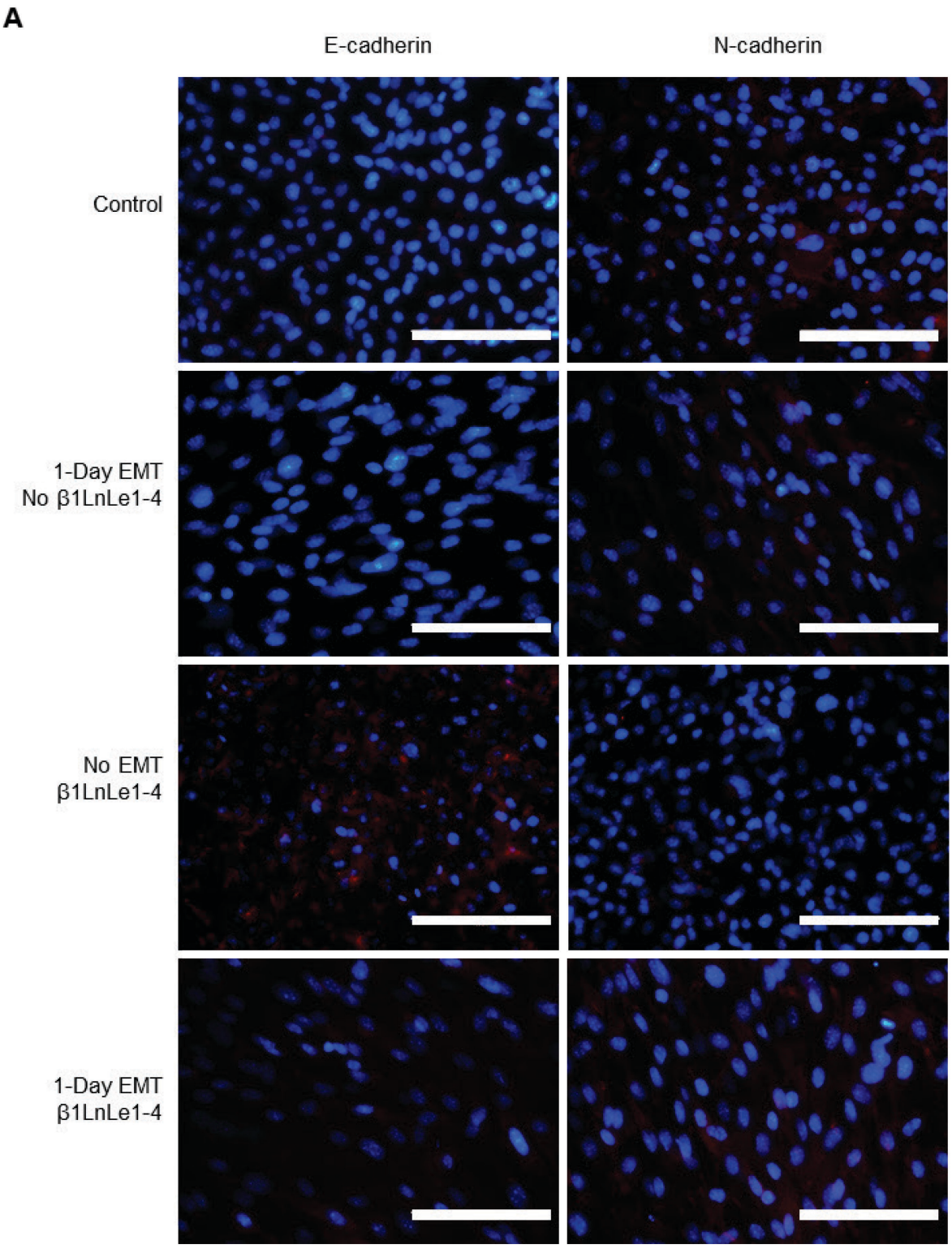


Figure 5 | Immunostaining of NMuMG Cells with TGFβ3 EMT Induction for 48 hrs

Representative images from fixed cells after 48 hrs of adding TGFβ3 and staining with antibodies for A, Anti-E-Cadherin, N-Cadherin and B, Anti-Fibronectin, and Actin. Some contrast and sharpening adjustments were made. Scale bar = 100μm.


A
E-cadherin
N-cadherin
Control
1-Day EMT
No β1LnLe1-4
No EMT
β1LnLe1-4
1-Day EMT
β1LnLe1-4

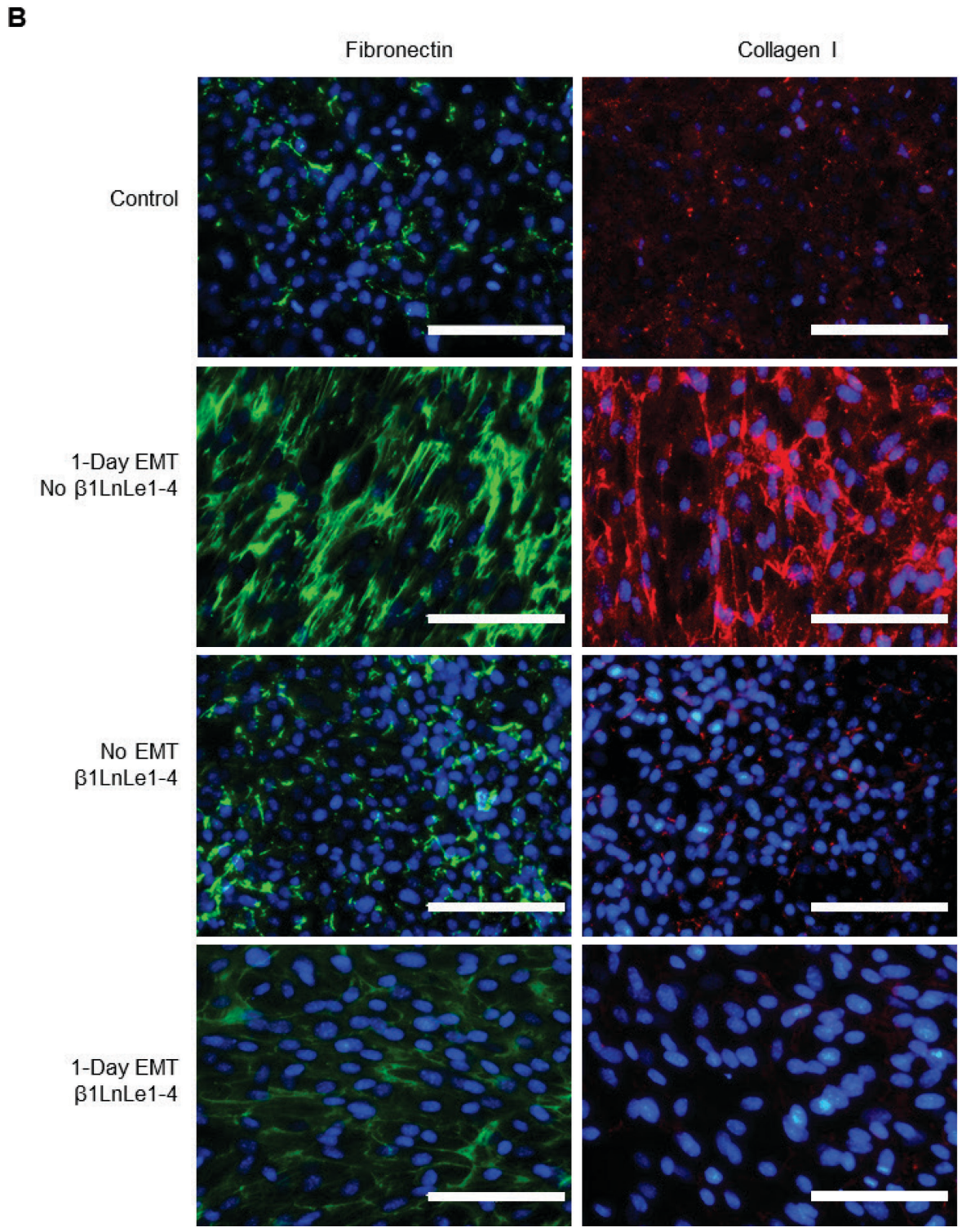


Figure 6 | Immunostaining of NMuMG Cells with TGFβ1 EMT Induction for 48 hrs
Representative images from fixed cells after 48 hrs of adding TGFβ1 and staining with antibodies for A, Anti-E-Cadherin, N-Cadherin and B, Anti-Fibronectin, and Collagen type I. For E-cadherin, N-cadherin, and collagen type I some contrast adjustment was made. Some contrast and sharpening adjustments were made. Scale bar = 100μm.

From the microscopy images we were able to determine that the fragment did not morphologically alter NMuMG cells significantly both in control and TGF-induced EMT. Additionally, TGFβ1 and TGFβ3 pathways were not significantly different, in that the cells undergo the same EMT phenotypic changes using either growth factor for both 24 and 48 hr time periods. These results were encouraging as it is undesirable for the fragment to interfere completely with the EMT process, as was the case with certain inhibitor drugs.[40] In wound healing, the critical EMT process must continue, but not progress to fibrosis. There was not qualitative evidence of cadherin switching, as problematic staining with the cadherin antibodies led to inconsistent imaging across samples. Reasons may include over-permeabilisation or poor antibody specificity due to the antibodies being raised against human proteins (though all were supposedly also successfully tested with mouse proteins). Evidence from previous literature where NMuMGs are stimulated with TGFβ1 or TGFβ3, however, suggests that the phenomenon can be visualised.[59,60]

2.1.2 Protein Expression Analysis

To characterise the change in expression of critical EMT genes, western blot and qPCR were used. In western blot analysis, presence of EMT-critical gene products E-Cadherin, N-Cadherin, and Fibronectin were successfully identified, though Collagen type I and EMMPRIN antibodies did not appear to work, possibly due to the denaturing process of preparing samples. Figure 7 shows that both E and N-Cadherin proteins were expressed, but EMT E/N-Cadherin switching is not entirely clear. Fibronectin appears to show a clear increase under EMT induction, especially when considering relative to GAPDH bands. EMT induction time was also tested, varying between 24 hrs and 4 days.

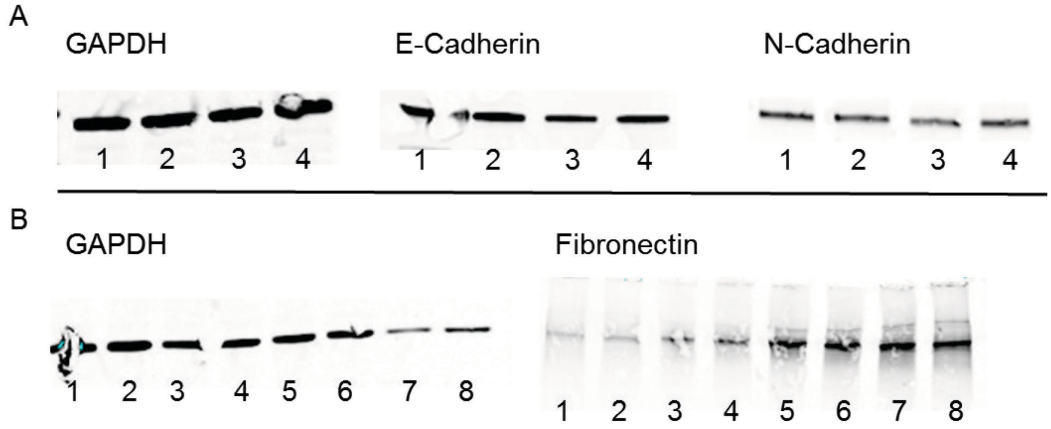


Figure 7 | Western Blot of EMT proteins
A, Anti - GAPDH, E-Cadherin, and N-Cadherin antibodies identify presence of critical EMT genes in NMuMG cells after inducing EMT for 24 hrs. Lane 1: Control NMuMG; Lane 2: β1LnLe1-4 fragment added; Lane 3: TGFβ3-induced EMT; Lane 4: β1LnLe1-4 and TGFβ3 EMT. B, GAPDH and

Fibronectin western blot in separate experiment looking at time-dependent EMT induction shows increase of fibronectin. Lane 1: Control; Lane 2: β1LnLe1-4 fragment; Lane 3: TGFβ3 for 24 hrs; Lane 4: β1LnLe1-4 fragment and TGFβ3 for 24 hrs; Lane 5: TGFβ3 for 48 hrs; Lane 6: β1LnLe1-4 fragment and TGFβ3 for 48 hrs; Lane 7: TGFβ3 for 4 days; Lane 7: β1LnLe1-4 fragment and TGFβ3 for 4 days.

The western blots showed that EMT-critical proteins were being expressed and expression was varying in response to EMT induction via TGFβ. To provide a more quantitative and sensitive evaluation of fragment influence and EMT signaling, qPCRs were performed. In the first set of qPCR experiments, TGFβ3 was added and EMT induced for 24 hrs, with the medium complemented with 10μM laminin fragment. Results in Figure 8 show that there is clear evidence of EMT events, notably down-regulation of E-cadherin, up-regulation of MMP2, collagen type I, and fibronectin. These effects show that the morphological change of NMuMGs is accompanied by changes in mRNA expression.

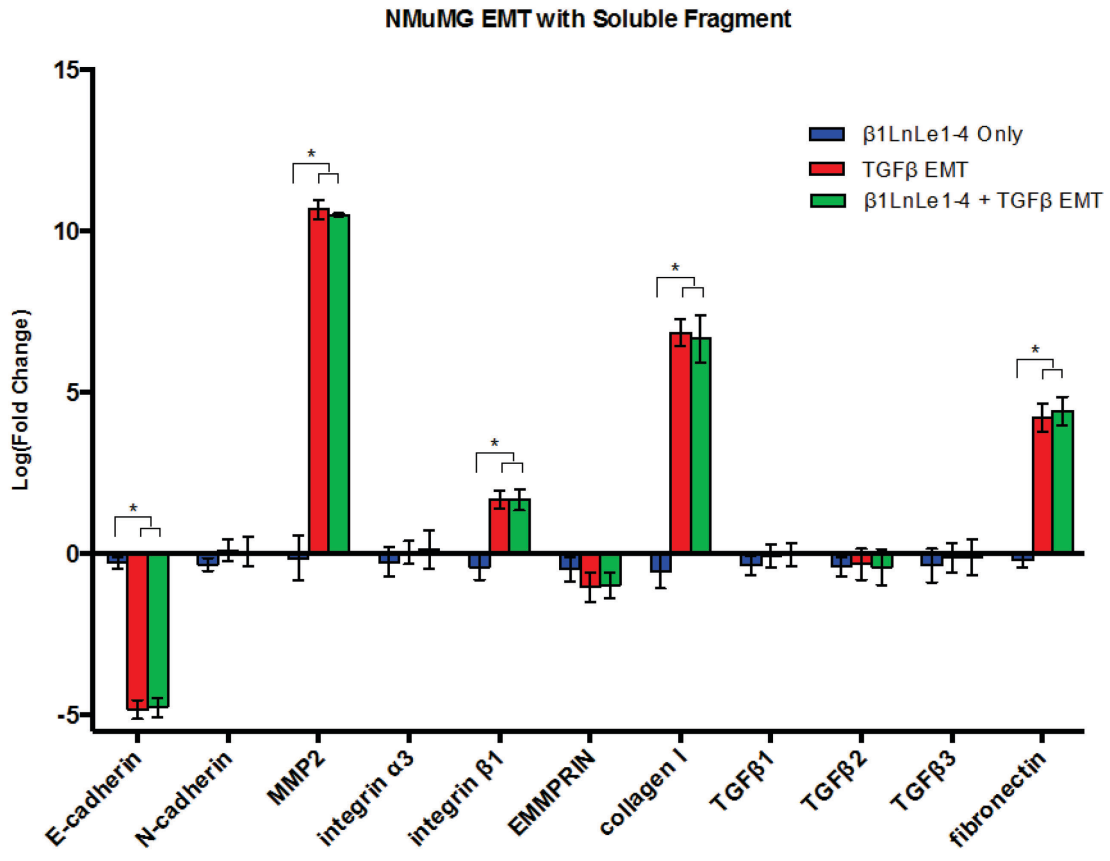
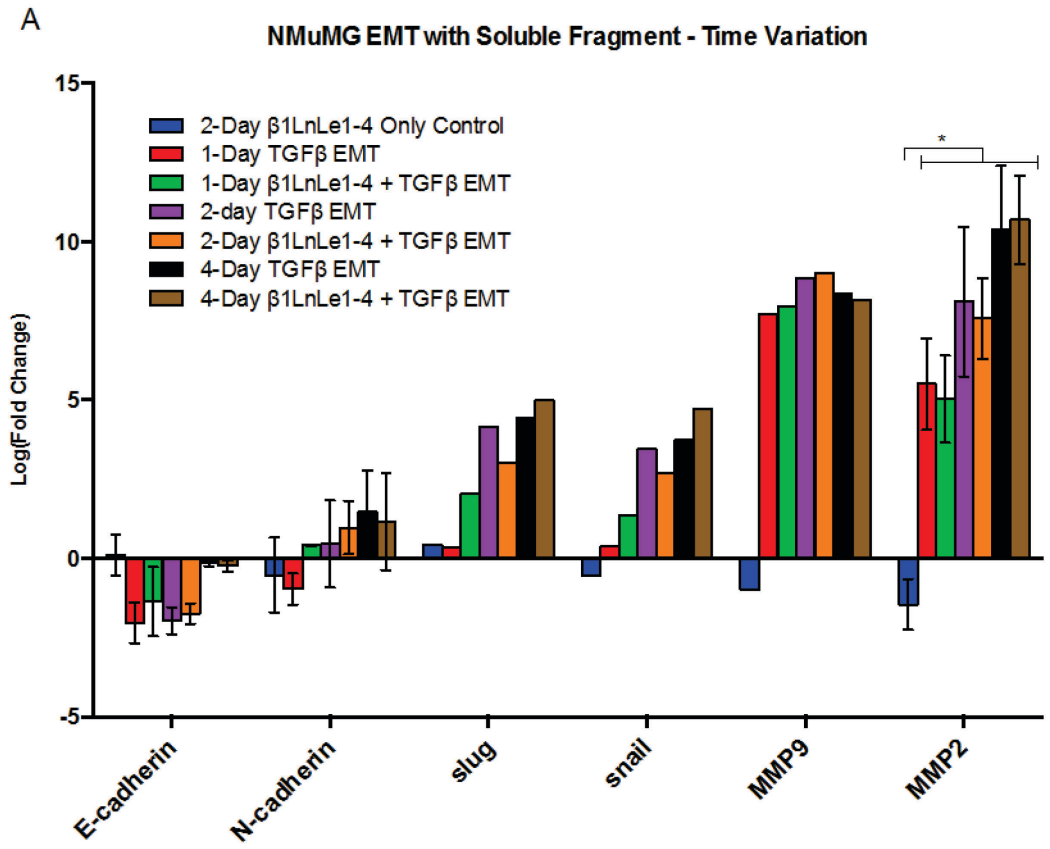


Figure 8 | qPCR for NMuMG with Soluble Laminin Fragment
EMT-related gene expression levels in terms of fold change relative to control non-EMT NMuMG cells. 1st bar (blue): β1LnLe1-4 only; 2nd bar (red): TGFβ EMT; 3rd bar (green): β1LnLe1-4 and TGFβ EMT. Log(Fold Change) > 0 indicates up-regulation while negative values indicate down-regulation. *P < 0.05 EMT conditions compared to non-EMT conditions. Error bars show standard error of mean (SEM) of replicates. For all genes N = 3.

To further characterise NMuMG genetic changes due to EMT, a time-dependent study was performed for 1 day, 2 days, and 4 days of inducing EMT via TGFβ3. Figure 9 shows that there is roughly a correspondence between days of EMT induced and the fold change in mRNA expression of certain genes. Here it appears that there are some changes caused by fragment influence, but unfortunately due to the high variability no statistical significance can be gained. Overall, however, there is a trend for MMP2 and collagen type I being affected by the presence of the laminin fragment. In order to enhance laminin fragment contact with NMuMG cells, the fragment was pre-adsorbed to the bottom of tissue culture plastic instead of added as a soluble factor. TGFβ1 was then added to induce EMT. Cells were treated with medium complemented with TGFβ1 for 2 hrs, 5 hrs, 24 hrs, and 4 days. Figure 10 shows that there are no EMT-characteristic gene-expression changes until TGFβ treatment for 5 and 24 hrs, while after 4 days the cells become overly confluent. Overall, this initial characterisation of NMuMG cells builds a foundation upon what is to be expected in the material system in terms of EMT gene expression level changes and possible fragment influence. Based on the most consistent results being from the 24 hr time point, all future EMT experiments had TGFβ1 added 24 hrs before sample characterization.



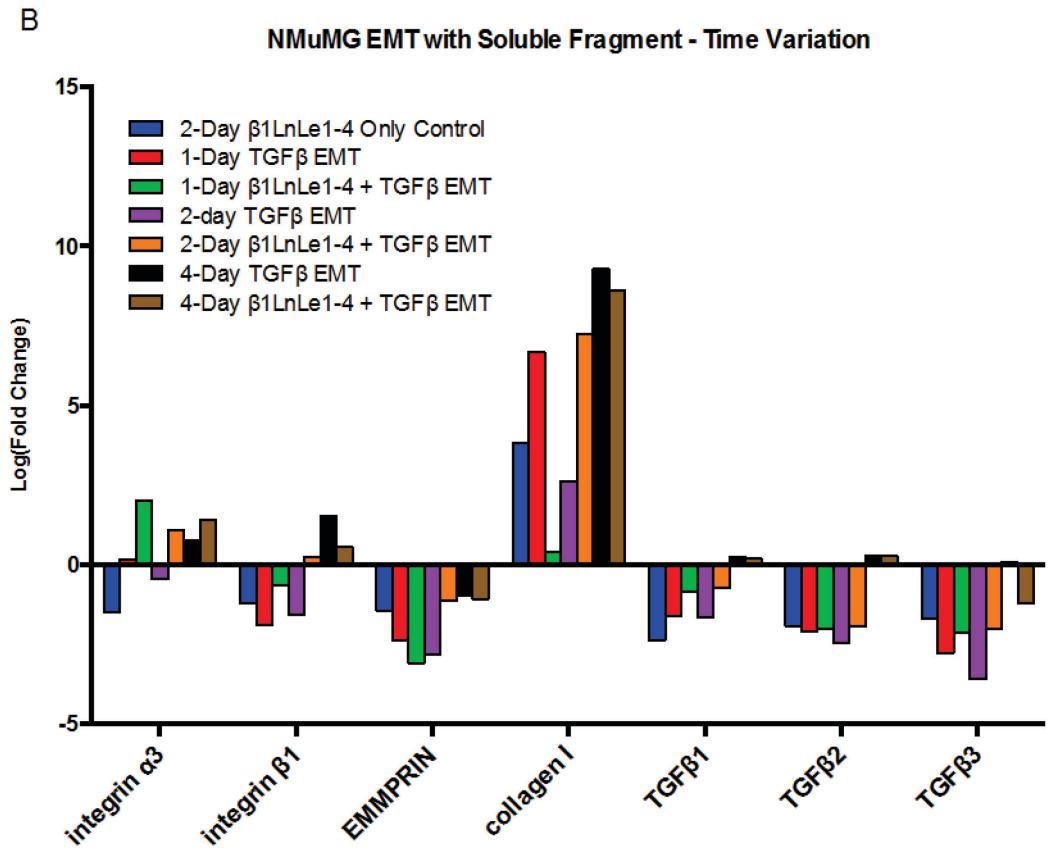
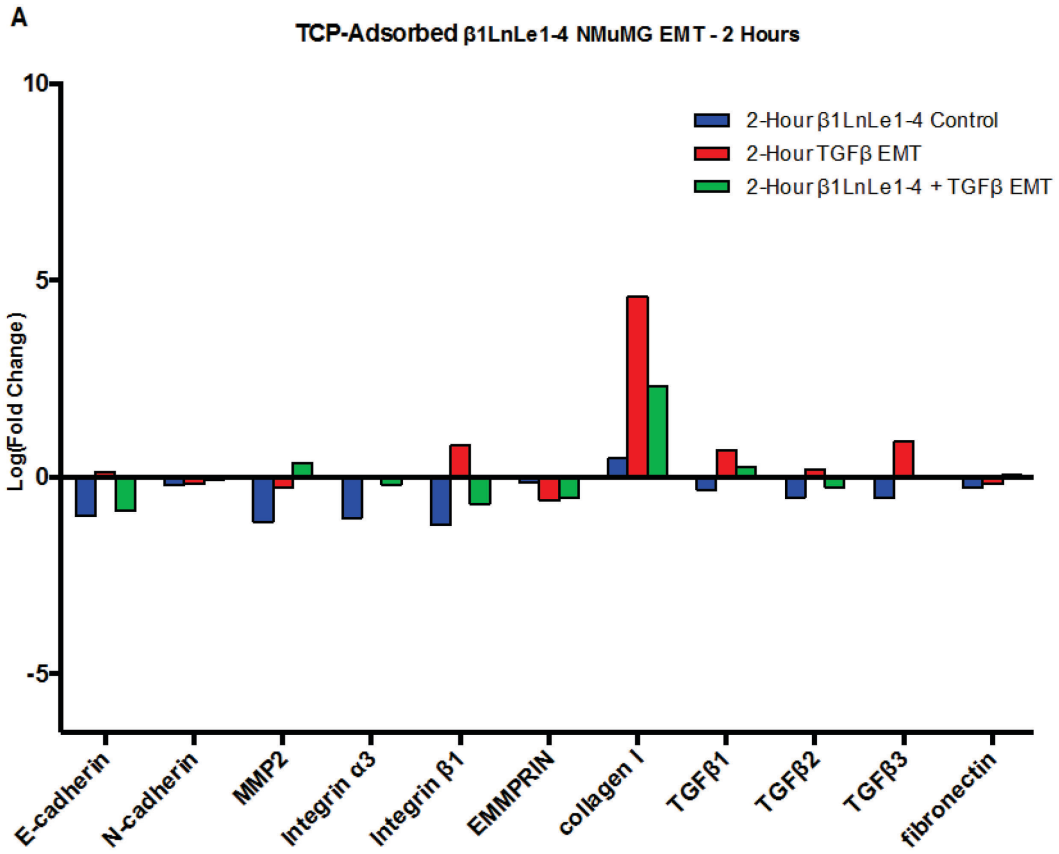
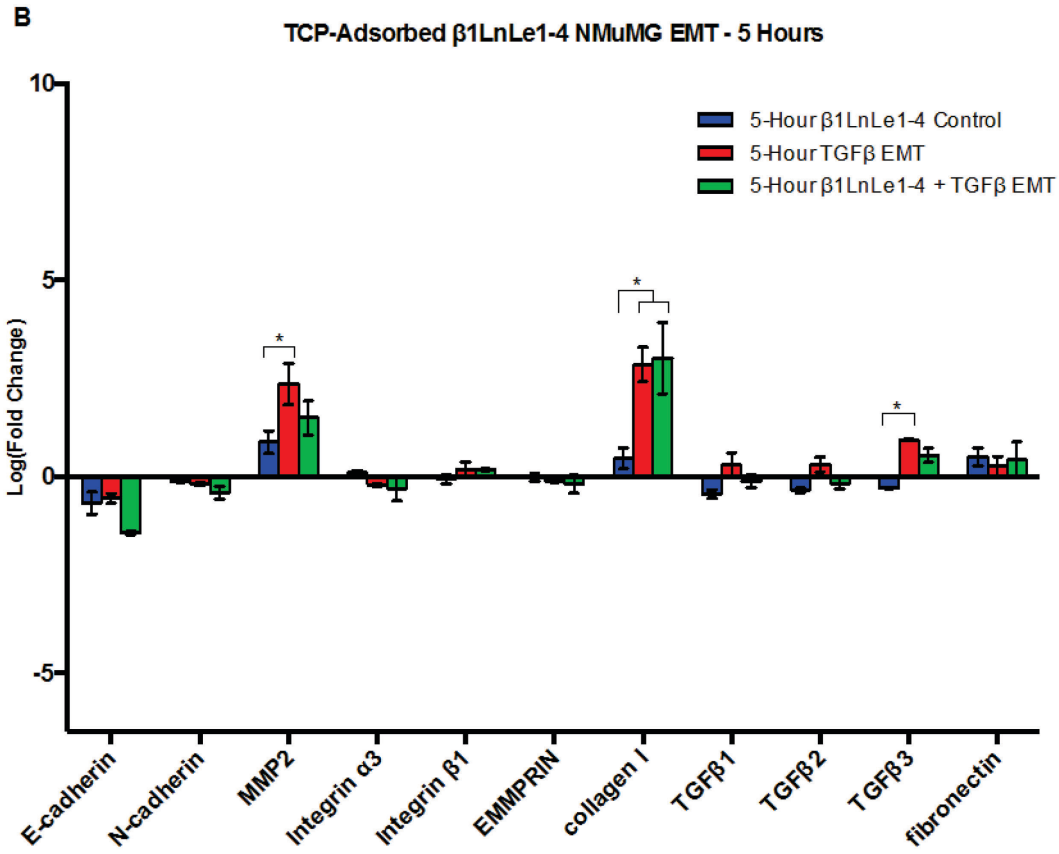


Figure 9 | qPCR for NMuMG with Soluble Laminin Fragment with Varying Times
EMT-related gene expression levels in terms of fold change relative to control non-EMT NMuMG cells. EMT was induced by adding TGFβ and waiting for either 1 day, 2 days, or 4 days, with the control cells harvested at the same time as the 2-day samples. 1st bar (blue): β1LnLe1-4 Only Control; 2nd bar (red): 1-Day TGFβ EMT; 3rd bar (green): 1-Day β1LnLe1-4 and TGFβ EMT; 4th bar (purple): 2-Day TGFβ EMT; 5th bar (orange): 2-Day β1LnLe1-4 and TGFβ EMT; 6th bar (black): 4-Day TGFβ EMT; 7th bar (brown): 4-Day β1LnLe1-4 and TGFβ EMT. Log(Fold Change) > 0 indicates up-regulation while negative values indicate down-regulation. *P < 0.05 EMT conditions compared to non-EMT conditions. The horizontal line indicates that every sample under the line is significant to the other indicator. Error bars show SEM of replicates. For E, N-Cadherin, MMP2 N = 2. For all other genes N = 1.


A
TCP-Adsorbed β1LnLe1-4 NMuMG EMT - 2 Hours
2-Hour β1LnLe1-4 Control
2-Hour TGFβ EMT
2-Hour β1LnLe1-4 + TGFβ EMT
Log(Fold Change)
10
5
0
-5
E-cadherin
N-cadherin
MMP2
Integrin α3
Integrin β1
EMMPRIN
collagen I
TGFβ1
TGFβ2
TGFβ3
fibronectin


B
TCP-Adsorbed β1LnLe1-4 NMuMG EMT - 5 Hours
5-Hour β1LnLe1-4 Control
5-Hour TGFβ EMT
5-Hour β1LnLe1-4 + TGFβ EMT
Log(Fold Change)
10
5
0
-5
*
*
*
E-cadherin
N-cadherin
MMP2
Integrin α3
Integrin β1
EMMPRIN
collagen I
TGFβ1
TGFβ2
TGFβ3
fibronectin

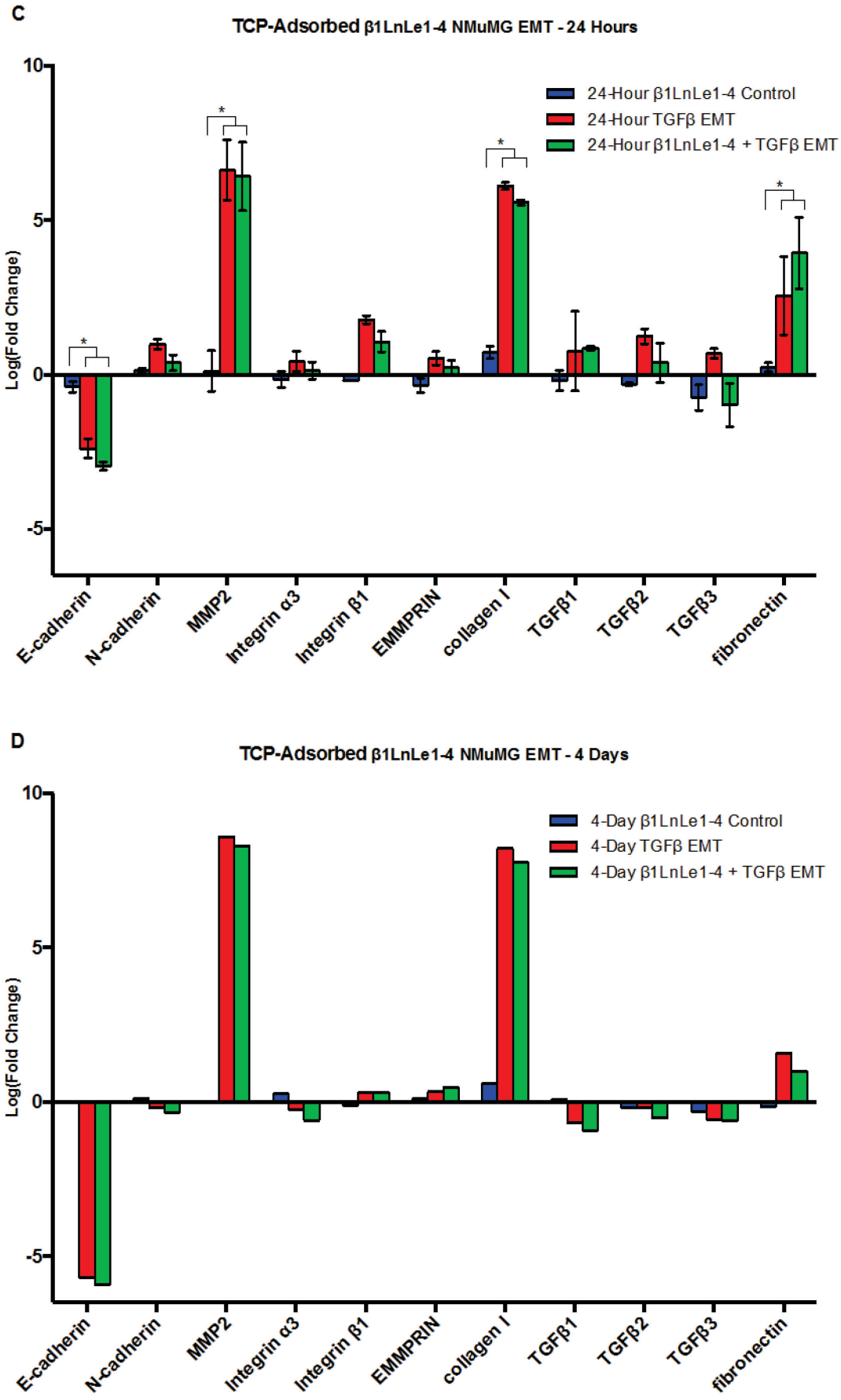


Figure 10 | qPCR for NMuMG with TCP-Adsorbed Laminin Fragment with Varying Times

EMT-related gene expression levels in terms of fold change relative to control 2-day non-EMT NMuMG cells for A) 2 hrs, B) 5 hrs, C) 24 hrs, D) 4 days after TGFβ1 addition. 1st bar (blue): β1LnLe1-4 Control; 2nd bar (red): TGFβ EMT; 3rd bar (green): β1LnLe1-4 and TGFβ EMT (all samples). *P < 0.05 EMT compared to non-EMT conditions. Error bars show SEM of replicates. For 2 hr genes, N = 1, for 5 hr genes N = 2, for 24 hr genes E, N-cadherin, MMP2, EMMPRIN, Fibronectin N = 3, and everything else N = 2, for 4 day genes N = 1.

2.2 Designing a Biomimetic Cryptic Basement Membrane System

2.2.1 Protein Binding Characterisation

In order to determine the optimal protein concentrations, incubation medium, and adsorption time, a preliminary characterisation of binding on pDA-coated PCL mats was performed. Collagen type I dissolved in acetic acid is diluted to 100μg/mL with either PBS or 10mM Tris pH 8.5 and incubated with PCL with and without pDA coating. To characterise protein binding, the antibody intensity of an anti-Collagen I antibody was measured using an infrared dye conjugated secondary antibody. Signal was quantified using an infrared (IR) detector (Figure 11A, C, D). Additionally, a BCA protein assay wacs performed, measuring the concentration of laminin-111 protein left in solution after PCL mats were incubated for varying periods from 5 min to 24 hrs as a proxy for protein adsorption onto the PCL mats (Figure 11B). Results indicate that PBS and 10mM Tris show approximately equal binding efficiency, so PBS was used for all further experiments. Interestingly, non-pDA coated PCL showed higher binding signal in the IR assay (Figure 11C). In non-air plasma treated samples, PCL not-coated with pDA continued to show higher protein binding (Figure 11D). Ultimately, it appeared that comparison between the binding on non-coated and pDA-coated PCL mats using IR was rendered difficult by quenching of the signal by the pDA coating, possibly due to the aromatic groups in the coating. Additionally, lower signal may also be a result of differences in changed surface properties that result in less nonspecific adsorption but tighter binding, due to interaction of pDA with thiol and amine groups through Michael addition or Schiff base reactions.[61] Hence, even if there was a greater amount of protein in non pDA mats, it is still more desirable to coat with pDA to ensure even and stable protein coating. Thus, the indirect method of measuring the protein removal from the solution was a better approach to determine protein binding. From the results of the BCA-binding assay, binding appeared to approach saturation around 6-8 hrs. As such, in the optimised system protein is dissolved in PBS and coated for at least 8 hrs to reach theoretical saturation.

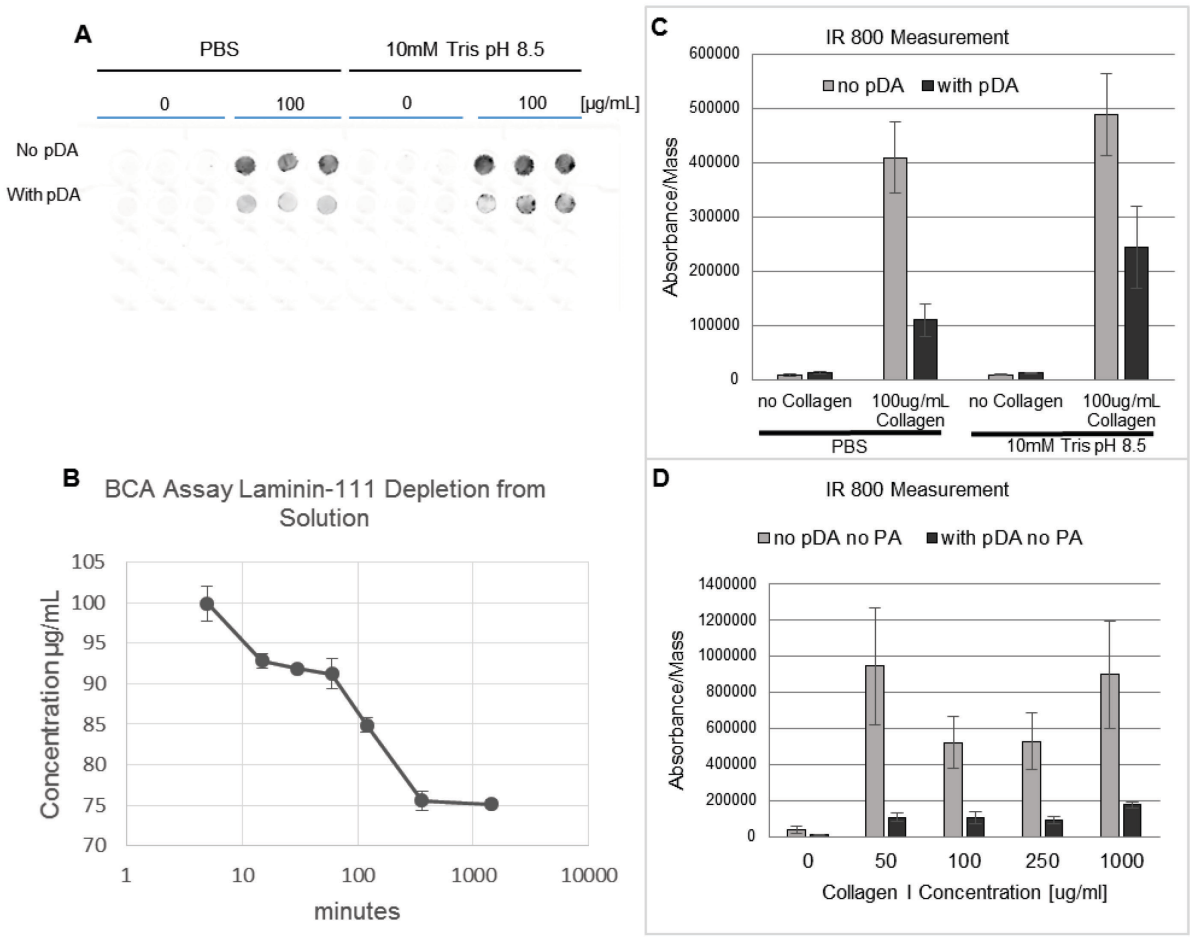


Figure 11 | Protein Binding Characterisation of Polydopamine Coated Poly(ε-caprolactone) Mats

A, Anti-Collagen type I antibodies show that protein is successfully bound to PCL mats after several gentle washing steps. Protein was dissolved in both PBS and Tris buffer to investigate their effect on binding. B, BCA protein assay shows amount of laminin-111 left in solution of pDA PCL mats over time. C, Quantification of IR absorbance signal from (A), normalised to dry mass of each PCL mat. D, Comparison of non-pDA and pDA coated mats without treatment of plasma air (PA) for 24 hrs. Sample size N = 1, n = 3. Error bars shown SEM of repeats.

To directly visualise protein-binding on pDA PCL mats, FITC-labelled laminin fragment was coated on the mats and imaged using confocal imaging and total internal reflection fluorescence (TIRF) microscopy (Figure 12D). The TIRF image indicates individual fragment presence. Cells seeded on mats were also fixed and stained for confocal imaging. A quantification of the fluorescence intensity signal normalised to a PBS only control shows that that fragment is stably bound, and increased concentration of fragment results in an increase in fluorescence intensity (Figure 12A-C)

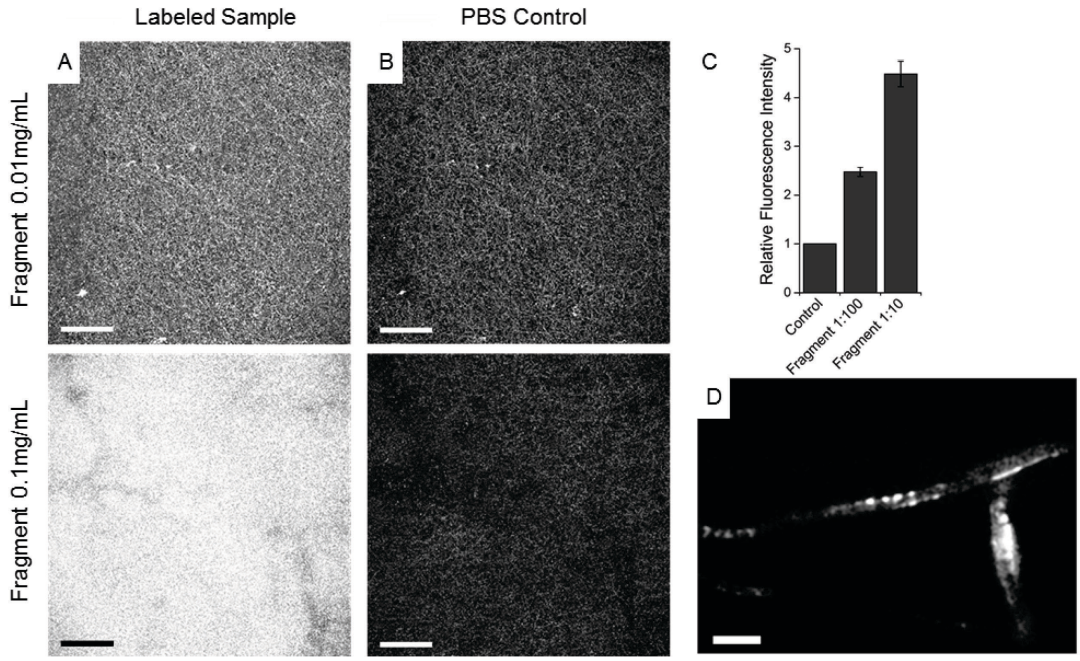
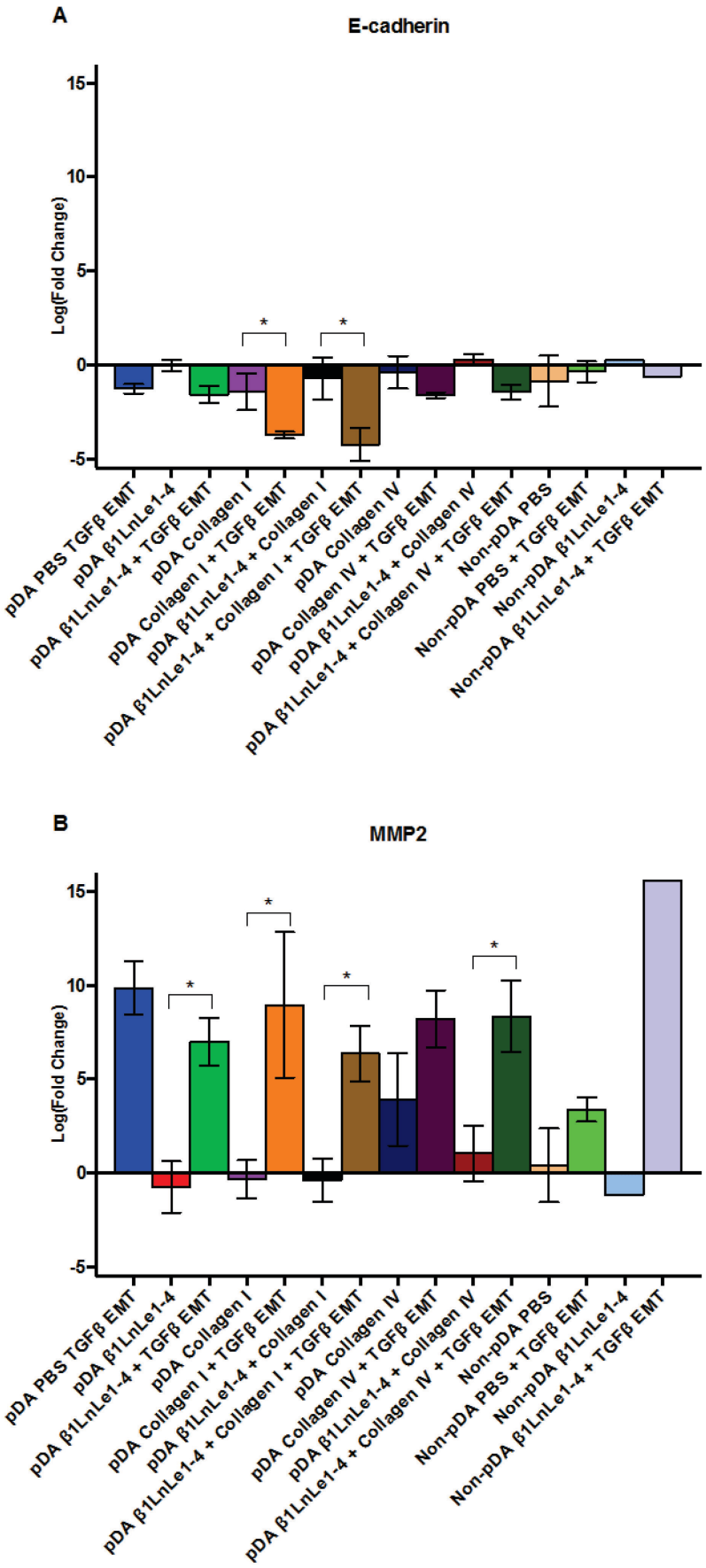
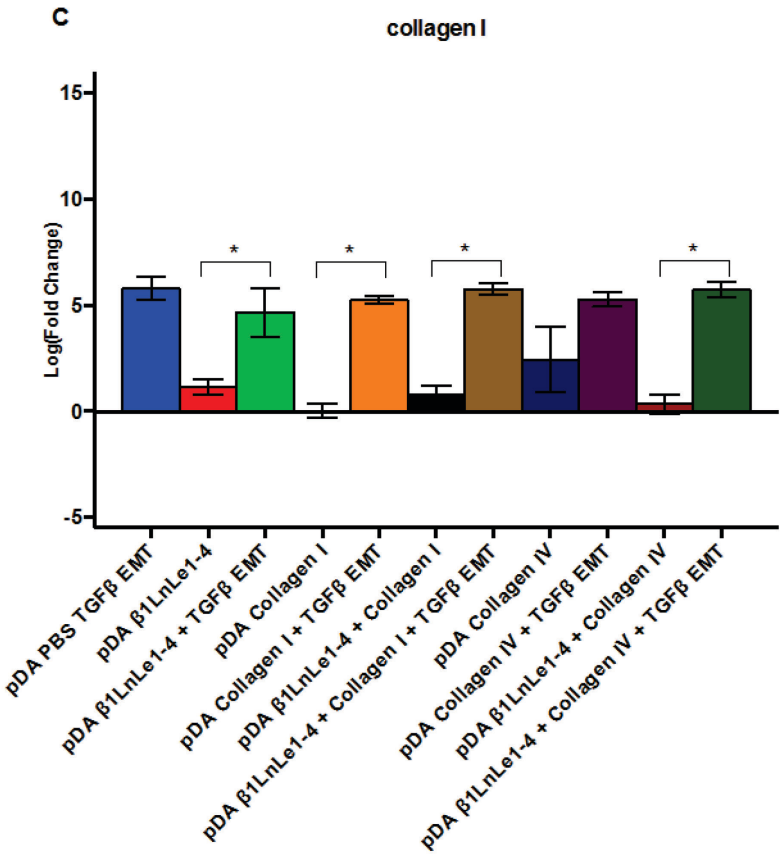


Figure 12 | TIRF and Confocal Images of Labelled pDA PCL Mats
A, Confocal images of PCL mats coated with FITC-labeled β1LnLe1-4 at concentrations of 0.01mg/mL and 0.1mg/mL. B, Control PBS only PCL mats for each experiment. Scale bars = 150μm C, Fluorescence intensity quantification of (A) normalised to (B) samples shows significant intensity signal for labelled laminin fragment. Error bars show SEM, n = 3. D, TIRF image of labelled fragment. Scale bar = 5μm. Images by Thomas von Erlach.

2.2.2 Characterisation of Effect of Biomimetic Material on Epithelial Cells

To see if EMT gene expression is affected by the material, qPCRs were performed to assess NMuMG epithelial cells undergoing TGFβ-induced EMT (Figure 13). Due to the small quantities of cells per sample, the heterogeneity of each condition gave high variation in genetic expression levels. Over the course of several repeats the fold change could vary by several orders of magnitude for the same condition, due to the topology of the PCL mat, the passage number of the cells, and small variations in handling the system. From combined repeats, MMP2, collagen I, and fibronectin expression during EMT with fragment appears to be down-regulated compared to the pDA PBS control, though multiple-hypothesis corrections do not cross $P<0.05$ when EMT conditions across different PCL pDA coatings are compared to the control condition (Figure 13B-D). The fragment itself changes some expression levels even without EMT induction, as expected from its bioactivity. Interestingly, in cells of epithelial phenotype on materials with only Collagen type IV coating, MMP2, Collagen I, and Fibronectin are all up-regulated, indicating bioactivity of Collagen IV on the PCL pDA mats without EMT induction.


A
E-cadherin
Log(Fold Change)
15
10
5
0
-5
*
*
pDA PBS TGFβ EMT
pDA β1LnLe1-4
pDA β1LnLe1-4 + TGFβ EMT
pDA Collagen I
pDA Collagen I + TGFβ EMT
pDA β1LnLe1-4 + Collagen I
pDA β1LnLe1-4 + Collagen I + TGFβ EMT
pDA Collagen IV
pDA Collagen IV + TGFβ EMT
pDA β1LnLe1-4 + Collagen IV
pDA β1LnLe1-4 + Collagen IV + TGFβ EMT
Non-pDA PBS
Non-pDA PBS + TGFβ EMT
Non-pDA β1LnLe1-4
Non-pDA β1LnLe1-4 + TGFβ EMT
B
MMP2
Log(Fold Change)
15
10
5
0
-5
*
*
*
*
pDA PBS TGFβ EMT
pDA β1LnLe1-4
pDA β1LnLe1-4 + TGFβ EMT
pDA Collagen I
pDA Collagen I + TGFβ EMT
pDA β1LnLe1-4 + Collagen I
pDA β1LnLe1-4 + Collagen I + TGFβ EMT
pDA Collagen IV
pDA Collagen IV + TGFβ EMT
pDA β1LnLe1-4 + Collagen IV
pDA β1LnLe1-4 + Collagen IV + TGFβ EMT
Non-pDA PBS
Non-pDA PBS + TGFβ EMT
Non-pDA β1LnLe1-4
Non-pDA β1LnLe1-4 + TGFβ EMT


C
collagen I
Log(Fold Change)
15
10
5
0
-5
*
*
*
*
pDA PBS TGFβ EMT
pDA β1LnLe1-4
pDA β1LnLe1-4 + TGFβ EMT
pDA Collagen I
pDA Collagen I + TGFβ EMT
pDA β1LnLe1-4 + Collagen I
pDA β1LnLe1-4 + Collagen I + TGFβ EMT
pDA Collagen IV
pDA Collagen IV + TGFβ EMT
pDA β1LnLe1-4 + Collagen IV
pDA β1LnLe1-4 + Collagen IV + TGFβ EMT

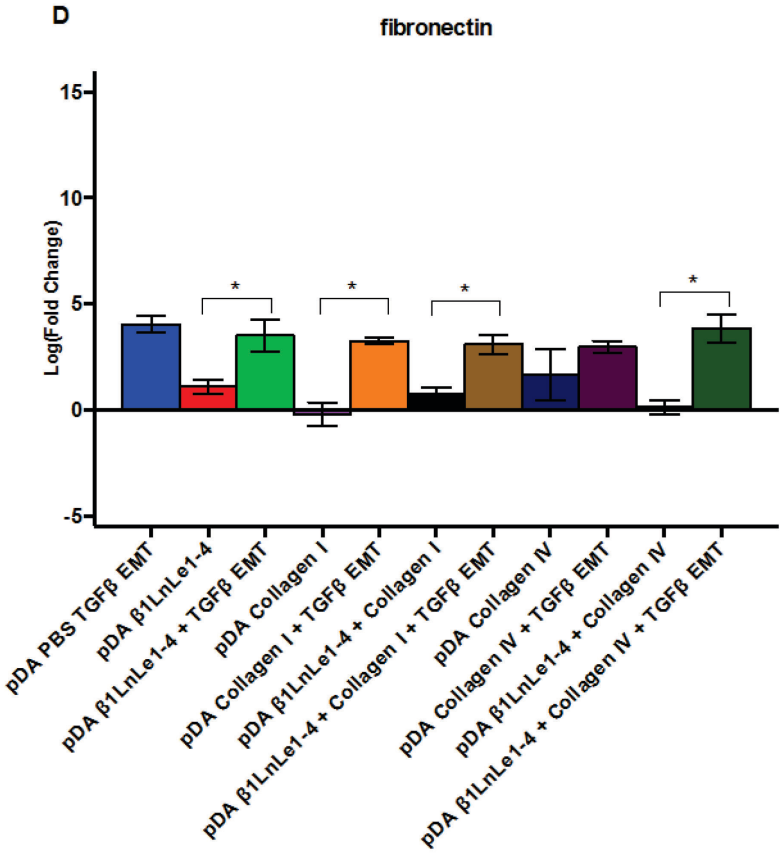

D
fibronectin
Log(Fold Change)
15
10
5
0
-5
*
*
*
*
pDA PBS TGFβ EMT
pDA β1LnLe1-4
pDA β1LnLe1-4 + TGFβ EMT
pDA Collagen I
pDA Collagen I + TGFβ EMT
pDA β1LnLe1-4 + Collagen I
pDA β1LnLe1-4 + Collagen I + TGFβ EMT
pDA Collagen IV
pDA Collagen IV + TGFβ EMT
pDA β1LnLe1-4 + Collagen IV
pDA β1LnLe1-4 + Collagen IV + TGFβ EMT

Figure 13 | qPCR Results of Cells Seeded on Different Materials

EMT-related gene expression levels in terms of fold change relative to control pDA PBS non-EMT NMuMG cells A) E-cadherin, B) MMP2, C) collagen type I, D) fibronectin for cells taken from PCL mats. Each of the bars from left to right shows: 1 (blue): pDA PBS TGFβ EMT; 2 (red): pDA β1LnLe1-4; 3 (green): pDA β1LnLe1-4 + TGFβ EMT; 4 (purple): pDA Collagen I; 5 (orange): pDA Collagen I + TGFβ EMT; 6 (black): pDA β1LnLe1-4 + Collagen I; 7 (brown): pDA β1LnLe1-4 + Collagen I + TGFβ EMT; 8 (dark blue): pDA Collagen IV; 9 (dark purple): pDA Collagen IV + TGFβ EMT; 10 (dark red): pDA β1LnLe1-4 + Collagen IV; 11 (dark green): pDA β1LnLe1-4 + Collagen IV + TGFβ EMT. For E-cadherin and MMP2 the further columns are 12 (light brown): Non-pDA PBS; 13 (light green) Non-pDA PBS + TGFβ EMT; 14 (light blue): Non-pDA β1LnLe1-4; 15 (light purple): Non-pDA β1LnLe1-4 + TGFβ EMT. *P < 0.05 EMT compared to non-EMT of similar treated PCL mat. Error bars show SEM of replicates. For pDA PBS TGFβ EMT, pDA β1LnLe1-4, and pDA β1LnLe1-4 + TGFβ EMT N = 6. For pDA with Collagen type I N = 2. For pDA with Collagen type IV N = 4. For non-pDA PBS and non-pDA PBS + TGFβ EMT N = 2. For all else N = 1.

3. Discussion

3.1 Characterisation of NMuMGs Undergoing EMT Shows Genetic and Morphological Changes

In this project study, a system using cryptic site signalling was designed to control the EMT in the application of fibrosis inhibition. In the first project aim, the goal was to characterise EMT and β1LnLe1-4 protein influence in the NMuMG cell line, with the goal of using this system to study the PCL pDA membrane. TGFβ-induced EMT in NMuMG cells was characterised by biochemical as well as molecular biological techniques, and observed morphological and gene expression changes corresponded strongly to EMT-like events. The morphological changes of EMT were apparent in light microscopy, as elongation and detachment of cells from rigid attachments were seen. In immunofluorescence studies, cytoskeletal differences were observed in actin conformation, along with changes in morphology of fibronectin and collagen I. Unfortunately, there was low immunofluorescent antibody signal for E-cadherin and N-cadherin, though both had signal in western blot analysis. This phenomenon may be due to over-permeabilisation of the cell membranes during the fixing procedure, insufficient concentration of primary or secondary antibodies, rapid photo-bleaching during the experiment, and/or poor antibody specificity. Ultimately with the view of focusing on fibrosis and EMT events, attempting to image the Cadherins by immunofluorescence was not pursued further in this study, but experiments currently ongoing indicate that the staining can be successful (data not shown). In western blot analysis, Fibronectin was seen to be strongly up-regulated, with E-Cadherin and N-Cadherin EMT-switching not as readily apparent, but later elucidated by qPCR. In qPCR studies, there is statistically significant E-cadherin down-regulation and up-regulation of MMP2,

MMP9, fibrogennectin – all corresponding to an EMT phenotype – along with clear up-regulation trends for other genes. The differences between TGFβ1 and TGFβ3 induced EMT were not significantly noticeable, and indeed the two isoforms, though appearing in different stages of development and in different tissues, compete for the same type I and type II receptors with approximately equal affinity, suggesting high similarity in activation strength and phenotype.[62] *In vivo*, it is thought that TGFβ3 has a role in cell migration during wound healing, while TGFβ1 is also secreted by damaged cells during wound healing to contribute to the inflammatory and repair response.[57,63]

The fragment β1LnLe1-4 influence was tested in this initial characterization system and showed many interesting trends. In immunofluorescence studies, Fibronectin and Collagen I appeared qualitatively different with fragment-medium supplemented wells after TGFβ1 EMT compared to control wells, but such a phenomenon could be due to staining artefacts, and it may be difficult to infer whether there was actual up or down-regulation. For qPCR studies of soluble laminin fragment there were potential trends in MMP2, TGFβ1, 2, 3 and EMMPRIN. When fragment was introduced as a soluble factor, it is possible that fragment concentration was too low for significant binding to occur in rapidly dividing NMuMG cells. Over time, as concentration of fragment from solution does not increase, and may possibly decrease due to binding, uptake, and degradation events, the population of cells continued to increase quite rapidly, thus potentially diluting the number of cells that have bound fragment. When fragment was coated onto the bottom of the tissue culture plastic, the increased fragment contact and possible availability of more cell binding sites noticeably altered qPCR mRNA expression. There appeared to be stronger trends towards down-regulation of MMP2, collagen type I, TGFβ3, TGFβ2, and EMMPRIN expression, suggesting that multiple complex EMT pathways including these proteins are involved. The rapidly dividing nature of NMuMG cells with complex EMT dynamics contributed to high variation of fold-change in gene expression across different experiments. This initial characterisation gave insight into how EMT genes are affected both undergoing TGFβ1 or TGFβ3-induced EMT and the influence of β1LnLe1-4 fragment. Trends show similar response to mouse ESCs in monolayer culture (Figure 1D) in effectively down-regulating a variety of EMT genes.[16] In conclusion, NMuMGs are a robust system for studying EMT and it appears that β1LnLe1-4 fragment does down-regulate critical EMT genes, including MMP2, as seen from previous studies with mESCs and hESCs.

3.2 The Biomimetic Material Affects EMT-Related Genes in NMuMGs

In the second project aim, a material system was optimized and characterized for stable protein binding. In the biomimetic material system, the polydopamine coating method of

immobilising functional peptides on pDA PCL was used specifically to engineer an artificial basement membrane that can influence EMT. Protein binding assays and immunostaining show that proteins such as collagen I, laminin-111, and laminin fragment are stably incorporated onto the surface of pDA PCL. While it is observed that there is higher protein binding IR signal in non-pDA coated PCL, it is thought that this increased signal may be an artefact due to interference by the aromatic groups in pDA or due to altered surface properties from the coating. As discussed previously, pDA coating is still desired for stable peptide binding and cell-seeding, especially because it guarantees a homogeneous and tight protein coating, which cannot be achieved on unprocessed PCL fibres.[61] The binding characterisation of fluorescently labelled β1LnLe1-4 by confocal and TIRF imaging shows direct incorporation of the peptide onto the surface, demonstrating that the system can present specific proteins to cells that are cultured on the material.

In the third aim, NMuMG cells were seeded on the material and their EMT behavior with and without β1LnLe1-4 fragment was studied. Experiments for qPCR show high variability on the material due to the sensitivity of cells to the topology of the PCL surface, which can vary across different batches of PCL, as well as the cell-material well chamber system that demands lower cell densities, increasing the presence of heterogenic artefacts (Figure 14). In PCL mats without polydopamine coating there is curiously different behaviour from both control PBS and EMT-induced conditions compared to similar conditions with pDA (Figure 13). One possibility is that non-pDA PCL mats do not stably bind the β1LnLe1-4 protein. Additionally, it is possible that without pDA coating the adhesion properties of NMuMG on these surfaces are considerably different from PCL with pDA coating, which would effect EMT gene expression levels.

The most potentially important result in the qPCR studies, however, is that there is a consistent decrease in MMP2 expression of cells undergoing EMT on the β1LnLe1-4 fragment as soluble factor, coated on TCP, and coated on PCL, pDA, as MMP2 has been implicated as a major factor of fibrosis.[30,64] While large variation and multiple-hypothesis correction leads to non-statistical significance, a more focused study specifically on MMP2, both with regards to gene expression and gene product levels, should clarify the result. There is also a definite trend of down-regulation on PCL pDA materials coated with both the fragment and collagen IV. One possibility is that the collagens may cover the bioactivity of laminin fragment due to steric effects. Notably, Collagen IV itself appears to have bioactivity in influencing EMT, noticeably up-regulating MMP2, collagen I, and fibronectin in non-EMT conditions. As it is a critical part of the basement membrane, Collagen IV's multi-functionality is not surprising. This trend may indicate that collagen IV is providing

biochemical and mechanical cues for NMuMGs on the PCL pDA coated material that may be inducing signalling events that are independent of TGFβ-induced EMT. If this EMT gene up-regulation activity by collagen IV was treated as independent from TGFβ EMT influence on genes, there would be a much stronger level of down-regulation of EMT genes for collagen IV and collagen IV with fragment samples (data not shown). However, it is highly unlikely that the two inputs are independent, and therefore it is uncertain how much influence each factor is contributing. The study of collagen IV and its possible cryptic and bioactive sites remains a fascinating area to be explored.

4. Conclusions

4.1 Further Optimizing the Biomimetic System

In this study, an artificial basement membrane was created *in vitro* that regulates EMT and fibrosis-related genes. Further experiments need to be performed to optimise and characterise the material and cells *in vitro* so that the system can progress to animal model studies of wound healing fibrosis. A wider range of EMT-related genes for cells on pDA PCL – including slug, snail, MMP9 – should be studied using qPCR. Additionally, since many MMPs are secreted as zymogens that require activation, it will be useful to conduct zymography to complement the qPCR results.[24] Zymography samples from cell-seeded PCL have been prepared to study MMP2 activity. The challenge in this characterisation is due to the low populations of cells in each well, which makes activity of MMP2 difficult to detect even after concentrating media proteins.

The stiffness, topology, and protein stability of PCL pDA mats will need to be more carefully characterised in potential animal models. Studies have shown that epithelial cells have varying motility and ability to form epithelial sheets depending on the characteristics of their base substrates.[47,65] It has been shown that matrix elasticity can direct lineage specification, which can be critically important in the EMT and wound healing.[66,67] PCL stiffness should be tuned to the wound-healing application being studied, and other necessary functionalization either from additional peptides or through controlled changes in alignment and density of PCL fibres can be explored.[48] Experiments optimizing the presentation of both collagen IV and laminin fragment may be performed to determine if there is a synergistic effect in down-regulating EMT genes. In the relatively simple coating system for this project, it appears that coating laminin fragment by itself remains the most effective artificial basement membrane system. Further coating studies over longer time periods can determine the stability of

proteins on pDA and establish more quantitative binding kinetics properties for more predictable optimization and preparation of mats. Additional characterisation of protein binding on pDA, zymography of MMP2, and qPCRs for additional EMT genes are currently underway.

4.2 Applications to Fibrotic Disease:

In this *in vitro* study, it was observed that EMT and fibrotic genes were down-regulated in qPCR studies. To investigate the impact of down-regulating critical EMT genes in reducing fibrosis, animal models of fibrotic tissue will need to be studied using a variety of characterisation techniques to probe tissue stiffness, the presence of myofibroblasts, abundance of proteins as collagen I, and levels of pro-fibrotic growth factors.[29,34,68,69] A model fibrotic wound healing system would typically be pulmonary, hepatic, or renal fibrosis pathologies that are found to be perpetuated by the EMT and in which the artificial basement membrane can serve as a bioactive scaffold and signaller.[32,33,70,71] Once the pDA PCL system has been characterised and optimised *in vitro* from the work that is being currently performed, future efforts in making the system medically relevant will require these animal studies. Early characterisations of polydopamine has shown low toxicity and immune response and may even reduce toxicity of other biomaterials.[72,73] Additionally, recent advancements in organ-on-chip systems may provide opportunity in studying fibrotic models with human kidney or liver tissue through control of base material, cell patterning, and nutrient flow.[74] In a recent study, a renal fibrosis EMT model had been built in a microfluidic chip.[75] Unfortunately, due to the relative novelty of such systems, no robust fibrotic models are currently known, so the most likely clinical translation path still lies in *in vivo* animal models.

4.3 Future Directions

The biologically active laminin fragment and other similar down-regulators of EMT have potential applications beyond wound healing, especially in cancer metastasis. In malignant cells, EMT may induce an auto-feedback loop by up-regulation of MMP-9 to cleave latent TGFβ, which would further increase expression and activation of EMT genes for cancer motility and transformation.[76] In murine breast cancer cells EMT induces up-regulated expression of pro-angiogenic factor vascular endothelial growth factor (VEGF) and thus increases tumor angiogenesis and viability.[77] In human hepatocellular carcinoma cells EMT activity has been implicated in angiogenesis and invasiveness, with down-regulation of EMT genes such as MMP2 reducing these tumorigenic events.[78] Preliminary characterisation of β1LnLe1-4 protein effects on human breast cancer cells is underway. Coupling EMT

regulators to artificial basement membrane systems such as pDA PCL will enhance localised delivery and optimal presentation of these signallers to cell receptors, thus potentially increasing the efficacy of the overall treatment. As further understanding of the mechanisms of EMT and its input signals come to light, along with the development of robust biomaterials, the field of biological tissue engineering can begin to deliver local, effective, and patient-specific treatment for a variety of EMT-related pathologies.

5. Materials and Methods

5.1 Cell Culture

5.1.1 Cell Handling

NMuMG cells (ATCC CRL-1636) were maintained in Dulbecco's Modified Eagle Medium (DMEM; Life Technologies) with 10% (v/v) foetal bovine serum (FBS; Life Technologies), 10μg/ml insulin (Sigma), and 100U/mL penicillin-streptomycin (Life Technologies) at 37°C and 5% CO2 grown on tissue culture plastic (TCP). Cells were detached with 0.05% (v/v) 1X trypsin-EDTA (Life Technologies) and passaged at 80% confluency (2-3 days). For cryopreservation, the growth medium is supplemented with 5% (v/v) DMSO (Sigma) and gradually frozen down and stored in liquid nitrogen.

5.1.2 EMT Induction and Fragment Addition

To induce EMT, TGFβ1 (Sigma) or TGFβ3 (Sigma) was added to cells at 80-90% confluency at a concentration of 10ng/ml in cell medium. Fragment not on PCL material was added in two different methods. For soluble fragment, cell medium was complemented with soluble recombinant β1LnLe1-4 at concentration at 10μM in PBS and added at time of initial cell seeding on TCP. For coated fragment, 6-well TCPs were coated with laminin β1LnLe1-4 fragment by incubating with 10μM fragment in PBS for 4 hrs at 37°C.

5.1.3 Recombinant β1LnLe1-4 Fragment Production

Recombinant laminin-111 fragment β1-LnLe1-4 was produced and purified according to previously published methods.[55] The β1-LnLe1-4 sequence was inserted into a pCEP-Pu vector coding with a C-terminal His_6-tag. Transfected human embryonic kidney HEK293 c18 cells (ATCC CRL-1573) were used for protein production and cultured at 37°C and 5% CO2. The culture medium has the composition: Dulbecco's modified Eagle's medium/nutrient mixture F-12 (Invitrogen) containing 10% (v/v) foetal bovine serum (FBS; Life Technologies),

2 mM glutamine, 10 units/ml penicillin, 100 µg/ml streptomycin, and 250 µg/ml Geneticin (all from Gibco). Transfection was performed using FuGENE 6 (Roche Diagnostics) and selected with 1 µg/ml puromycin (Sigma). Transfected cells were grown to confluence in HYPERFlask vessels (Corning), washed with PBS, and incubated with serum-free medium for 3 weeks with weekly medium changes. The laminin- 111 fragment was purified from serum-free conditioned medium by nickel affinity chromatography using 5 ml HisTrap FF columns (GE Healthcare) and an ÄKTA FPLC system (GE Healthcare). The purified protein was concentrated to 1 mg/ml using Amicon ultracentrifugal 10K MWCO units (Fisher Scientific UK), analyzed by SDS-PAGE, and stored at -20°C. All steps were performed by Christine-Maria Horejs.

5.2 qPCR:

5.2.1 Cell Sample Preparation

For standard plate culturing, cells were harvested as described before and lysed in 350µL RLT buffer (Qiagen). For cells on PCL mats, the mat itself was placed into 350µL RLT buffer solution and vigorously vortexed.

5.2.2 RNA Extraction and Purification

RNA was isolated using the RNeasy Mini Kit (Qiagen) according to manufacturer's standard protocol for each sample as follows: 1) Lysate is pipetted into a QIAshredder spin column placed in a 2 mL collection tube and centrifuged for 2 min at full speed. 2) 350µL 70% ethanol is added to the homogenised lysate and mixed will by pipetting. 3) The 700µL sample is transferred to an RNeasy spin column placed in a 2mL collection tube and centrifuged for 15s at 10,000rpm in a centrifuge (Eppendorf Microcentrifuge 5424). 4) The flow-through is discarded and 700µL RW1 buffer is added to the spin column. The column is centrifuged again for 15s at 10,000rpm and the flow-through discarded. 5) 500µL RPE buffer is then added. The column is centrifuged for 15s at 10,000rpm and flow through discarded. 6) The previous step is repeated once again before the RNEasy spin column is placed in a new 2mL collection tube and centrifuged at full speed for 1 min. The RNeasy spin column is then placed in a new collection tube. 7) 30µL RNase-free water is added to the spin column membrane and the column is centrifuged for 1 min at 10,000 rpm to elute the RNA.

5.2.3 Reverse Transcription

Reverse transcription into cDNA was performed using a QuantiTect Reverse Transcription Kit (Qiagen) according to manufacturer's standard protocol for each sample as follows: 1) The concentration of RNA is determined using Nanodrop 2000 (Thermo Scientific) and is then diluted to 40ng/μL. 2) 12μL of RNA and 2μL of gDNA wipeout buffer are mixed in PCR-tubes (Axygen) and incubated for 2 min at 42°C in a thermal cycler, then placed back on ice. 3) The reverse-transcription master mix per sample is prepared with 1μL Quantiscript reverse transcriptase, 4 μL Quantiscript RT buffer, and 1μL RT primer mix. 4) This mixture is added to the RNA in the PCR tube to make a total of 20μL reaction volume. 5) In the thermal cycler, the tube is incubated for 15 min at 42°C and then 3 min at 95°C. 6) For long term storage, this complementary DNA (cDNA) mixture is stored at -20°C.

5.2.4 qPCR of cDNA Samples

QuantiTect SYBR Green PCR Kit (Qiagen) was used according to manufacturer's protocol for each sample as follows: 1) cDNA samples prepared previously were diluted 1:10 in RNase free water. 2) Primers (see next section) at 10μM were mixed to1μL (forward + reverse) and added to 5μL SYBR green. 3) 4μL diluted cDNA and 6μL SYBR mix were mixed together in the final volume. 4) Thermocycling and SYBR green signal detection were both performed on a Corbett Rotorgene 6000 (Qiagen), with extension temperature at 72°C and denaturing temperature at 95°C. The annealing temperatures of all primers were at 55°C. Each sample was run in duplicate and signal was averaged in the analysis.

5.2.5 Primers:

The following primers were used (Invitrogen unless specified):

GAPDH: [Forward (For), 5'-TGGTATCGTGGAAGGACTCATGA-3';
Reverse (Rev), 5'-ATGCCAGTGAGCTTCCCGTTCAG-3']
MMP2: [For, 5′-ATGGCAAGTATGGCTTCTG-3′;
Rev, 5′-GTAGGAGGTGCCCTGGAAG-3′]
MMP9: [For, 5'-TGTACCGCTATGGTTACAC-3';
Rev, 5'-CGGCGACACCAAACTGGAT-3']
E-cadherin: [For, 5′-CGAGAGAGTTACCCTACATA-3′;
Rev, 5′-GTGTTGGGGGCATCATCATC-3′)]
N-cadherin: [For, 5′-AGGGTGGACGTCATTGTAGC-3′;
Rev, 5′-CTGTTGGGGTCTGTCAGGAT-3′]
Slug: [For, 5′-ACATTAGAACTCACACTGGGGA-3′;
Rev, 5′-GCAGAAGCGACATTCTGGAG-3′]
Snail: [For, 5′-CATCCTTGGGGCGTGTAAGT-3′;
Rev, 5′-ATGGCATGGGGGTCTGAAAG-3′]

Collagen Type I: [For, 5'-TAAGGGTCCCCAATGGTGAGA-3';
Rev, 5'-GGGTCCCTCGACTCCTACAT-3']
TGFβ-1: [For, 5'-CCACCTGCAAGACCATCGAC-3';
Rev, 5'-CTGGCGAGCCTTAGTTTGGAC-3']
TGFβ-2: [For, 5'-CTTCGACGTGACAGACGCT-3';
Rev, 5'-GCAGGGGCAGTGTAAACTTATT-3']
TGFβ-3: [For, 5'-GGACTTCGGCCACATCAAGAA-3';
Rev, 5'-TAGGGGACGTGGGTCATCAC-3']
EMMPRIN: [For, 5'-CCTGCATACGAAGTACATAGTGG -3';
Rev, 5'-TGATTTCTTTCGGACCTTGATCC -3']
Integrin α3: [For, 5'-ACTGTGAACGGATGGACATTTC-3';
Rev, 5'-ACAGACCAGGACTCTACCTGC-3']
Integrin β1: [For, 5'-ATGCAAATCTTGCGGAGAAT -3';
Rev, 5'-TTTGCTGCGATTGGTGACATT-3']
Fibronectin 1: [For, 5'-CCCTATCTCTGATACCGTTGTCC-3';
Rev, 5'-TGCCGCAACTACTGTGATTCGG-3']; (qSTAR primers from Origene)

5.2.6 Analysis:

Real-time PCR data was analysed by the comparative Ct method.[79-81] In this method, the fold change is defined as $2^{-\Delta\Delta Ct}$, where $-\Delta\Delta Ct = [(Ct\ gene\ of\ interest - Ct\ internal\ control)\ variable\ sample - (Ct\ gene\ of\ interest - Ct\ internal\ control)\ control\ sample)]$. Ct is defined as the cycle where signal crosses a set threshold (see appendix for thresholds). The normalised control for NMuMG cells was the no fragment no EMT condition. The normalised control for the material system for NMuMG cells was pDA PCL with PBS mats (no protein coating). The internal control gene is GAPDH. Data is shown as Log(fold change) so that down-regulation events are scaled equally to up-regulation events. For statistical significance of differences in expression between one EMT and one non-EMT condition across multiple genes, ANOVA test with Bonferroni correction was used. For significance between a non-EMT condition and multiple EMT conditions for one gene Dunnett's test was used. Tests were performed using GraphPad Prism software.

5.3 Western Blot

Cells were lysed with RIPA buffer with protease inhibitors (Sigma). Cell lysate samples were shaken vigorously and centrifuged at 4°C. The proteins were then separated by SDS-PAGE, transferred onto nitrocellulose membranes, and blocked with blocking buffer – 5% (w/v) milk

powder (Sigma) in TBST (20mM Tris-HCl, 136mM NaCl, 1% (v/v) Tween-20) –for 1 hr. The membranes were incubated in primary antibodies in blocking buffer overnight at 4^{o}C, and exposed to secondary antibodies in blocking buffer for one hr before being imaged and analysed using Odyssey LiCor Software (LiCor).

5.4 Immunostaining

NMuMG cells were fixed in 4% (v/v) paraformaldehyde for 20 min at room temperature. They were then permeabilised in 0.1% (v/v) Triton X-100 for 5 min and blocked with 3% (w/v) BSA solution for 1 hr at room temperature. Samples were incubated in primary antibodies in BSA overnight and in secondary antibodies for 1 hr at room temperature. Confocal images were collected by a Zeiss LSM-510 inverted confocal microscope and processed using Fiji (ImageJ). For all other fluorescence images an Evos FL Cell Imaging System (Life Technologies) was used.

Primary antibodies: anti-GAPDH (1:200) (Santa-Cruz sc32233), anti-E-Cadherin (1:200) (BD 610181), anti-N-Cadherin (1:200) (Santa-Cruz sc59987), anti-Fibronectin (1:500) (Abcam 23750), anti-Collagen I (Abcam 34710), anti-Actin (1:100) (AlexaFluor 488 phalloidin), anti-EMMPRIN (1:500) (ebioscience1601471082 and Abcam 70062).

Secondary antibodies: Alexafluor series (1:1000) (555, 568, 488 goat anti-mouse) and LiCor IRDyes (1:1200) (680 and 800 goat anti-mouse, goat anti-rabbit)

5.5 Polydopamine Coated Poly(ε-caprolactone)

5.5.1 Electrospinning:

Electrospinning of poly(ε-caprolactone) (PCL) membranes was performed according to previously described methods on a custom-made electrospinning setup.[48] PCL with number average M_n molecular weight of 80,000 (Sigma) was dissolved in 1,1,1,3,3,3-hexafluoroisopropanol (HFIP) at a concentration of 12% (w/v). The solution was pushed through an 18-gauge blunt-tip needle at a flow rate of 2ml/hr. A voltage of 16kV was applied to the needle and the fibres formed were collected onto a mandrel situated 11cm from the needle tip and rotating at a speed of 1m/s. This procedure results in randomly aligned fibres that are approximately 1µm in diameter (Figure 2B).

5.5.2 Polydopamine Coating

Eight mm diameter circular mats were cut from the electrospun PCL sheet using a hollow punch (Boehm). The mats were then air plasma-treated using a Plasma Prep 5 (Gala

Instrumente) at 50% power and 0.4mbar for 1 min to render them hydrophilic and ensure uniform pDA coating.[82] Dopamine hydrochloride (Sigma) was dissolved at 2mg/mL in ~20mL of 10mM Tris with pH 8.5.[51] The Tris solution was prepared using Tris-base (Sigma) and titrated with HCl and NaOH using a pH meter. The PCL mats were stirred in the polydopamine solution for 4 hrs in an opened vial. The mats are then washed overnight with distilled water changed approximately four times until no pDA release is observed.

5.5.3 IR Protein Binding Assay

Polydopamine coated PCL disks were prepared as described above, air-dried and weighed. Collagen I solution was prepared by diluting rat tail collagen I (BD) to 100μg/mL in PBS or 10mM pH 8.5 Tris. The disks were incubated in 200μL of collagen type I solution for 24 hrs. Each plate was sealed thoroughly to prevent evaporation. The disks were blocked in 1μg/mL BSA solution, incubated in anti-collagen I antibody (see above) for 2 hrs followed by the secondary antibodies (IR 800) for 1 hr, then imaged and analysed using Odyssey LiCor Software (LiCor). Each sample was run in triplicate and infrared signal quantified and normalised to dry mass.

5.5.4 BCA Protein Assay

Samples of pDA PCL disks were incubated in 200μL of 100μg/mL laminin-111 (Sigma) diluted in PBS for time periods of 5, 15, 30, 60, 120 min, 6 hrs, and 24 hrs in 48-well plates (Corning). A standard concentration curve from 0 to 100μg/mL was also prepared from the laminin-111 (without PCL). BCA protein assay kit (Pierce) was used according to manufacturer's protocol (Pierce) as follows: For each sample 200μL BCA reagent mix – 50 parts BCA reagent A to 1 part BCA reagent B – was added. The samples were incubated at 60^{o}C for 30 minutes and then cooled down and read on a spectrophotometer plate reader. The signal was normalised to non-incubated control wells and the concentration of protein remaining in the well was derived from fitting to the concentration curve.

5.5.5 Protein Coating for Cell-Seeding:

The PCL pDA mats were sterilised by placing them for 30 min in 70% (v/v) EtOH-distilled water solution. All subsequent steps were performed in a cell hood under sterile conditions and reagents. The mats were washed three times with phosphate-buffered saline (PBS; Life Technologies) and put into a 48-well plate (Corning). Laminin fragment in PBS at 9μg/ml was added and the mats were incubated at 37^{o}C for 8 hrs. Subsequently, the mats were washed three times again with PBS. Rat tail collagen type I in acetic acid (BD) or collagen type IV in HCl (BD) diluted to 100 μg/ml or 10 μg/ml respectively in PBS was added to the

appropriate wells and the plate was incubated for 16 hrs, followed by washing the mats three times with PBS.

5.5.6 Preparation of PCL Cell Chambers:

Cell chambers were made from domed 8-cap and tube strips for PCR (Axygen). Using a razor blade, the top dome part of the caps was cut off and the remaining caps were separated from each other. The tubes were cut such that the bottom cone was separated from the top. The top of the tubes and the cut caps can then sandwich a PCL mat, holding it in place, while creating a small chamber for cell media to be put on top. Figure 14 illustrates the configuration. PCL cell chambers (caps and tube tops) were sterilised in 70% (v/v) EtOH and rinsed several times with PBS. Each tube top and cap were put together with a pDA-coated PCL mat in between and placed in a 24-well plate (Corning). The final assembly was rinsed twice with PBS and once with cell medium. All liquid was then aspirated off and 200μL media was dispensed in each well (but not inside the chamber caps) and placed in an incubator in preparation for cell seeding.

5.6 Cell Handling on PCL Mats

5.6.1 Cell Seeding on PCL

Cells were harvested as described previously and counted using a haemocytometer. They were then diluted to the concentration of 12,000 cells / 50μL. 50μL of cell solution was then gently pipetted into each cell chamber on top of the PCL mat. Cells were then allowed to settle for 5 to 10 min, and then 550μL of media was carefully pipetted into each well so that the cell chamber does not leak dry. The plate was then incubated as described previously.

5.6.2 EMT Induction on PCL

All media was carefully aspirated from each well, and 1mL of media complemented with concentration of 10ng/μL TGFβ1 was added into each well. For control samples medium without TGFβ was added.

5.7 Imaging

5.7.1 Light Imaging

Light microscopy images were collected on an IX51 inverted microscope (Olympus)

5.7.2 TIRF and Confocal Imaging Sample Preparation

Cell-seeded pDA PCL mats were fixed in the same manner described previously while still in the cell chambers. After cells were fixed and washed, the mats were taken out of the chambers. The cells were permeabilised in 0.1% (v/v) Triton for 5 min and then blocked for 45 min with 3% (w/v) BSA in PBS. Antibody application and imaging were subsequently performed by Christine-Maria Horejs and Thomas von Erlach. TIRF imaging was performed on a Zeiss Axiovert 200 manual inverted microscope with a 488 laser diode, 100X/1.45W alpha Plan-Fluar objective, and back illuminated EM-CCD camera (Hamamatsu C9100-13). Confocal imaging was performed on a SP5 Leica laser-scanning confocal fluorescence microscope with HC PL APO 10x 0.40 CS air objective.

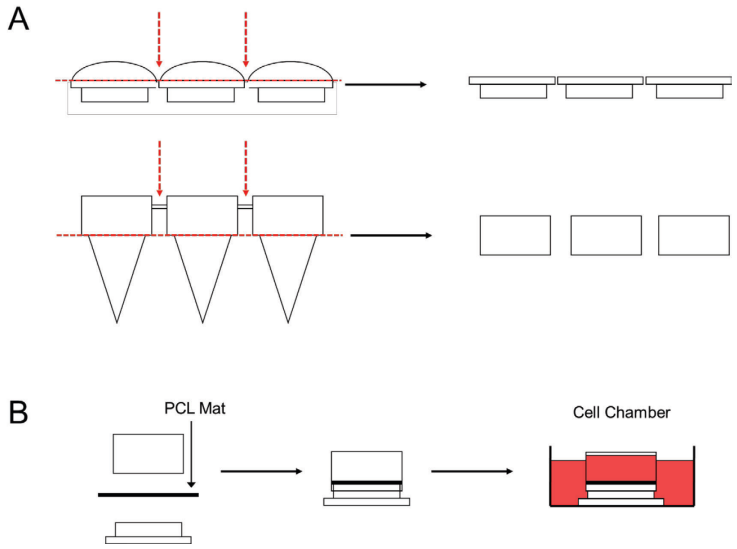


Figure 14 | Construction of Cell Chamber
A, PCR strip-tubes and caps are cut along the red lines to yield the bottom of the caps and the top of the tubes. B, The PCL mat is sandwiched between the tube-top and cap-bottom. The configuration is placed in a 24-well plate to create a cell chamber. The outside of the chamber is filled with media to prevent leakage and drying out of the cells.

6. References

1 Frantz, C., Stewart, K. M. & Weaver, V. M. The extracellular matrix at a glance. *Journal of cell science* **123**, 4195-4200, doi:Doi 10.1242/Jcs.023820 (2010).

2 Shekaran, A. & Garcia, A. J. Extracellular matrix-mimetic adhesive biomaterials for bone repair. *Journal of biomedical materials research. Part A* **96**, 261-272, doi:10.1002/jbm.a.32979 (2011).

3 Schenk, S. & Quaranta, V. Tales from the crypt[ic] sites of the extracellular matrix. *Trends in cell biology* **13**, 366-375 (2003).

4 Giannelli, G., Falk-Marzillier, J., Schiraldi, O., Stetler-Stevenson, W. G. & Quaranta, V. Induction of cell migration by matrix metalloprotease-2 cleavage of laminin-5. *Science* **277**, 225-228 (1997).

5 Davis, G. E., Bayless, K. J., Davis, M. J. & Meininger, G. A. Regulation of tissue injury responses by the exposure of matricryptic sites within extracellular matrix molecules. *The American journal of pathology* **156**, 1489-1498, doi:10.1016/S0002-9440(10)65020-1 (2000).
6 Kalluri, R. Basement membranes: Structure, assembly and role in tumour angiogenesis. *Nat Rev Cancer* **3**, 422-433, doi:Doi 10.1038/Nrc1094 (2003).
7 Colognato, H. & Yurchenco, P. D. Form and function: the laminin family of heterotrimers. *Developmental dynamics : an official publication of the American Association of Anatomists* **218**, 213-234, doi:10.1002/(SICI)1097-0177(200006)218:2<213::AID-DVDY1>3.0.CO;2-R (2000).
8 Hohenester, E. & Yurchenco, P. D. Laminins in basement membrane assembly. *Cell adhesion & migration* **7**, 56-63, doi:10.4161/cam.21831 (2013).
9 Yurchenco, P. D. & Cheng, Y. S. Self-assembly and calcium-binding sites in laminin. A three-arm interaction model. *The Journal of biological chemistry* **268**, 17286-17299 (1993).
10 McKee, K. K., Harrison, D., Capizzi, S. & Yurchenco, P. D. Role of laminin terminal globular domains in basement membrane assembly. *The Journal of biological chemistry* **282**, 21437-21447, doi:10.1074/jbc.M702963200 (2007).
11 Yurchenco, P. D., Sung, U., Ward, M. D., Yamada, Y. & O'Rear, J. J. Recombinant laminin G domain mediates myoblast adhesion and heparin binding. *The Journal of biological chemistry* **268**, 8356-8365 (1993).
12 Yurchenco, P. D., Cheng, Y. S. & Colognato, H. Laminin forms an independent network in basement membranes. *The Journal of cell biology* **117**, 1119-1133 (1992).
13 Li, S., Edgar, D., Fassler, R., Wadsworth, W. & Yurchenco, P. D. The role of laminin in embryonic cell polarization and tissue organization. *Developmental cell* **4**, 613-624 (2003).
14 Ekblom, P., Lonai, P. & Talts, J. F. Expression and biological role of laminin-1. *Matrix biology : journal of the International Society for Matrix Biology* **22**, 35-47 (2003).
15 Miner, J. H. & Yurchenco, P. D. Laminin functions in tissue morphogenesis. *Annu Rev Cell Dev Biol* **20**, 255-284, doi:10.1146/annurev.cellbio.20.010403.094555 (2004).
16 Horejs, C. M., Serio, A., Purvis, A., Gormley, A. J., Bertazzo, S., Poliniewicz, A., Wang, A. J., DiMaggio, P., Hohenester, E. & Stevens, M. M. Biologically-active laminin-111 fragment that modulates the epithelial-to-mesenchymal transition in embryonic stem cells. *Proceedings of the National Academy of Sciences of the United States of America* **111**, 5908-5913, doi:10.1073/pnas.1403139111 (2014).
17 Eastham, A. M., Spencer, H., Soncin, F., Ritson, S., Merry, C. L., Stern, P. L. & Ward, C. M. Epithelial-mesenchymal transition events during human embryonic stem cell differentiation. *Cancer research* **67**, 11254-11262, doi:10.1158/0008-5472.CAN-07-2253 (2007).
18 Thiery, J. P., Acloque, H., Huang, R. Y. & Nieto, M. A. Epithelial-mesenchymal transitions in development and disease. *Cell* **139**, 871-890, doi:10.1016/j.cell.2009.11.007 (2009).
19 Haynes, J., Srivastava, J., Madson, N., Wittmann, T. & Barber, D. L. Dynamic actin remodeling during epithelial-mesenchymal transition depends on increased moesin expression. *Molecular biology of the cell* **22**, 4750-4764, doi:10.1091/mbc.E11-02-0119 (2011).
20 Wheelock, M. J., Shintani, Y., Maeda, M., Fukumoto, Y. & Johnson, K. R. Cadherin switching. *Journal of cell science* **121**, 727-735, doi:10.1242/jcs.000455 (2008).
21 Liu, G., Zhang, X., Lin, H., Wang, H., Li, Q., Ni, J. & Zhu, C. Effects of E-cadherin on mouse embryo implantation and expression of matrix metalloproteinase-2 and -9. *Biochemical and biophysical research communications* **343**, 832-838, doi:10.1016/j.bbrc.2006.02.189 (2006).
22 Lee, J. M., Dedhar, S., Kalluri, R. & Thompson, E. W. The epithelial-mesenchymal transition: new insights in signaling, development, and disease. *The Journal of cell biology* **172**, 973-981, doi:10.1083/jcb.200601018 (2006).
23 Visse, R. & Nagase, H. Matrix metalloproteinases and tissue inhibitors of metalloproteinases: structure, function, and biochemistry. *Circulation research* **92**, 827-839, doi:10.1161/01.RES.0000070112.80711.3D (2003).
24 Sternlicht, M. D. & Werb, Z. How matrix metalloproteinases regulate cell behavior. *Annu Rev Cell Dev Bi* **17**, 463-516, doi:DOI 10.1146/annurev.cellbio.17.1.463 (2001).
25 Coussens, L. M., Fingleton, B. & Matrisian, L. M. Matrix metalloproteinase inhibitors and cancer: trials and tribulations. *Science* **295**, 2387-2392, doi:10.1126/science.1067100 (2002).
26 Wang, Z., Symons, J. M., Goldstein, S. L., McDonald, A., Miner, J. H. & Kreidberg, J. A. (Alpha)3(beta)1 integrin regulates epithelial cytoskeletal organization. *Journal of cell science* **112 (Pt 17)**, 2925-2935 (1999).

27 Kreidberg, J. A. Functions of alpha3beta1 integrin. *Current opinion in cell biology* **12**, 548-553 (2000).
28 Berditchevski, F., Chang, S., Bodorova, J. & Hemler, M. E. Generation of monoclonal antibodies to integrin-associated proteins. Evidence that alpha3beta1 complexes with EMMPRIN/basigin/OX47/M6. *The Journal of biological chemistry* **272**, 29174-29180 (1997).
29 Wynn, T. A. & Ramalingam, T. R. Mechanisms of fibrosis: therapeutic translation for fibrotic disease. *Nature medicine* **18**, 1028-1040, doi:10.1038/nm.2807 (2012).
30 Hemmann, S., Graf, J., Roderfeld, M. & Roeb, E. Expression of MMPs and TIMPs in liver fibrosis - a systematic review with special emphasis on anti-fibrotic strategies. *Journal of hepatology* **46**, 955-975, doi:10.1016/j.jhep.2007.02.003 (2007).
31 Iwano, M., Plieth, D., Danoff, T. M., Xue, C., Okada, H. & Neilson, E. G. Evidence that fibroblasts derive from epithelium during tissue fibrosis. *The Journal of clinical investigation* **110**, 341-350, doi:10.1172/JCI15518 (2002).
32 Zeisberg, E. M., Tarnavski, O., Zeisberg, M., Dorfman, A. L., McMullen, J. R., Gustafsson, E., Chandraker, A., Yuan, X., Pu, W. T., Roberts, A. B., Neilson, E. G., Sayegh, M. H., Izumo, S. & Kalluri, R. Endothelial-to-mesenchymal transition contributes to cardiac fibrosis. *Nature medicine* **13**, 952-961, doi:10.1038/nm1613 (2007).
33 Zeisberg, M., Yang, C., Martino, M., Duncan, M. B., Rieder, F., Tanjore, H. & Kalluri, R. Fibroblasts derive from hepatocytes in liver fibrosis via epithelial to mesenchymal transition. *The Journal of biological chemistry* **282**, 23337-23347, doi:10.1074/jbc.M700194200 (2007).
34 Lee, K. & Nelson, C. M. New insights into the regulation of epithelial-mesenchymal transition and tissue fibrosis. *International review of cell and molecular biology* **294**, 171-221, doi:10.1016/B978-0-12-394305-7.00004-5 (2012).
35 Zhou, X., Hovell, C. J., Pawley, S., Hutchings, M. I., Arthur, M. J., Iredale, J. P. & Benyon, R. C. Expression of matrix metalloproteinase-2 and -14 persists during early resolution of experimental liver fibrosis and might contribute to fibrolysis. *Liver international : official journal of the International Association for the Study of the Liver* **24**, 492-501, doi:10.1111/j.1478-3231.2004.0946.x (2004).
36 Huang, Y. H., Shi, M. N., Zheng, W. D., Zhang, L. J., Chen, Z. X. & Wang, X. Z. Therapeutic effect of interleukin-10 on CCl4-induced hepatic fibrosis in rats. *World journal of gastroenterology : WJG* **12**, 1386-1391 (2006).
37 Takahara, T., Sugiyama, K., Zhang, L. P., Ando, O., Fujii, M., Yata, Y., Bo, J., Xue, F., Minemura, M. & Watanabe, A. Cotreatment with interferon-alpha and -gamma reduces liver fibrosis in a rat model. *Hepatology research : the official journal of the Japan Society of Hepatology* **28**, 146-154, doi:10.1016/j.hepres.2003.11.003 (2004).
38 Castro, M. M. & Tanus-Santos, J. E. Inhibition of Matrix Metalloproteinases (MMPs) as a Potential Strategy to Ameliorate Hypertension-Induced Cardiovascular Alterations. *Curr Drug Targets* **14**, 335-343 (2013).
39 Turk, B. Targeting proteases: successes, failures and future prospects. *Nature reviews. Drug discovery* **5**, 785-799, doi:10.1038/nrd2092 (2006).
40 Aref, A. R., Huang, R. Y., Yu, W., Chua, K. N., Sun, W., Tu, T. Y., Bai, J., Sim, W. J., Zervantonakis, I. K., Thiery, J. P. & Kamm, R. D. Screening therapeutic EMT blocking agents in a three-dimensional microenvironment. *Integrative biology : quantitative biosciences from nano to macro* **5**, 381-389, doi:10.1039/c2ib20209c (2013).
41 Purcell, B. P., Lobb, D., Charati, M. B., Dorsey, S. M., Wade, R. J., Zellars, K. N., Doviak, H., Pettaway, S., Logdon, C. B., Shuman, J. A., Freels, P. D., Gorman, J. H., 3rd, Gorman, R. C., Spinale, F. G. & Burdick, J. A. Injectable and bioresponsive hydrogels for on-demand matrix metalloproteinase inhibition. *Nature materials* **13**, 653-661, doi:10.1038/nmat3922 (2014).
42 Place, E. S., Evans, N. D. & Stevens, M. M. Complexity in biomaterials for tissue engineering. *Nature materials* **8**, 457-470, doi:10.1038/nmat2441 (2009).
43 Rahmany, M. B. & Van Dyke, M. Biomimetic approaches to modulate cellular adhesion in biomaterials: A review. *Acta Biomater* **9**, 5431-5437, doi:DOI 10.1016/j.actbio.2012.11.019 (2013).
44 Pashuck, E. T. & Stevens, M. M. Designing Regenerative Biomaterial Therapies for the Clinic. *Sci Transl Med* **4**, doi:ARTN 160sr4, DOI 10.1126/scitranslmed.3002717 (2012).
45 Gill, B. J., Gibbons, D. L., Roudsari, L. C., Saik, J. E., Rizvi, Z. H., Roybal, J. D., Kurie, J. M. & West, J. L. A synthetic matrix with independently tunable biochemistry and mechanical properties to study epithelial morphogenesis and EMT in a lung adenocarcinoma model. *Cancer research* **72**, 6013-6023, doi:10.1158/0008-5472.CAN-12-0895 (2012).

46 Sewell-Loftin, M. K., Chun, Y. W., Khademhosseini, A. & Merryman, W. D. EMT-inducing biomaterials for heart valve engineering: taking cues from developmental biology. *Journal of cardiovascular translational research* **4**, 658-671, doi:10.1007/s12265-011-9300-4 (2011).
47 Beckstead, B. L., Pan, S., Bhrany, A. D., Bratt-Leal, A. M., Ratner, B. D. & Giachelli, C. M. Esophageal epithelial cell interaction with synthetic and natural scaffolds for tissue engineering. *Biomaterials* **26**, 6217-6228, doi:10.1016/j.biomaterials.2005.04.010 (2005).
48 McCullen, S. D., Autefage, H., Callanan, A., Gentleman, E. & Stevens, M. M. Anisotropic fibrous scaffolds for articular cartilage regeneration. *Tissue engineering. Part A* **18**, 2073-2083, doi:10.1089/ten.TEA.2011.0606 (2012).
49 Lee, H., Dellatore, S. M., Miller, W. M. & Messersmith, P. B. Mussel-inspired surface chemistry for multifunctional coatings. *Science* **318**, 426-430, doi:10.1126/science.1147241 (2007).
50 Lee, H., Scherer, N. F. & Messersmith, P. B. Single-molecule mechanics of mussel adhesion. *Proceedings of the National Academy of Sciences of the United States of America* **103**, 12999-13003, doi:10.1073/pnas.0605552103 (2006).
51 Ko, E., Yang, K., Shin, J. & Cho, S. W. Polydopamine-assisted osteoinductive peptide immobilization of polymer scaffolds for enhanced bone regeneration by human adipose-derived stem cells. *Biomacromolecules* **14**, 3202-3213, doi:10.1021/bm4008343 (2013).
52 Shin, Y. M., Lee, Y. B., Kim, S. J., Kang, J. K., Park, J. C., Jang, W. & Shin, H. Mussel-Inspired Immobilization of Vascular Endothelial Growth Factor (VEGF) for Enhanced Endothelialization of Vascular Grafts. *Biomacromolecules* **13**, 2020-2028, doi:DOI 10.1021/bm300194b (2012).
53 Ku, S. H., Ryu, J., Hong, S. K., Lee, H. & Park, C. B. General functionalization route for cell adhesion on non-wetting surfaces. *Biomaterials* **31**, 2535-2541, doi:10.1016/j.biomaterials.2009.12.020 (2010).
54 Ku, S. H. & Park, C. B. Human endothelial cell growth on mussel-inspired nanofiber scaffold for vascular tissue engineering. *Biomaterials* **31**, 9431-9437, doi:10.1016/j.biomaterials.2010.08.071 (2010).
55 Purvis, A. & Hohenester, E. Laminin network formation studied by reconstitution of ternary nodes in solution. *The Journal of biological chemistry* **287**, 44270-44277, doi:10.1074/jbc.M112.418426 (2012).
56 Miettinen, P. J., Ebner, R., Lopez, A. R. & Derynck, R. TGF-beta induced transdifferentiation of mammary epithelial cells to mesenchymal cells: involvement of type I receptors. *The Journal of cell biology* **127**, 2021-2036 (1994).
57 Lopez-Novoa, J. M. & Nieto, M. A. Inflammation and EMT: an alliance towards organ fibrosis and cancer progression. *EMBO molecular medicine* **1**, 303-314, doi:10.1002/emmm.200900043 (2009).
58 Lamouille, S. & Derynck, R. Cell size and invasion in TGF-beta-induced epithelial to mesenchymal transition is regulated by activation of the mTOR pathway. *The Journal of cell biology* **178**, 437-451, doi:10.1083/jcb.200611146 (2007).
59 Shirakihara, T., Saitoh, M. & Miyazono, K. Differential regulation of epithelial and mesenchymal markers by deltaEF1 proteins in epithelial mesenchymal transition induced by TGF-beta. *Molecular biology of the cell* **18**, 3533-3544, doi:10.1091/mbc.E07-03-0249 (2007).
60 Bhowmick, N. A., Ghiassi, M., Bakin, A., Aakre, M., Lundquist, C. A., Engel, M. E., Arteaga, C. L. & Moses, H. L. Transforming growth factor-beta1 mediates epithelial to mesenchymal transdifferentiation through a RhoA-dependent mechanism. *Molecular biology of the cell* **12**, 27-36 (2001).
61 Nielsen, S. R., Besenbacher, F. & Chen, M. Mussel inspired surface functionalization of electrospun nanofibers for bio-applications. *Phys Chem Chem Phys* **15**, 17029-17037, doi:10.1039/c3cp52651h (2013).
62 Lyons, R. M., Miller, D. A., Graycar, J. L., Moses, H. L. & Derynck, R. Differential binding of transforming growth factor-beta 1, -beta 2, and -beta 3 by fibroblasts and epithelial cells measured by affinity cross-linking of cell surface receptors. *Molecular endocrinology* **5**, 1887-1896, doi:10.1210/mend-5-12-1887 (1991).
63 Bandyopadhyay, B., Fan, J., Guan, S., Li, Y., Chen, M., Woodley, D. T. & Li, W. A "traffic control" role for TGFbeta3: orchestrating dermal and epidermal cell motility during wound healing. *The Journal of cell biology* **172**, 1093-1105, doi:10.1083/jcb.200507111 (2006).
64 Corbel, M., Belleguic, C., Boichot, E. & Lagente, V. Involvement of gelatinases (MMP-2 and MMP-9) in the development of airway inflammation and pulmonary fibrosis. *Cell Biol Toxicol* **18**, 51-61 (2002).

65 Wu, T. H., Li, C. H., Tang, M. J., Liang, J. I., Chen, C. H. & Yeh, M. L. Migration speed and directionality switch of normal epithelial cells after TGF-beta1-induced EMT (tEMT) on micro-structured polydimethylsiloxane (PDMS) substrates with variations in stiffness and topographic patterning. *Cell communication & adhesion* **20**, 115-126, doi:10.3109/15419061.2013.833194 (2013).
66 Engler, A. J., Sen, S., Sweeney, H. L. & Discher, D. E. Matrix elasticity directs stem cell lineage specification. *Cell* **126**, 677-689, doi:10.1016/j.cell.2006.06.044 (2006).
67 Cox, T. R. & Erler, J. T. Remodeling and homeostasis of the extracellular matrix: implications for fibrotic diseases and cancer. *Disease models & mechanisms* **4**, 165-178, doi:10.1242/dmm.004077 (2011).
68 Willis, B. C. & Borok, Z. TGF-beta-induced EMT: mechanisms and implications for fibrotic lung disease. *American journal of physiology. Lung cellular and molecular physiology* **293**, L525-534, doi:10.1152/ajplung.00163.2007 (2007).
69 Wynn, T. A. Integrating mechanisms of pulmonary fibrosis. *The Journal of experimental medicine* **208**, 1339-1350, doi:10.1084/jem.20110551 (2011).
70 Carew, R. M., Wang, B. & Kantharidis, P. The role of EMT in renal fibrosis. *Cell and tissue research* **347**, 103-116, doi:10.1007/s00441-011-1227-1 (2012).
71 Griffith, L. G., Wells, A. & Stolz, D. B. Engineering liver. *Hepatology* **60**, 1426-1434, doi:10.1002/hep.27150 (2014).
72 Hong, S., Kim, K. Y., Wook, H. J., Park, S. Y., Lee, K. D., Lee, D. Y. & Lee, H. Attenuation of the in vivo toxicity of biomaterials by polydopamine surface modification. *Nanomedicine* **6**, 793-801, doi:10.2217/nnm.11.76 (2011).
73 Liu, X., Cao, J., Li, H., Li, J., Jin, Q., Ren, K. & Ji, J. Mussel-inspired polydopamine: a biocompatible and ultrastable coating for nanoparticles in vivo. *ACS nano* **7**, 9384-9395, doi:10.1021/nn404117j (2013).
74 Bhatia, S. N. & Ingber, D. E. Microfluidic organs-on-chips. *Nature biotechnology* **32**, 760-772, doi:10.1038/nbt.2989 (2014).
75 Zhou, M., Ma, H., Lin, H. & Qin, J. Induction of epithelial-to-mesenchymal transition in proximal tubular epithelial cells on microfluidic devices. *Biomaterials* **35**, 1390-1401, doi:10.1016/j.biomaterials.2013.10.070 (2014).
76 Yu, Q. & Stamenkovic, I. Cell surface-localized matrix metalloproteinase-9 proteolytically activates TGF-beta and promotes tumor invasion and angiogenesis. *Genes & development* **14**, 163-176 (2000).
77 Fantozzi, A., Gruber, D. C., Pisarsky, L., Heck, C., Kunita, A., Yilmaz, M., Meyer-Schaller, N., Cornille, K., Hopfer, U., Bentires-Alj, M. & Christofori, G. VEGF-mediated angiogenesis links EMT-induced cancer stemness to tumor initiation. *Cancer research* **74**, 1566-1575, doi:10.1158/0008-5472.CAN-13-1641 (2014).
78 Xiao, H., Cheng, S., Tong, R., Lv, Z., Ding, C., Du, C., Xie, H., Zhou, L., Wu, J. & Zheng, S. BAG3 regulates epithelial-mesenchymal transition and angiogenesis in human hepatocellular carcinoma. *Laboratory investigation; a journal of technical methods and pathology* **94**, 252-261, doi:10.1038/labinvest.2013.151 (2014).
79 Pfaffl, M. W. A new mathematical model for relative quantification in real-time RT-PCR. *Nucleic acids research* **29**, e45 (2001).
80 Livak, K. J. & Schmittgen, T. D. Analysis of relative gene expression data using real-time quantitative PCR and the 2(-Delta Delta C(T)) Method. *Methods* **25**, 402-408, doi:10.1006/meth.2001.1262 (2001).
81 Schmittgen, T. D. & Livak, K. J. Analyzing real-time PCR data by the comparative C(T) method. *Nature protocols* **3**, 1101-1108 (2008).
82 Jacobs, T., De Geyter, N., Morent, R., Desmet, T., Dubruel, P. & Leys, C. Plasma treatment of polycaprolactone at medium pressure. *Surf Coat Tech* **205**, S543-S547, doi:DOI 10.1016/j.surfcoat.2011.02.012 (2011).

7. **Appendix**

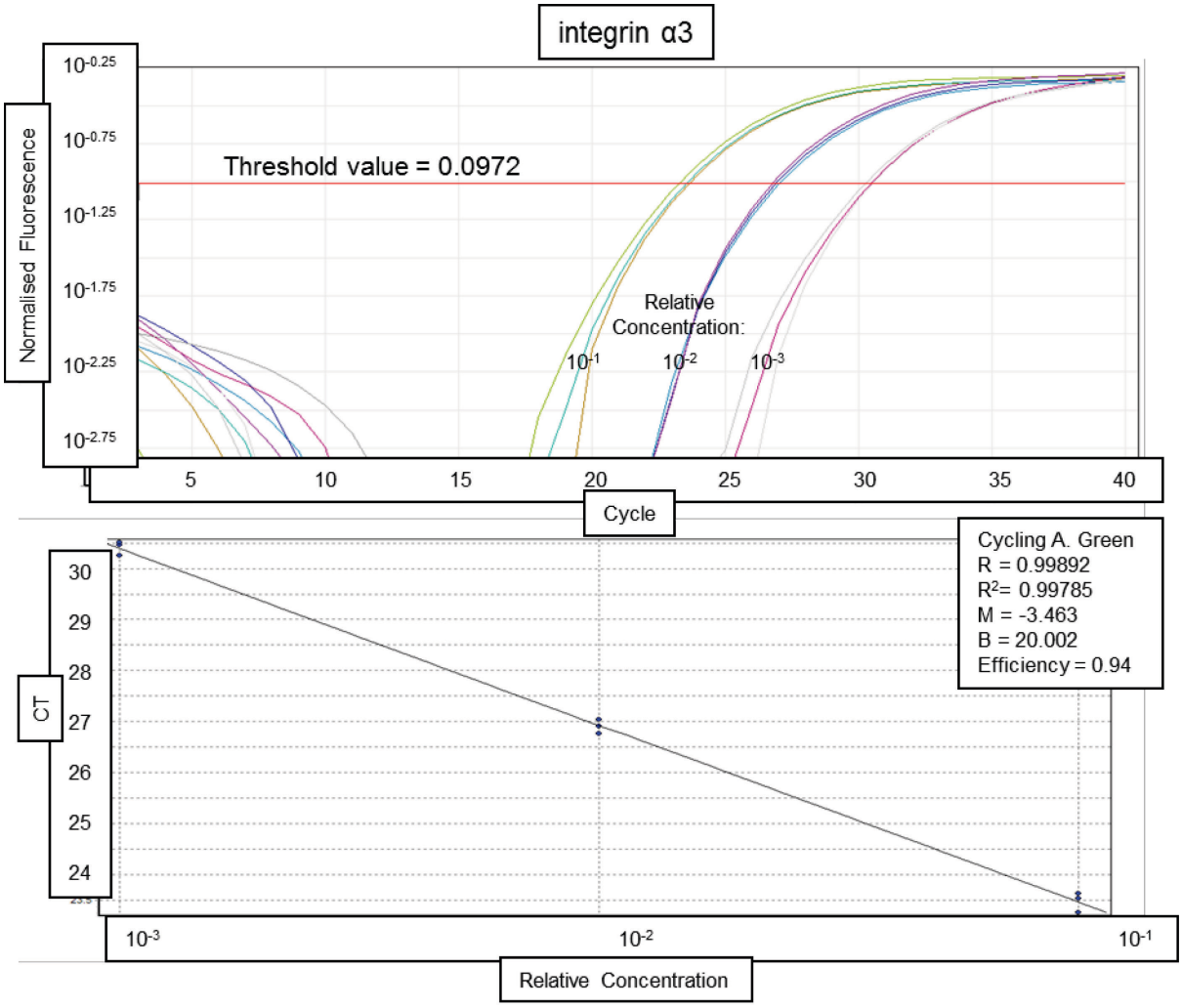
7.1 List of Abbreviations

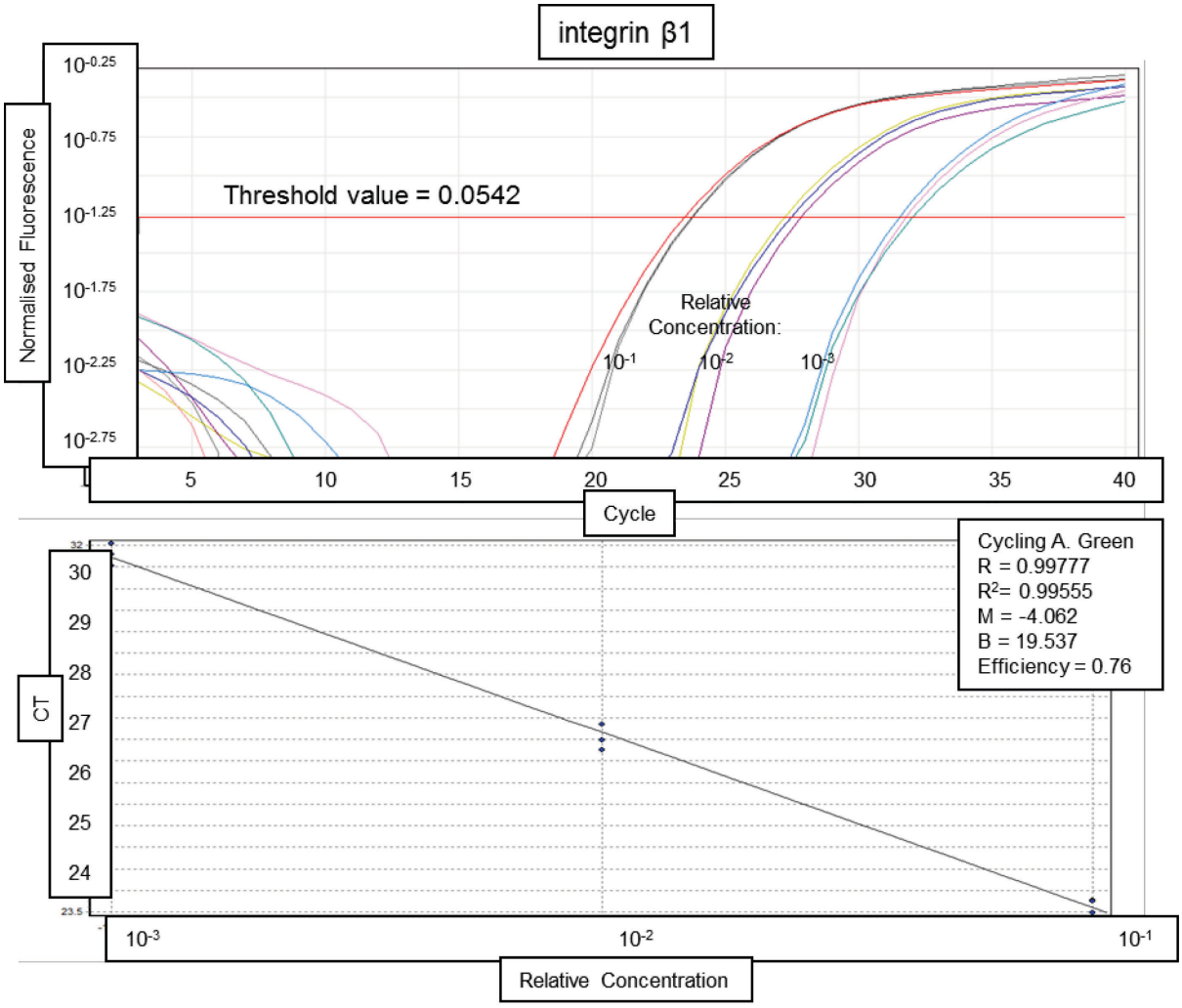
Acronym	**Meaning**
BM	Basement Membrane
cDNA	Complementary Deoxyribonucleic Acid
DMEM	Dulbecco's Modified Eagle Medium
ECM	Extracellular Matrix
EMMPRIN	Extracellular Matrix Metalloproteinase Inducer
EMT	Epithelial-to-Mesenchymal Transition
EndoMT	Endothelial-to-Mesenchymal Transition
ESC	Embryonic Stem Cell
FBS	Foetal Bovine Serum
HFIP	1,1,1,3,3,3-Hexafluoroisopropanol
IR	Infrared
LC-MS	Liquid Chromatography Tandem Mass Spectrometry
LE	Laminin-type Epidermal Growth Factor-like
LG	Laminin Globular
LN	Laminin N-terminal
MMP	Matrix Metalloproteinase
MMS	Molecular Mass Standard
NMuMG	*Mus Musculus* Mammary Gland Epithelial Cells
PA	Plasma Air
PCL	Poly(ε-caprolactone)
pDA	Polydopamine
qPCR	Quantitative Polymerase Chain Reaction

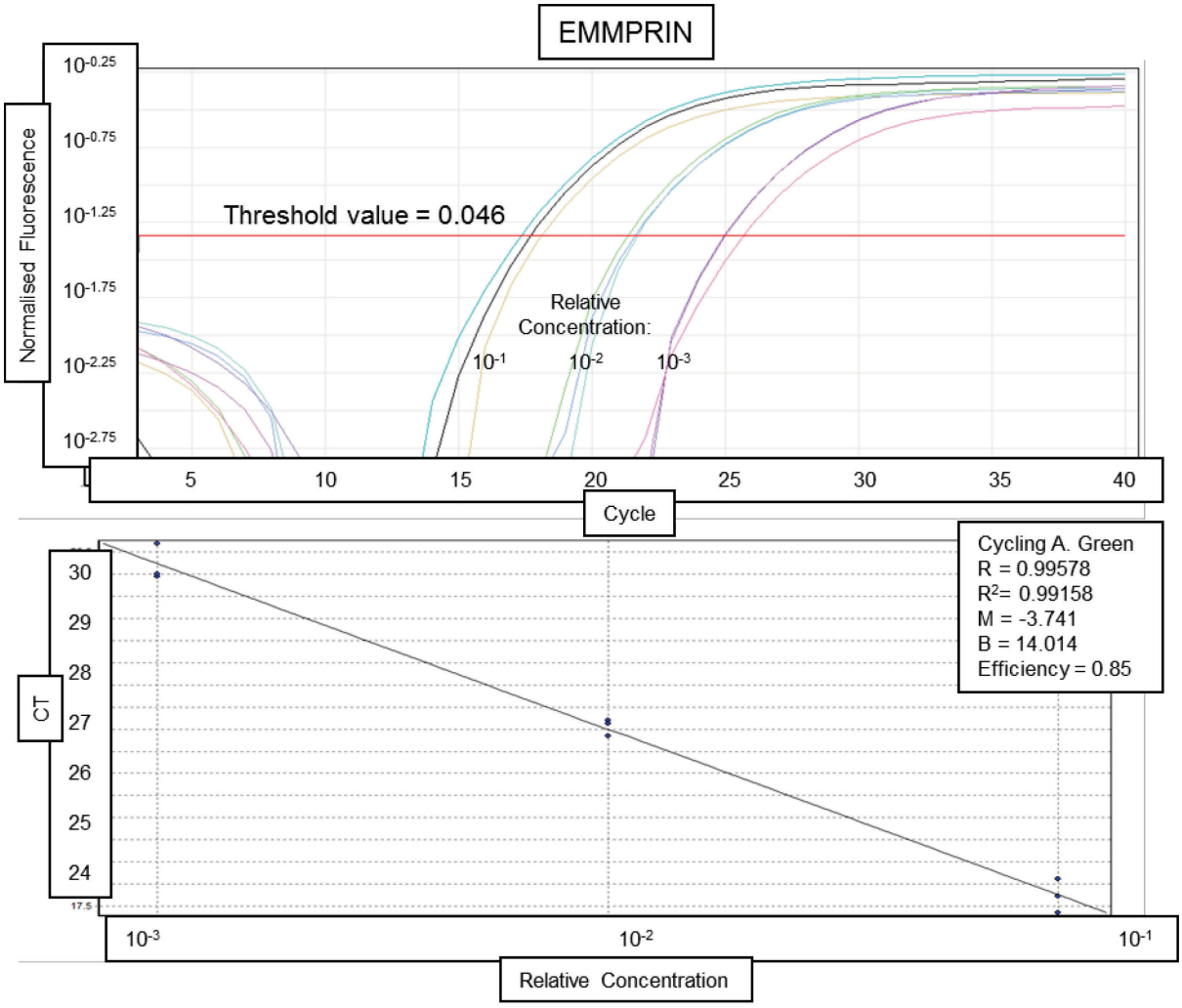
SEM	Scanning Electron Microscope/ Standard Error of Mean
TCP	Tissue Culture Plastic
TGFβ	Transforming Growth Factor β
TIRF	Total Internal Reflection Fluorescence
VEGF	Vascular Endothelial Growth Factor

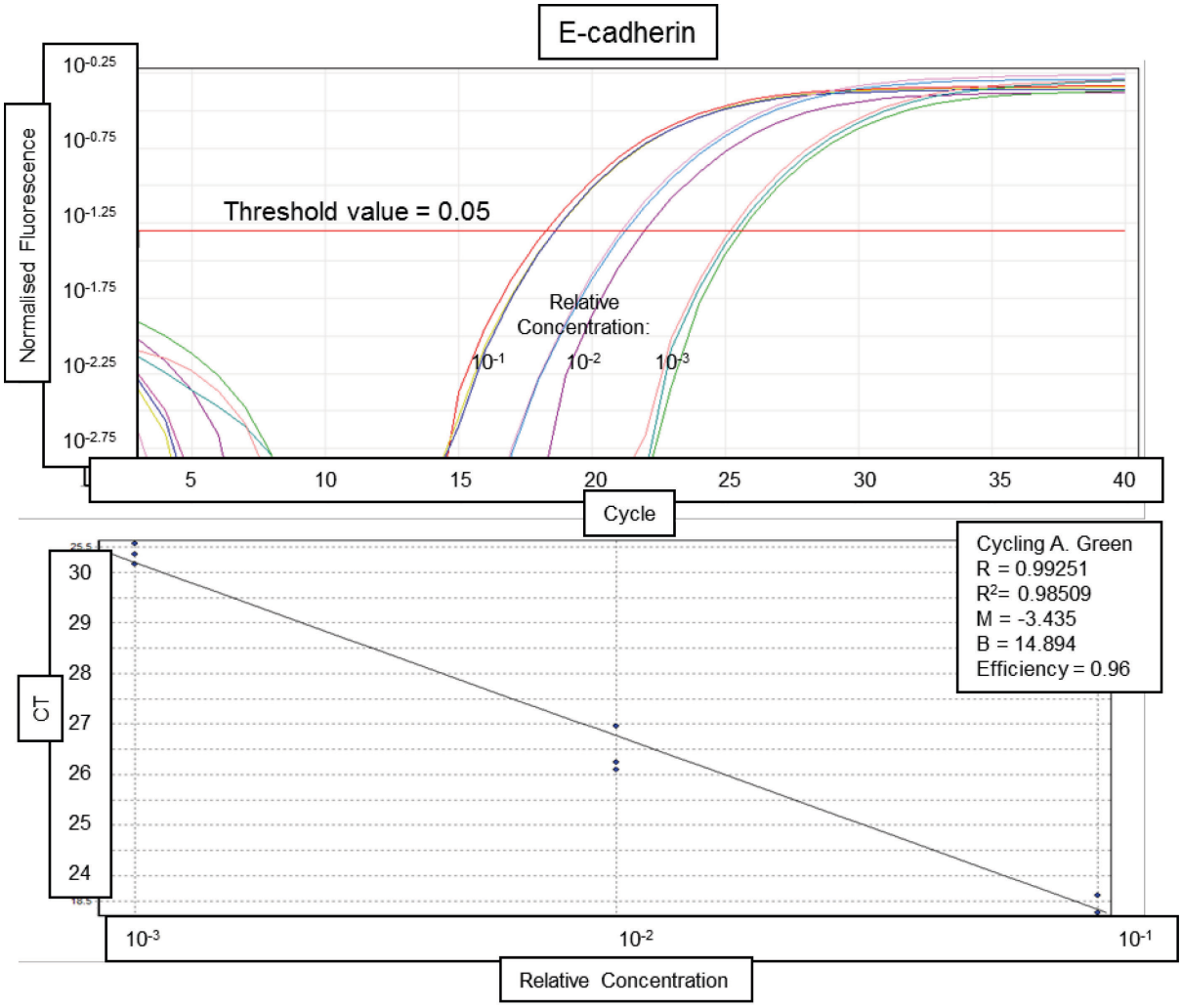
7.2 RT-PCR primer threshold validations

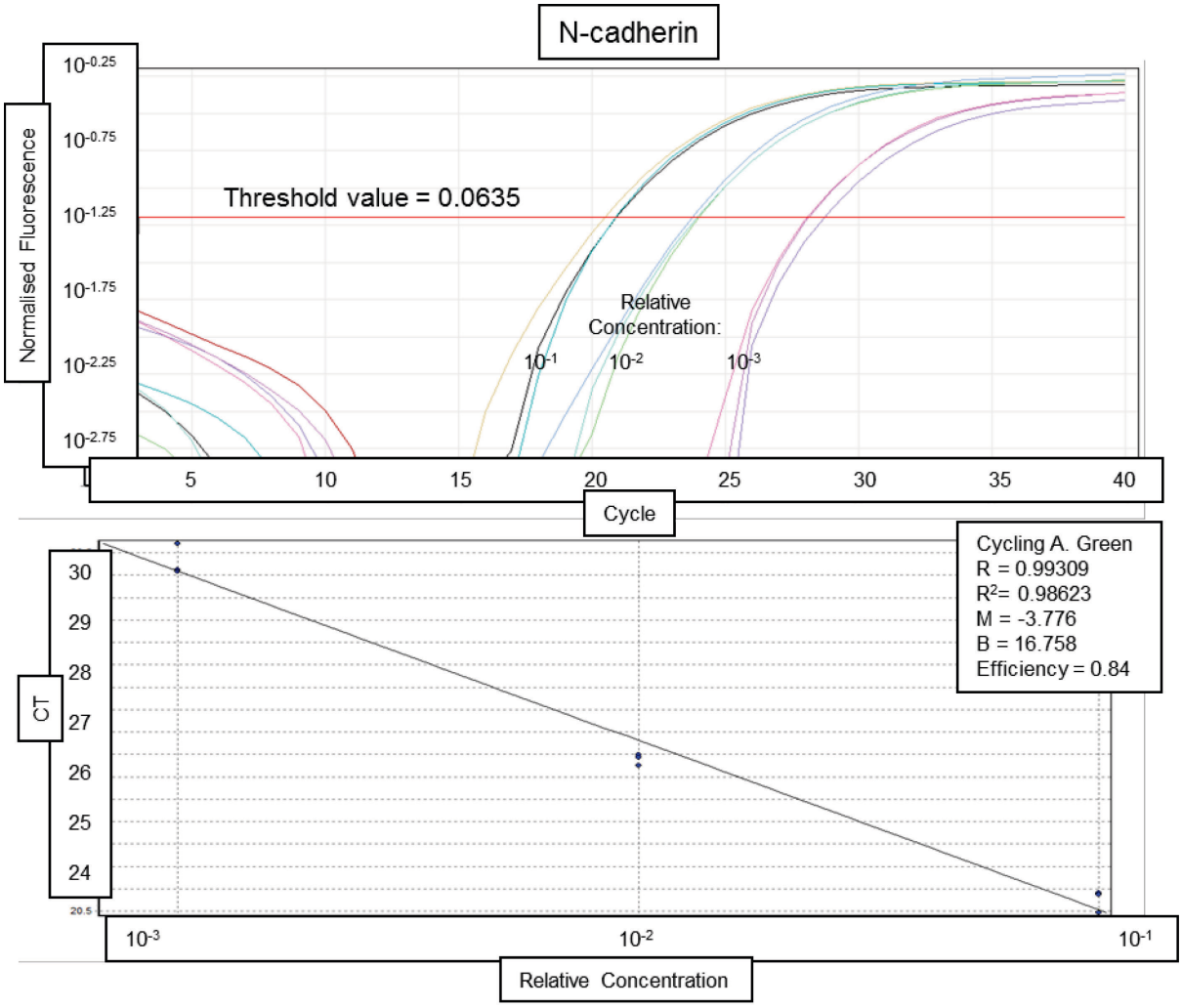
For threshold calculations, primers were added to cDNA of NMuMG non-EMT samples diluted 1:10, 1:100, 1:1000, and fluorescence was measured according to the qPCR procedure described previously. Threshold value was determined as the normalised fluorescence that gives threshold cycle (CT) values resulting in a linear curve that maximizes fit for the dilutions in log-space. Each dilution has n = 3, with curves that are closely clustered together.

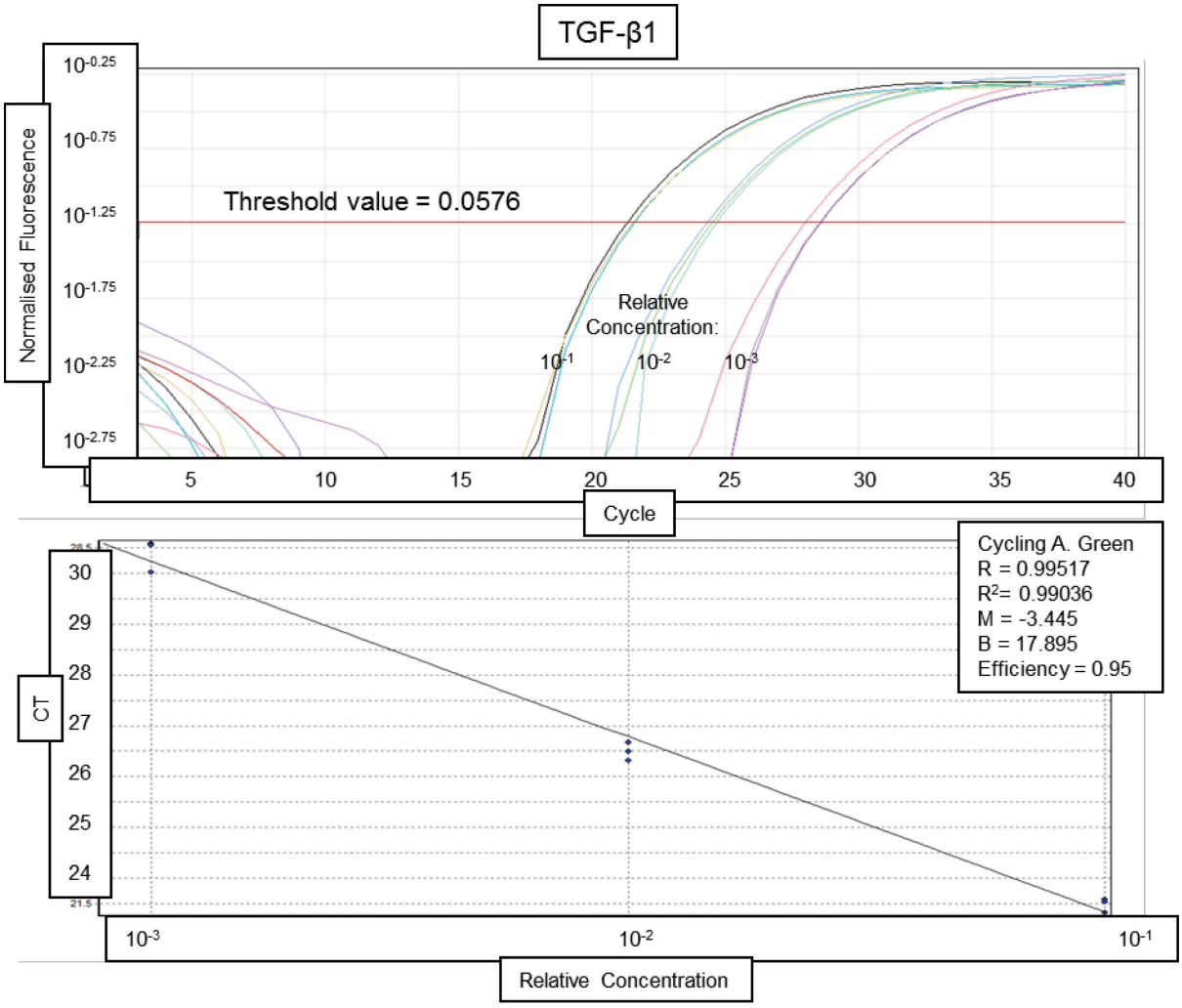

integrin α3
Normalised Fluorescence
10-0.25
10-0.75
10-1.25
10-1.75
10-2.25
10-2.75
Threshold value = 0.0972
Relative Concentration:
10-1
10-2
10-3
5
10
15
20
25
30
35
40
Cycle
CT
30
29
28
27
26
25
24
Cycling A. Green
R = 0.99892
R2= 0.99785
M = -3.463
B = 20.002
Efficiency = 0.94
10-3
10-2
10-1
Relative Concentration

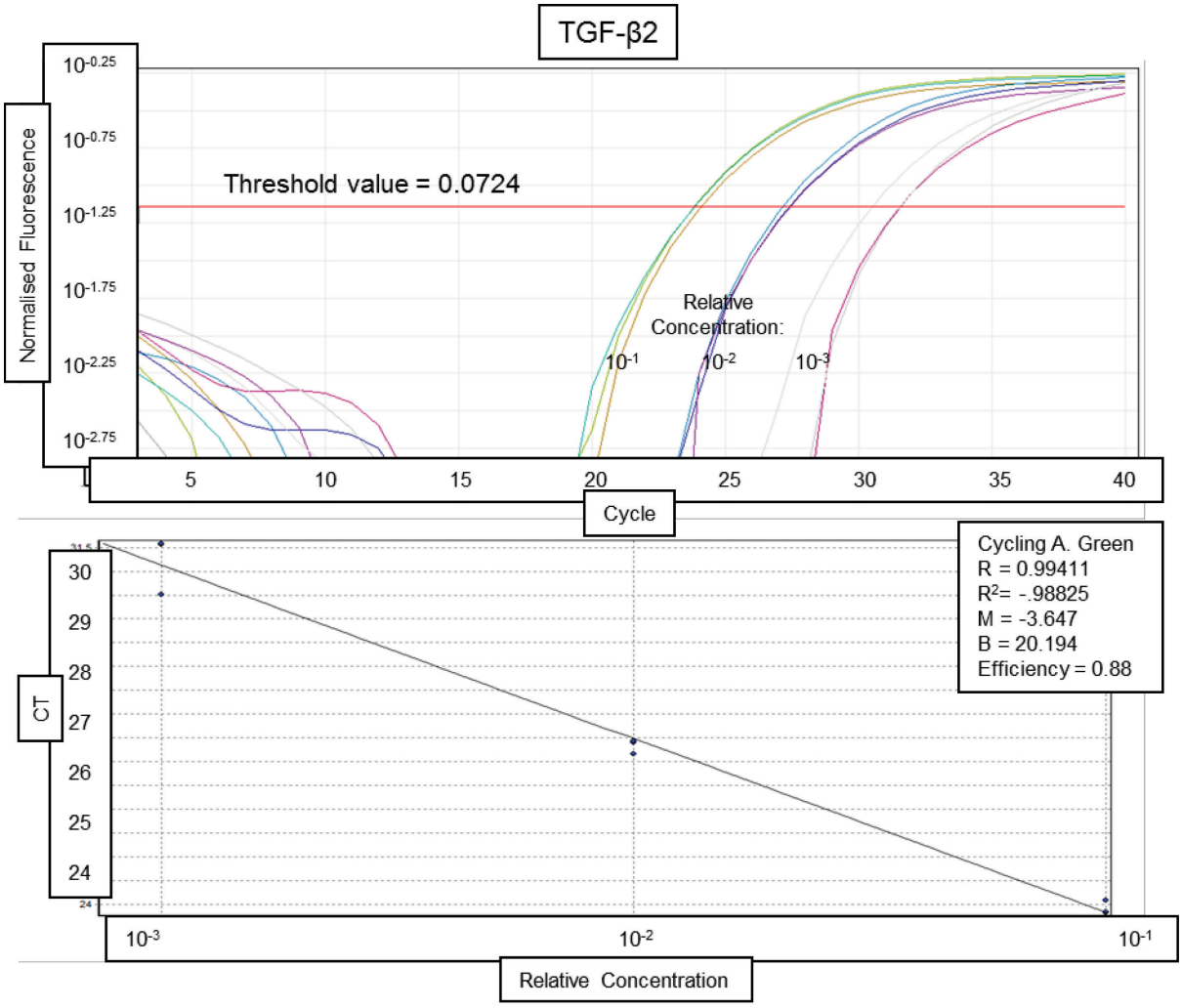

integrin β1
Normalised Fluorescence
10-0.25
10-0.75
10-1.25
10-1.75
10-2.25
10-2.75
Threshold value = 0.0542
Relative Concentration:
10-1
10-2
10-3
5
10
15
20
25
30
35
40
Cycle
CT
32
30
29
28
27
26
25
24
23.5
Cycling A. Green
R = 0.99777
R2= 0.99555
M = -4.062
B = 19.537
Efficiency = 0.76
10-3
10-2
10-1
Relative Concentration

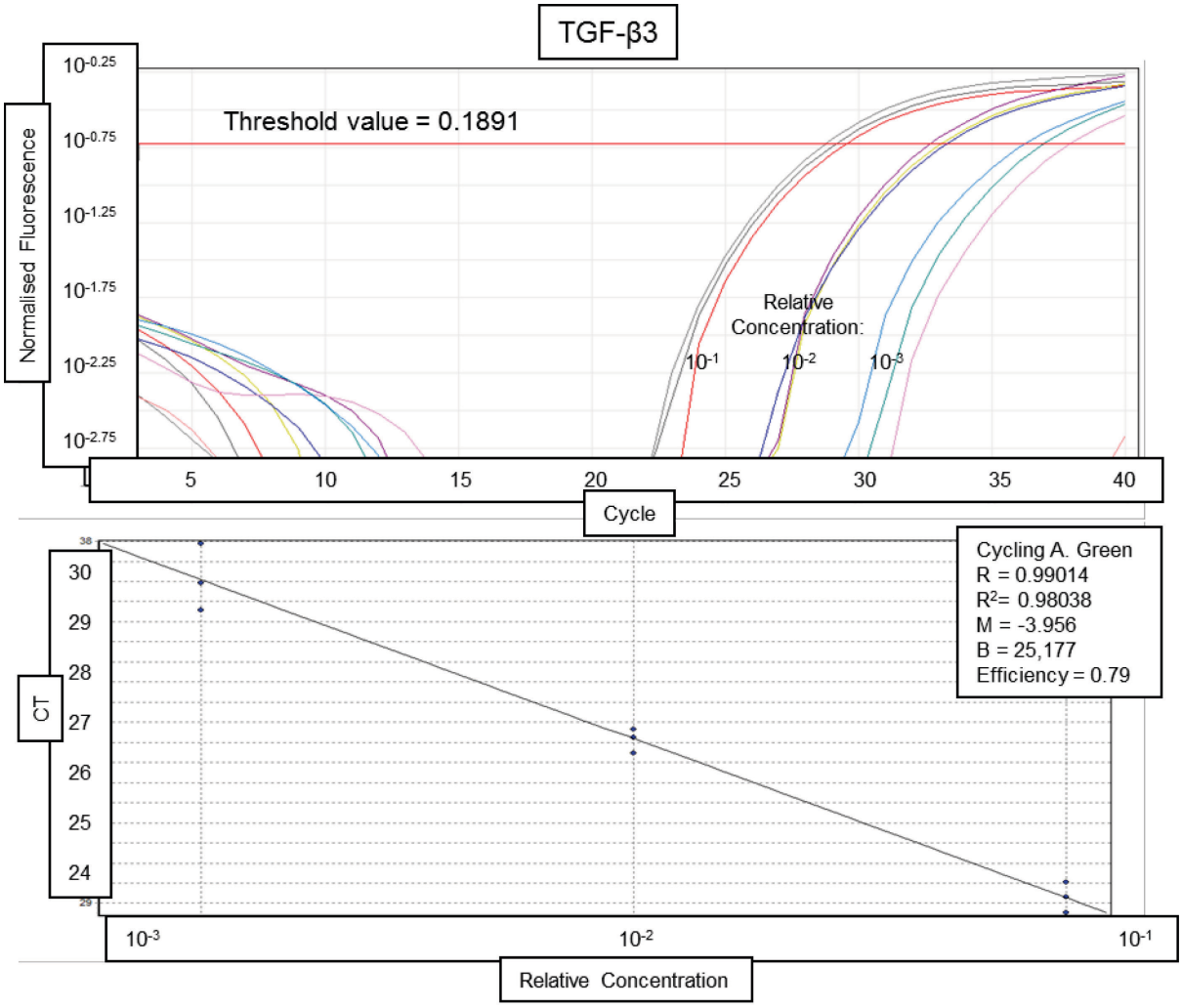

EMMPRIN
Normalised Fluorescence
$10^{-0.25}$
$10^{-0.75}$
$10^{-1.25}$
$10^{-1.75}$
$10^{-2.25}$
$10^{-2.75}$
Threshold value = 0.046
Relative Concentration:
10^{-1}
10^{-2}
10^{-3}
5
10
15
20
25
30
35
40
Cycle
CT
30
29
28
27
26
25
24
Cycling A. Green
R = 0.99578
R^2= 0.99158
M = -3.741
B = 14.014
Efficiency = 0.85
10^{-3}
10^{-2}
10^{-1}
Relative Concentration

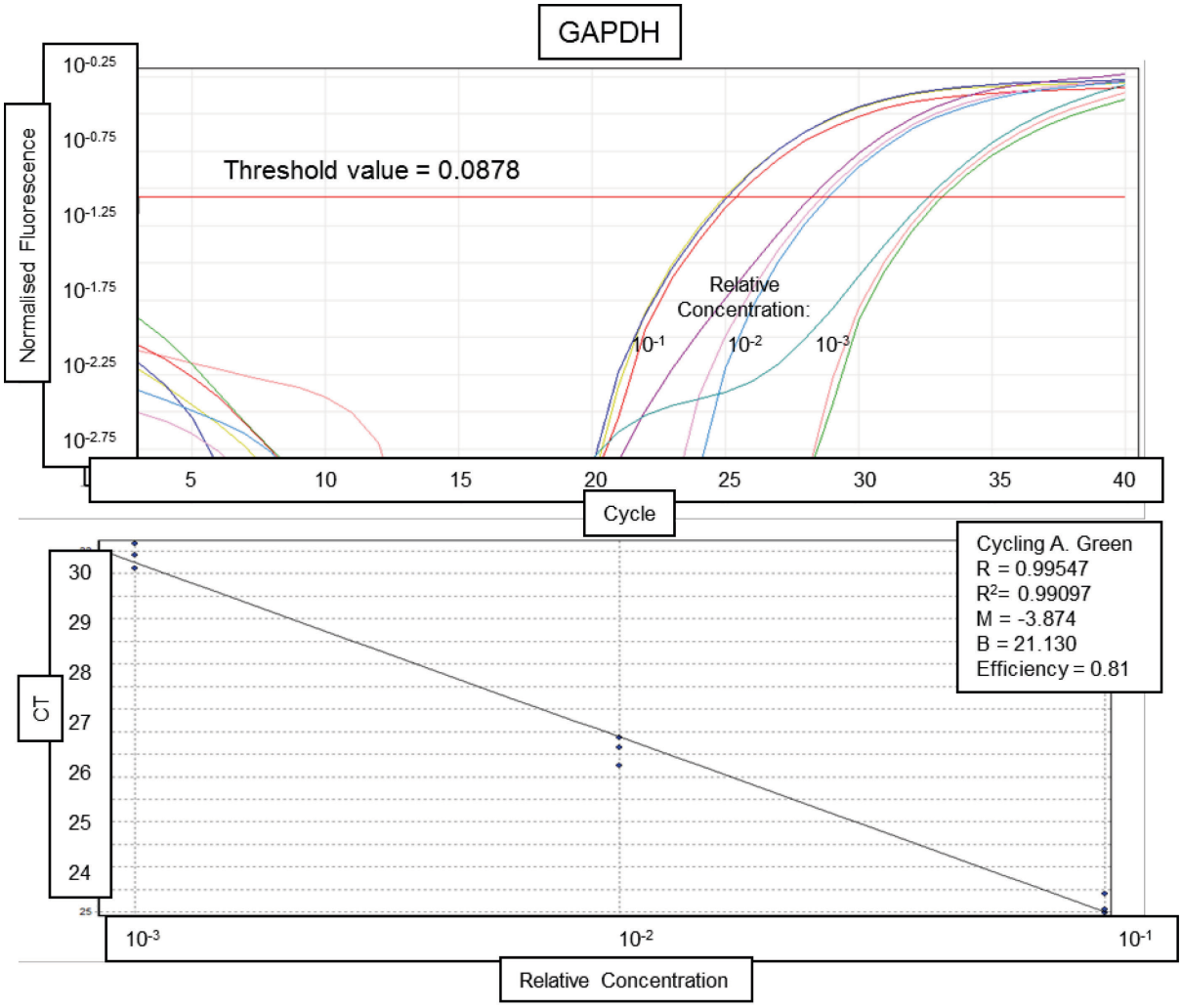

E-cadherin
Normalised Fluorescence
$10^{-0.25}$
$10^{-0.75}$
$10^{-1.25}$
$10^{-1.75}$
$10^{-2.25}$
$10^{-2.75}$
Threshold value = 0.05
Relative Concentration:
10^{-1}
10^{-2}
10^{-3}
5
10
15
20
25
30
35
40
Cycle
CT
30
29
28
27
26
25
24
Cycling A. Green
R = 0.99251
R^2= 0.98509
M = -3.435
B = 14.894
Efficiency = 0.96
10^{-3}
10^{-2}
10^{-1}
Relative Concentration

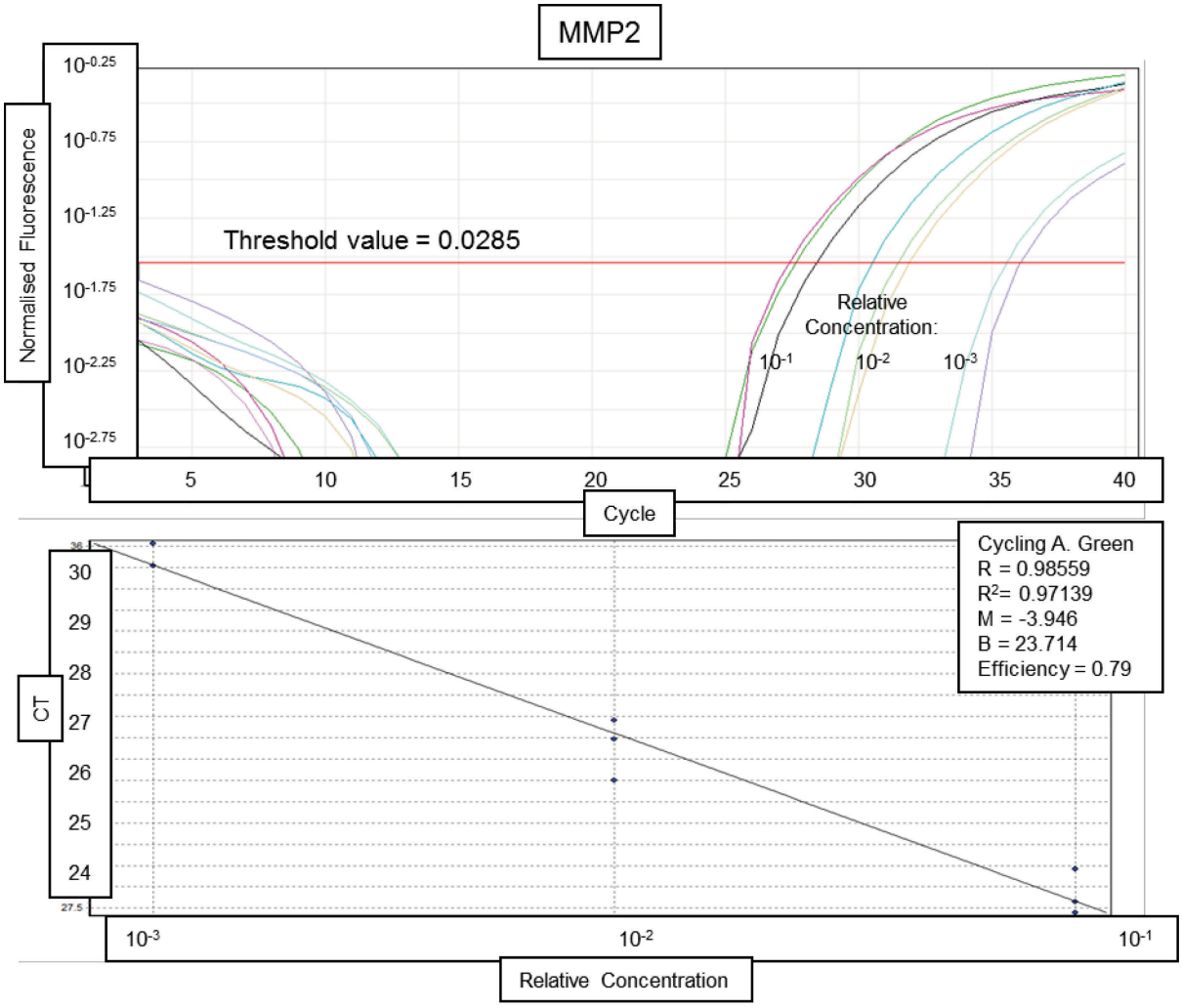

N-cadherin
Normalised Fluorescence
10-0.25
10-0.75
10-1.25
10-1.75
10-2.25
10-2.75
Threshold value = 0.0635
Relative Concentration:
10-1
10-2
10-3
5
10
15
20
25
30
35
40
Cycle
CT
30
29
28
27
26
25
24
20.5
Cycling A. Green
R = 0.99309
R2= 0.98623
M = -3.776
B = 16.758
Efficiency = 0.84
10-3
10-2
10-1
Relative Concentration

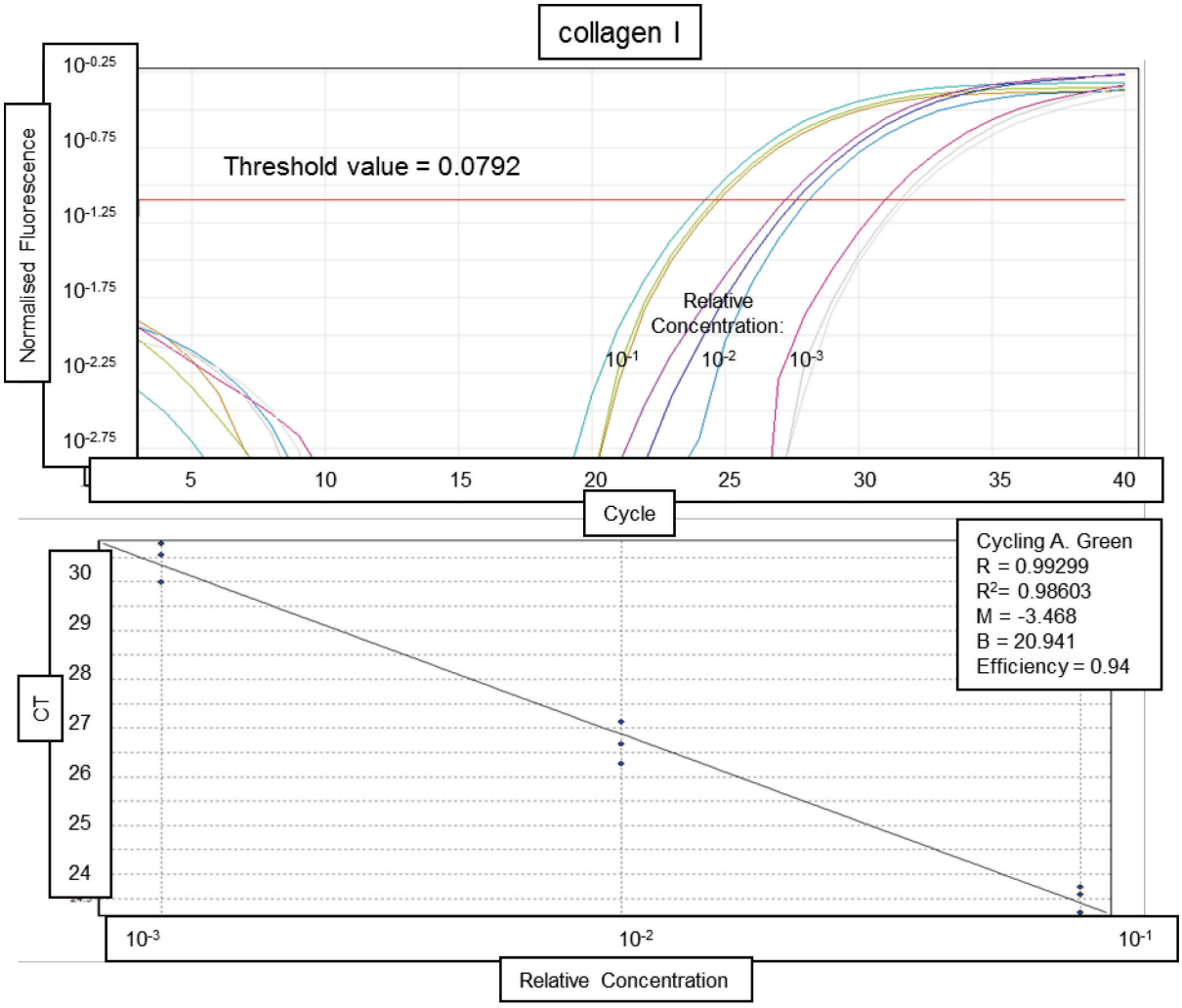

TGF-β1
Normalised Fluorescence
10-0.25
10-0.75
10-1.25
10-1.75
10-2.25
10-2.75
Threshold value = 0.0576
Relative Concentration:
10-1
10-2
10-3
5
10
15
20
25
30
35
40
Cycle
CT
30
29
28
27
26
25
24
Cycling A. Green
R = 0.99517
R2= 0.99036
M = -3.445
B = 17.895
Efficiency = 0.95
10-3
10-2
10-1
Relative Concentration

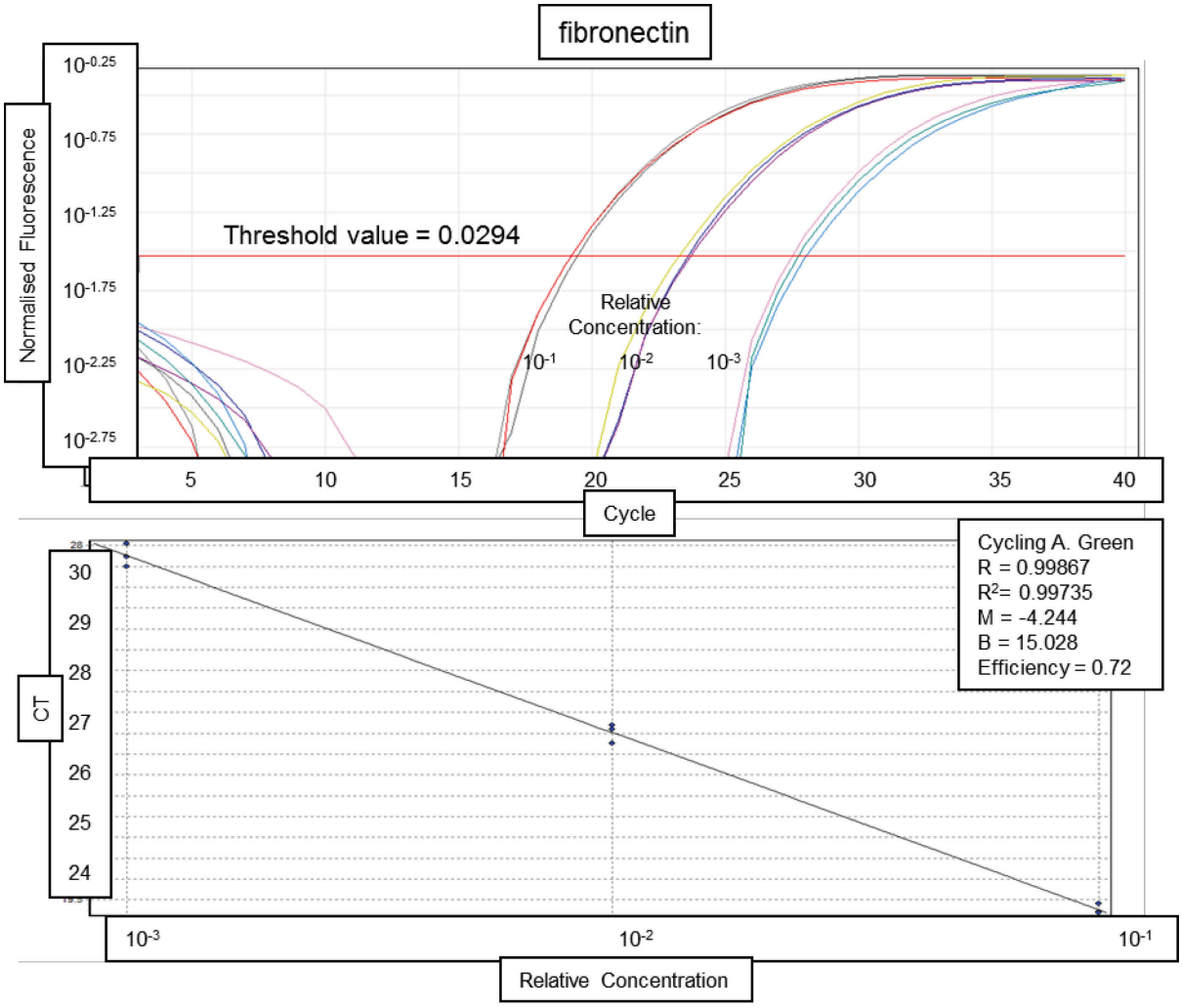

TGF-β2
Normalised Fluorescence
10-0.25
10-0.75
10-1.25
10-1.75
10-2.25
10-2.75
Threshold value = 0.0724
Relative Concentration:
10-1
10-2
10-3
5
10
15
20
25
30
35
40
Cycle
CT
30
29
28
27
26
25
24
Cycling A. Green
R = 0.99411
R2= -.98825
M = -3.647
B = 20.194
Efficiency = 0.88
10-3
10-2
10-1
Relative Concentration


TGF-β3
Threshold value = 0.1891
Normalised Fluorescence
10-0.25
10-0.75
10-1.25
10-1.75
10-2.25
10-2.75
Relative Concentration:
10-1
10-2
10-3
5
10
15
20
25
30
35
40
Cycle
CT
30
29
28
27
26
25
24
10-3
10-2
10-1
Relative Concentration
Cycling A. Green
R = 0.99014
R2= 0.98038
M = -3.956
B = 25,177
Efficiency = 0.79


GAPDH
Normalised Fluorescence
10-0.25
10-0.75
10-1.25
10-1.75
10-2.25
10-2.75
Threshold value = 0.0878
Relative Concentration:
10-1
10-2
10-3
5
10
15
20
25
30
35
40
Cycle
CT
30
29
28
27
26
25
24
Cycling A. Green
R = 0.99547
R2= 0.99097
M = -3.874
B = 21.130
Efficiency = 0.81
10-3
10-2
10-1
Relative Concentration


MMP2
Normalised Fluorescence
$10^{-0.25}$
$10^{-0.75}$
$10^{-1.25}$
$10^{-1.75}$
$10^{-2.25}$
$10^{-2.75}$
Threshold value = 0.0285
Relative Concentration:
10^{-1}
10^{-2}
10^{-3}
5
10
15
20
25
30
35
40
Cycle
CT
30
29
28
27
26
25
24
Cycling A. Green
R = 0.98559
R^2= 0.97139
M = -3.946
B = 23.714
Efficiency = 0.79
10^{-3}
10^{-2}
10^{-1}
Relative Concentration


collagen I
Normalised Fluorescence
$10^{-0.25}$
$10^{-0.75}$
$10^{-1.25}$
$10^{-1.75}$
$10^{-2.25}$
$10^{-2.75}$
Threshold value = 0.0792
Relative Concentration:
10^{-1}
10^{-2}
10^{-3}
5
10
15
20
25
30
35
40
Cycle
CT
30
29
28
27
26
25
24
Cycling A. Green
R = 0.99299
R^2= 0.98603
M = -3.468
B = 20.941
Efficiency = 0.94
10^{-3}
10^{-2}
10^{-1}
Relative Concentration


fibronectin
Normalised Fluorescence
10-0.25
10-0.75
10-1.25
10-1.75
10-2.25
10-2.75
Threshold value = 0.0294
Relative Concentration:
10-1
10-2
10-3
5
10
15
20
25
30
35
40
Cycle
CT
30
29
28
27
26
25
24
Cycling A. Green
R = 0.99867
R2= 0.99735
M = -4.244
B = 15.028
Efficiency = 0.72
10-3
10-2
10-1
Relative Concentration